

1-2014

# Hydrologic Modeling in Semi-Arid Agricultural Region : An Integrated Approach to Study Water Resources in Southern San Joaquin Valley, California

Sagarika Roy  
*Montclair State University*

Follow this and additional works at: <https://digitalcommons.montclair.edu/etd>

 Part of the [Environmental Sciences Commons](#)

---

## Recommended Citation

Roy, Sagarika, "Hydrologic Modeling in Semi-Arid Agricultural Region : An Integrated Approach to Study Water Resources in Southern San Joaquin Valley, California" (2014). *Theses, Dissertations and Culminating Projects*. 194.  
<https://digitalcommons.montclair.edu/etd/194>

This Dissertation is brought to you for free and open access by Montclair State University Digital Commons. It has been accepted for inclusion in Theses, Dissertations and Culminating Projects by an authorized administrator of Montclair State University Digital Commons. For more information, please contact [digitalcommons@montclair.edu](mailto:digitalcommons@montclair.edu).

HYDROLOGIC MODELING IN SEMI-ARID AGRICULTURAL REGION: AN  
INTEGRATED APPROACH TO STUDY WATER RESOURCES IN SOUTHERN  
SAN JOAQUIN VALLEY, CALIFORNIA

A DISSERTATION

Submitted to the Faculty of  
Montclair State University in partial fulfillment  
of the requirements  
for the degree of Doctor of Philosophy

by

SAGARIKA ROY

Montclair State University

Montclair, NJ

2015

Dissertation Chair: Duke Ophori, PhD

Copyright © 2015 by *Sagarika Roy*. All rights reserved.

MONTCLAIR STATE UNIVERSITY

THE GRADUATE SCHOOL

DISSERTATION APPROVAL

We hereby approve the Dissertation

**HYDROLOGIC MODELING IN SEMI-ARID AGRICULTURAL REGION: AN  
INTEGRATED APPROACH TO STUDY WATER RESOURCES IN SOUTHERN  
SAN JOAQUIN VALLEY, CALIFORNIA**

of

**SAGARIKA ROY**

Candidate for the Degree:

Doctor of Philosophy in Environmental Management

Department of Earth & Environmental Studies

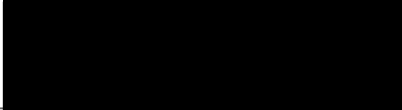
Certified by:

  
\_\_\_\_\_

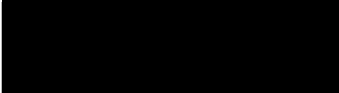
Dr. Joan C. Ficke  
(Dean of Graduate School)

6/8/15  
\_\_\_\_\_  
(Date)

Dissertation Committee:

  
\_\_\_\_\_

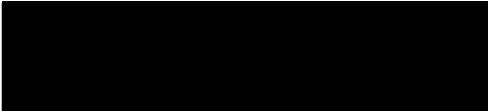
Dr. Duke Ophori

  
\_\_\_\_\_

Dr. Mark Chopping

  
\_\_\_\_\_

Dr. Joshua Galster

  
\_\_\_\_\_

Dr. Solomon Gbondo-Tugbawa

## ABSTRACT

# HYDROLOGIC MODELING IN SEMI-ARID AGRICULTURAL REGION: AN INTEGRATED APPROACH TO STUDY WATER RESOURCES IN SOUTHERN SAN JOAQUIN VALLEY, CALIFORNIA

by Sagarika Roy

Drought is one of the most severe natural hazards in the world. This research aims at assessing the limited water resources for better crop-water irrigation and conservation of a drought affected agricultural area in California.

Evapotranspiration (ET) is one of the most important parameter to study crop water use for irrigation scheduling and water management. The remote sensing based ET estimation using Surface Energy Balance Algorithm for Land (SEBAL) is the efficient way to understand crop water use. Crop Water Stress Index (CWSI) quantifies plant stress under different field conditions. The remote sensing approach allows efficient irrigation by applying water when symptoms of water stress appear. To avoid water stress and poor productivity, agriculture relies heavily on surface-water diversions and groundwater extraction. The flow of percolated irrigated water and identification of potential recharge area in the field can minimize the water stress. A thorough understanding of the ET processes and reliable estimates of ET as well as precipitation are required to obtain reliable estimates for water balance.

Results show that the average actual evapotranspiration (ET<sub>a</sub>) estimated from SEBAL, and Penman-Monteith (PM) was 0.67 mm/h and 0.75 mm/h respectively, with a mean percent difference of 0.109%. The analysis shows that the CWSI when greater than

0.5 resulted in maximum stress whereas the well-irrigated almond crops have CWSI less than 0.24. The flow of groundwater can indirectly influence the status of water stress and ET. It was observed that the groundwater is flowing towards the east of the study area. Excess irrigated water contributes to groundwater recharge. The average Water Surface Elevation (WSE) in 1955 for the growing season (May to July) is 161.04 m. This value is low when compared to those of 2009, 2010, and 2011, which are 237.14 m, 236.28 m, and 235.74 m respectively. The result shows that the average WSE in the wells increased. The total annual deficit in the region is  $135.66 \pm 11.3$  mm and the total annual surplus is  $291.47 \pm 24.29$  mm. Irrigation should apply when this region undergoes a period of moisture deficit in the months of May to July. From September to October are months of soil water recharge; from November to early February is the period of water surplus due to winter rainfall. It was observed that the growers should apply a depth of approximately  $79.37 \pm 11.3$  mm to replenish the soil moisture storage over the entire field in the growing season of almond orchards.

## **ACKNOWLEDGEMENT**

I am thankful to Almighty God for the many blessings that He bestowed upon me and my loved ones throughout the course of my life.

My first debt of gratitude must go to my principal supervisor Professor Duke Ophori for his immense knowledge, guidance and encouragement in the completion of my research. He patiently provided the constructive feedback, support and advice necessary for me to advance through the doctoral program and complete my dissertation. Special thanks to my committee, Dr. Joshua Galster, Ph.D., Dr. Mark Chopping, Ph.D., and Dr. Solomon Gbondo-Tugbawa, Ph.D., for their guidance and useful suggestions. Their guidance has served me well and I owe them my heartfelt appreciation.

I wish to express my sincere thanks to Professor Dibyendu Sarkar, Ph.D., Program Director of the Ph.D. Environmental Management Program for his mentoring in building my academic progress. I would also like to extend my thanks to the faculty and staff in the Department of Earth & Environmental Studies at Montclair State University for providing their outstanding contributions in my academic growth at Montclair. I am thankful to many graduate students, fellow PhD students, and seniors for providing a cohort environment filled with fun, learning and wisdom.

I am thankful to NASA – Student Airborne Research Program 2009, National Suborbital Education and Research Center (NSERC) of the University of North Dakota for two months external research at the University of California, Irvine and collection of data at Paramount Farm in California. In addition, I would like to thank the MASTER

teams from NASA AMES, Paramount Farms for the use of their facilities, the CSTARS field team from University of California Davis (UCD) for their collaboration, and Blake Sanden, Irrigation and Agronomy farm advisor, UCD for coordination, data exchanges, and fieldwork.

I would also like to thank the Graduate School and the College of Science and Mathematics (CSAM) at Montclair State University for their financial support in form of graduate assistantships and tuition waiver scholarships, without which this research could not be possible.

I am grateful to my parents and my brother for their constant support from India. I am thankful to my husband and in-laws for their understanding and co-operation that allowed me to pursue my work. Final thanks to my little Archisha for her relentless efforts to keep me focused on the important things in life, rather than staring at a computer screen.



## **DEDICATION**

*To Bulu Roy and the Late Manoranjan Roy*

## TABLE OF CONTENTS

<b>Content</b>	<b>Page</b>
ABSTRACT.....	<i>iv</i>
ACKNOWLEDGEMENTS.....	<i>vi</i>
DEDICATION.....	<i>viii</i>
LIST OF TABLES.....	<i>xiv</i>
LIST OF FIGURES.....	<i>xv</i>
<b>CHAPTER 1.....</b>	<b>1</b>
1. Introduction.....	1
1.1 Research Objectives.....	16
1.2 Organization of Thesis.....	17
1.3 References.....	18
<b>CHAPTER 2.....</b>	<b>20</b>
ESTIMATION OF ACTUAL EVAPOTRANSPIRATION USING SURFACE ENERGY BALANCE ALGORITHMS FOR LAND MODEL: A CASE STUDY IN KERN COUNTY, CALIFORNIA	

<b>Content</b>	<b>Page</b>
Abstract.....	20
2. Introduction.....	22
2.1 Materials and Methods.....	23
2.1.1 Study area.....	23
2.1.2 Data.....	24
2.1.3 SEBAL model description.....	26
2.1.4 Program Model and Flowchart.....	30
2.1.5 Image Classification & Masking.....	33
2.2 Results and Discussion.....	38
2.2.1 ET estimation results.....	38
2.2.2 Spatial Analysis of ET <sub>a</sub> , NDVI and T <sub>c</sub> .....	40
2.2.3 Validation of SEBAL ET with Penman-Monteith ET.....	43
2.3 Conclusions.....	46
2.4 References.....	47

<b>Content</b>	<b>Page</b>
<b>CHAPTER 3</b> .....	<b>51</b>
ESTIMATION OF CROP WATER STRESS INDEX IN ALMOND ORCHARDS USING THERMAL AERIAL IMAGERY.	
Abstract.....	51
3. Introduction.....	52
3.1 Materials and Method.....	54
3.2 Results and Discussion.....	64
3.3 Conclusions.....	69
3.4 References.....	70
<b>CHAPTER 4</b> .....	<b>72</b>
SIMULATION OF REGIONAL GROUNDWATER FLOW USING MODFLOW IN SOUTHERN SAN JOAQUIN VALLEY, CALIFORNIA.	
Abstract.....	72
4. Introduction.....	74
4.1 Materials and Methods.....	76

<b>Content</b>	<b>Page</b>
4.1.1 Study Area.....	76
4.1.2 Hydrogeology.....	78
4.1.3 Hydrologic framework and Conceptualizing.....	83
4.1.4 Numerical Model.....	87
4.2 Results and Discussion.....	88
4.3 Conclusions.....	97
4.4 References.....	98
<b>CHAPTER 5.....</b>	<b>101</b>
<p>ASSESSMENT OF WATER BALANCE OF THE SEMI-ARID REGION IN  SOUTHERN SAN JOAQUIN VALLEY CALIFORNIA USING THORNTHWAITE  AND MATHER’S MODEL.</p>	
Abstract.....	101
5. Introduction.....	103
5.1 Materials and Method.....	104
5.1.1 Study Area.....	104

<b>Content</b>	<b>Page</b>
5.1.2 Hydrogeology.....	107
5.1.3 Available Data.....	110
5.1.4 The Thornthwaite and Mather's (T M) Model.....	112
5.2 Results and Discussion.....	116
5.3 Conclusions.....	121
5.4 References.....	123
<b>SUMMARY.....</b>	<b>126</b>

## LIST OF TABLES

<b>Table</b>	<b>Page</b>
Table 2-1. A confusion matrix generated from the classification between training data and testing data.....	37
Table 2-2. Comparison of ET <sub>a</sub> among SEBAL, PM, and Field data .....	44
Table 2-3. ET (mm/day) estimates for current year, previous year and historic data for the month of July.....	45
Table 3-1. Baseline parameters for various crops-sunlight conditions (Idso, 1982).....	63
Table 4-1. Soil texture and soil moisture capacity in Paramount Farm (Ratliff et al., 1983) .....	80
Table 4-2. Aquifer parameters .....	84
Table 4-3. Description of observational wells in the locations monitored by DWR.....	85
Table 5-1. Estimated available water capacities for various soil-texture groups.....	109
Table 5-2. Calculation of accumulated potential water loss (APWL) in mm.....	115
Table 5-3. Average monthly water balance computation for almond orchard (AWC= 63.5 mm) in mm.....	117
Table 5-4. Summary of P, PET, AET, and Runoff.....	118

## LIST OF FIGURES

<b>Figure</b>	<b>Page</b>
Figure 1-1. False color composite (Band 1, Band 2, and Band 6) of MASTER image showing Paramount Farm in Southern San Joaquin Valley, California.....	7
Figure 2-1. False color composite (Band 1, Band 2, and Band 6) of MASTER image for Paramount Farm in southern San Joaquin Valley.....	25
Figure 2-2. Flow chart representing the steps included in the ENVI+IDL programming for coding SEBAL algorithms in IDL.....	32
Figure 2-3a: Supervised classification using maximum likelihood for Almond orchards, non-photosynthetic plant (NPV), urban, water, soil, pistachio orchards, and other green vegetations.....	35
Figure 2-3b. Post classification: Building Mask. White scale shows the Almond class pixel.....	36
Figure 2-4. The actual evapotranspiration map of almond crop distribution.....	36
Figure 2-5. Curve of relationship of hourly evapotranspiration (ET <sub>a</sub> ) with vegetation Index (NDVI) for almond orchards.....	41
Figure 2-6. Curve of relationship of hourly evapotranspiration (ET <sub>a</sub> ) with canopy temperature (T <sub>c</sub> ) for almond orchards.....	41
Figure 2-7. Curve of relationship between Vegetation Indices (NDVI) and canopy temperature (T <sub>c</sub> ).....	42



<b>Figure</b>	<b>Page</b>
Figure 2-8. Comparison of remotely sensed ETa (SEBAL) with Penman-Monteith method ( $p < 0.0001$ ).....	41
Figure 3-1a. False color composite (Band 1, Band 2, and Band 6) of MASTER image for Paramount Farm in southern San Joaquin Valley.....	56
Figure 3-1b. Aerial photograph of the almond orchard in Paramount Farm taken from the flight DC-8 (Above). Field photograph of the almond orchard in Paramount Farm in California (Below).....	57
Figure 3-2. Experimental design to compute CWSI.....	58
Figure 3-3. The red line shows the maximum water stress baseline where the CWSI of point A is approximately 1. The blue line is non water-stress shows the crop is well- watered with CWSI is 0 at point C. Whereas at Point B, the crop is moderately stressed with CWSI 0.5. Figure adapted from Idso and Jackson et al. 1981.....	62
Figure 3-4. The image shows the location of the thermal IR radiometer measurements and the regions used for the canopy temperature calibration.....	66
Figure 3-5. Non-stressed baselines for CWSI calculation of almond orchards ( $p < 0.0001$ ).....	67
Figure 3-6. CWSI value of almond orchards.....	68
Figure 4-1. False color composite (Band 1, Band 2 and Band 6) of MASTER image for Paramount farm in Southern San Joaquin Valley .....	73
Figure 4-2. Map showing elevation derived from U.S.G.S topographic base map .....	81

<b>Figure</b>	<b>Page</b>
Figure 4-3. Supervised classification using maximum likelihood for almond orchards, non-photosynthetic plant (NPV), urban, water, soil, pistachio orchards, and other green vegetations.....	82
Figure 4-4. Conceptual framework of hydro-stratigraphic units in the study area.....	86
Figure 4-5a. Showing horizontal cross-section of piezometric surface map based on the steady state simulation model.....	90
Figure 4-5b. Groundwater flowing in vertical cross-section in I and J axis to analyze the recharge and discharge areas.....	91
Figure 4-6. A horizontal view of bottom layer (K axis) showing the potential areas of recharge in red.....	93
Figure 4-7. A horizontal view (k axis) for the map showing groundwater drawdown after the first stress period.....	94
Figure 4-8. A plot showing the simulated head and observed head in five wells in the study area.....	94
Figure 4-9. Yearly Groundwater demand from the year 2006 through 2012.....	96
Figure 4-10. A comparison between the groundwater levels between 1955 with 2009, 2010 and 2011.....	96
Figure 5-1. False color composite (Band 1, Band 2 and Band 6) of MASTER image for Paramount farm in Southern San Joaquin Valley.....	106

<b>Figure</b>	<b>Page</b>
Figure 5-2. Supervised classification using maximum likelihood for almond orchards, non-photosynthetic plant (NPV), urban, water, soil, pistachio orchards, and other green vegetations.....	111
Figure 5-3. Water balance status of the study area.....	120

## CHAPTER 1

### 1. Introduction

The Central Valley in California is known to the world as a productive agricultural region. More than 250 different crops are grown there on 20,000 square acres (California Department of Food and Agriculture, 2009). According to U.S. Census Bureau (2002), the population of California is expected to increase nearly by 50 million people by 2025. The water demands in this region are used mainly for irrigation. Therefore, the increasing population and growing demand for water in the period of drought is expected to increase the reliance on groundwater and surface water (Burow, Karen R et al., 2004). Drought is one of the most severe natural hazards in the world. America's most famous drought, the 1930's Dust Bowl, undermined agricultural production throughout the Great Plains, and displaced as many as 2.5 million people (National Climatic Data Center, 2009. "Drought: A Paleo Perspective – 20<sup>th</sup>Century Drought"). The potential of drought in California is a matter of serious concern particularly when there is extensive agricultural production in the Central Valley. The water delivery for the Central Valley Project (CVP) reduced at 10 percent of contractor's allocations to be used for irrigation in 2009 compared to 40 percent in 2008 and 50 percent in 2007 (California Department of Water Resources, 2009). This is a very critical situation; farmers relied on the groundwater to accommodate the water shortage caused by CVP allowances. Moreover, the State does not have a record of how much water is pumped from an aquifer because the agricultural industry has prevented the State from

adopting regulations for pumping water from wells. The water years 2007-09 were the 12<sup>th</sup> consecutive three-year drought-period in recorded climatic history based on precipitation index (California Department of Water Resources, 2010). In terms of hydrological perspective, the droughts in the late 1920s, 1970s, and 1980s were considered more severe; however, the drought in the year 2009 severely affected the agriculture, ecosystem health, and hydropower production sectors on a massive scale. It not only increased the demands for freshwater, but also changed the operating rules at reservoirs for reduction in pumping of water from the Sacramento-San Joaquin Delta (DWR, 2010).

The State experienced agricultural losses of \$ 308 million in 2008 due to water scarcity (California Department of Food and Agriculture, 2009). As a result, crop prices remained high throughout the drought period from national and international markets. Consequently, unemployment almost doubled statewide from 5.4% to 11.3% during 2005 to 2009 from agricultural loss. Michael et al. (2010) observed that agricultural support jobs declined by 1.5% (2,500 jobs) to 2.3 % (3,750 jobs) in the San Joaquin Valley by the end of 2009-drought period (Employment Development Department 2005-2010). These statistics highlighted the problem of severe and chronic poverty (Congressional Research Service, 2005).

This project focuses on the Paramount Farm (35°30'N, 119°39'W) in San Joaquin Valley, California (Figure 1-1). This study area was selected because it is the world's largest supplier of almonds. It has an extreme Mediterranean climate with an annual rainfall of 98.5 mm, which rains during the winter months (December to February), and

remains arid during the growing months (May to August). The total annual rainfall of the farm was 98.5 mm in the 2009 study period, suggesting serious drought in the area. These orchards are a long-term investment and require specific irrigation scheduling. However, they can provide excellent returns to growers over a prolonged period. In addition, these crops are sensitive to over-irrigation, which can result in hull-rot disease. In view of the fact that only 10% of contractor's total water was allocated by CVP for irrigation purposes, an optimum balance amount of water is required for irrigation as well as conservation. This research aims at assessing the limited water resources in semi-arid regions for irrigation and water conservations based on the following chapters (chapter 2 to 5).

Actual Evapotranspiration (ET<sub>a</sub>) is one of the most important parameters of water balance, irrigation scheduling, and in analyzing crop water stress. The remote sensing approach allows for more complete understanding of ET over a large area using Surface Energy Balance Algorithms for Land (SEBAL) model originally developed by Bastiaanssen et al., (1998, 2005) (**Chapter 2**). In this chapter, an airborne image was obtained from MODIS/ASTER airborne simulator (MASTER) onboard the NASA DC-8 aircraft. This simulator has the characteristics of both the EOS Terra Advanced Space borne Thermal Emission Reflection Radiometer (ASTER) and Moderate Resolution Imaging Spectro-radiometer (MODIS) sensors (Hook et al., 2000). Meteorological data such as incoming solar radiation, relative humidity, air temperature, and wind speed are available from the California Irrigation Management Information System (CIMIS) located in Belridge, California (station no. 146).

Crop Water Stress Index (CWSI) is used to estimate the water requirement. The CWSI method suggested by Idso et al. (1981) quantifies plant stress associated with water deficit under field conditions. Due to scarcity of water, the crop depends on the soil moisture availability. Therefore, to avoid the water stress and poor productivity, the irrigated agriculture relies heavily on surface-water diversions, and groundwater extractions (**Chapter 3**).

After the development of the ground-water basin and surface water diversions, the irrigation water from agriculture percolates to recharge the groundwater and irrigation pumpage is the main reason for groundwater discharge (Davis et al., 1959 and Burrow et al., 2004). Assessing the potential recharge areas in the field can inform management decisions that minimize the water stress. The primary source of recharge is through percolation of irrigation water. This chapter attempts to analyze the flow of groundwater in recharge areas and in water stressed areas (**Chapter 4**).

The water regimes of the farm are well understood by water balance assessment. Water balance is the balance between incoming water (precipitation) and outgoing water (ET, groundwater recharge, and stream flow). A thorough understanding of the ET processes and reliable estimates of ET as well as precipitation (P) are required to obtain water balance computation of the area annually. The little difference between P and ET determines what is left for recharge and runoff (**Chapter 5**). This study also attempts to elucidate complete hydro-geologic characterization of the aquifer system and irrigation scheduling of a large farmland dominated by orchards that depends mostly on the rainfall assuming that the CVP deliveries could be nil during a drought year.

**Contribution of chapter 2.**

In this chapter, energy balance equations based on SEBAL method (Bastiaanssen et al., 1998) was coded in Interactive Data Language (IDL) programming in ENVI 4.0 imaging software for estimating ET in each pixel of the almond orchards. The code was applied on the thermal imagery of MASTER data. This is an alternate approach used to estimate ET using SEBAL model originally developed by Bastiaanssen et al., (1995). The coded SEBAL based ET results were validated with ground based ET using Penman-Monteith method computed by field based CIMIS data.

**Contribution in chapter 3.**

Aerial remote measurement using MASTER thermal band data was used to measure canopy temperature. The first calibration of MASTER imagery shows that the average canopy temperature is 5.02 °C greater than air temperature. This is a problem because the test field was well watered and the transpiration occurring should cause a canopy temperature lower than the air temperature. Therefore, the differential value should be negative. In addition, the in situ thermal IR Radiometer measurements of canopy temperature ( $T_c$ ) were lower than ambient air temperature ( $T_a$ ). Therefore another calibration was applied where the canopy temperatures measured by the thermal IR radiometer in the field was averaged for three different trees to get a representative temperature for the canopy for those almond trees. The locations of these trees were known so the temperatures from the nine surrounding pixels were averaged from the aerial remote sensing MASTER image. The difference between the MASTER temperatures and the thermal IR radiometer temperatures were calculated and then



averaged. The average difference of 7.87 °C was applied to the MASTER data. Therefore, the calibration of field with remote sensing temperatures was found to be appropriate such that  $T_c - T_a$  is negative which allowed for the calculation of CWSI. The thermal data obtained from MASTER was used for the canopy temperature of the almond trees. The air temperature, relative humidity, vapor pressure, wind speed, solar radiation was obtained from the CIMIS station located in Belridge (station number 143) at Lost Hills. It was assumed that the almond orchards completely covered the soil surface, and there are no bare soils exposed in the MASTER image, and therefore the soil temperature was neglected from the image.

#### **Contribution in chapter 4.**

The contribution of this work was to analyze the water stress, low ET in the study area (objective 1 & 2), and study the groundwater flow in order to identify the recharge areas within the field. Identification of potential zones of recharge in the field can help the land manager, and farmers to minimize potential water stress. The excess water from well-irrigated crops percolates to groundwater recharge. Percolated recharge groundwater provides a farm with water conservation, as the recharged water is perhaps utilized for uptake by water stressed crops.

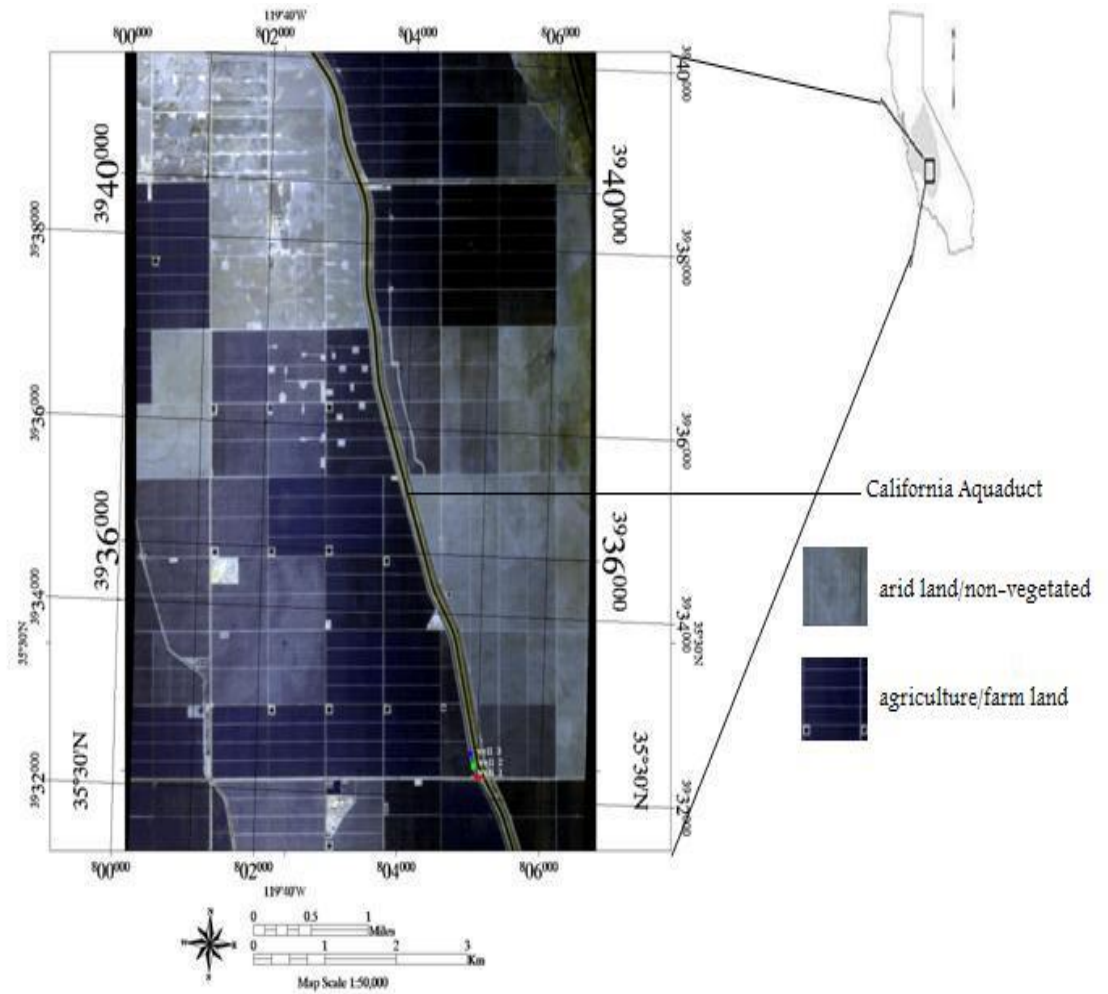


**Figure 1-1.** False color composite (Band 1, Band 2 and Band 6) of MASTER image showing Paramount farm in Southern San Joaquin Valley, California. Blocks shows reflectances of various types of crops in dark tone. Bright tone shows reflectances of non-vegetated/arid areas

Chapter 4 also attempts to analyze the flow of groundwater from the well-irrigated farm. There are no previously research studies related to Paramount Farm groundwater flow. In this study, groundwater flow was simulated by three-dimensional finite-difference model using MODFLOW-2000 developed by United States Geological Survey (USGS) to study the irrigation water recharge and the flow direction of the infiltrated water. This study maps the potential zones for recharge and discharge of groundwater and changes in the water-table head in the study area. Such studies provide an opportunity to analyze the soil moisture surplus and deficit, which helped to quantify the water balance (objective 4). The hypothesis of the study was that the groundwater levels increased since 1955 because of the development of surface water diversion by CVP and percolation of excess irrigated water.

#### **Contribution in chapter 5.**

The land use/land cover classification map was generated from supervised maximum likelihood classification using remote sensing techniques. This was used to compute Available Water Capacity (AWC) for almond orchards class. The water balance using Thornthwaite and Mather (TM) method uses input data from precipitation to predict the water availability. This quantification assumed that the CVP deliveries could be less than 10% of contractor's allocation, and perhaps zero in the future. Based on the precipitation as the only input, the study quantifies soil moisture storage, potential water loss, water deficit, and water surplus for the year.

The overarching goals of this research and study were to integrate remote sensing and hydrology to evaluate energy fluxes for estimation of ET and CWSI; study the movement of ground water; assess the change in water table from irrigation, and quantify the water balance of the farm. The spatial distribution of CWSI and ET in almond was determined through remote sensing using a high spatial resolution of multispectral MASTER image.

The research questions were:

- (1) Will the crop evapotranspiration (ET) have any effect on the water budget or energy budget?
- (2) How the almond orchard will yield under the water stress condition with limited irrigation?
- (3) How do we address drought potential for better harvests?
- (4) How should irrigation timings be scheduled?
- (5) When is water essential for irrigation?
- (6) Are ET and water stress the best indicators?
- (7) Is the groundwater declining? Can irrigated water recharge the groundwater?

Moreover, how is the percolated water flow useful for farm water conservation?

Remote sensing data and hydrologic model output were used to answer questions about ET, aquifer flow dynamics, water budgets, and energy budgets in the study area.

## Conclusions

The remote sensing approach allows for a more complete understanding of ET over the large area of Paramount Farm. In this study, the energy balance equations based on SEBAL model was programmed using IDL code embedded in the ENVI image processing software originally developed by Bastiaanssen et al., (1998, 2005). The customized SEBAL model takes into account the value of sensible heat flux (H) for dry pixels, assuming there are no wet pixels (water bodies) in the study area. The value of  $\Delta T$  is determined from the hot pixel in the MASTER image. Results show that the remote sensing estimate of ET is an alternative to the conventional method using PM method. The average ET<sub>a</sub> estimated from customized SEBAL and PM are 0.67 mm/h and to 0.75 mm/h respectively and the mean percent-difference between them is 0.10%. The remote sensing thermal infrared crop water stress provides a useful tool for understanding crop water requirements. CWSI is based on the energy balance theory explained by Jackson et al. (1981) and Idso et al. (1981) and they suggested that the incoming net radiation is dissipated into sensible heat flux (H) and latent heat flux (LE). These outgoing fluxes H and LE are responsible for heating the air and evapotranspiration respectively (<http://hydrology1.nmsu.edu/teaching/soil698/CWSI.html>). This study attempts to use aerial remote sensing method to compute CWSI. Results show that the average CWSI for well-irrigated almond crop was 0.24, while the water stress crops has CSWI greater than 0.5. The flow of groundwater can indirectly influence the status of water stress and ET. Results show that the groundwater flow can contribute to soil moisture availability. MODFLOW 2000 model was used to simulate the irrigation water recharge and flow of

groundwater. Result shows that the groundwater is flowing towards the east of the study area. The average Water Surface Elevation (WSE) in 1955 for the growing season (May to July) is 161.04 m compared with those of 2009, 2010, and 2011 that are 237.14 m, 236.28 m, and 235.74 m respectively. Therefore, the result shows that the water-table has increased since 1955 due to infiltration of irrigated water and development of surface water diversions in the study area. This research was also useful to understand the soil moisture surplus and deficit for computing the water balance. The water balance study using the TM model is very helpful in finding out the periods of moisture deficit and moisture surplus for the region. Results show that the annual deficit in the field is  $135.85 \pm 11.3$  mm and the annual surplus is  $291.47 \pm 24.29$  mm. Hence, to prevent water stress, irrigation was required when the absolute value of Accumulated Potential Water Loss (APWL) is highest, typically in the months of May, June, and July. In addition, this region was subjected to a period of moisture deficit in the months of May to July. From the middle of September through October, soils benefit from recharge, whereas from November to early February there typically exists a period of water surplus from winter rainfall. The result shows that the area-weighted total runoff was  $1086.56 \pm 58.4$  mm from total precipitation of  $98.55 \pm 8.2$  mm annually. The water budget is used to determine the amount of water required to replenish the soil moisture loss for irrigation scheduling. Therefore, the amount of water required for irrigation in the month of July (either runoff or groundwater percolation) is  $79.37 \pm 11.3$  mm. Furthermore, the field requires irrigation with at least 20 mm of water to ensure uniform and adequate soil water availability in the study area. Water balance approach using the TM model will be useful

for the local population to assess their crop calendar and irrigation requirements based upon the periods of deficit or surplus.

### **Environmental Management Implications**

The environment and the water resource play a dual relationship. In this research, the environment in the agricultural sector requires sufficient quantity of water for irrigation and productivity for better socio-economic development. On the other hand, environment provides services and decision support to allocate water in every sector such as terrestrial ecosystem services, irrigation, urban, domestic, and industrial uses for judicial water rights. In addition, economic factor is also included when there is agricultural sector involved in large-scale irrigations. Managing limited water resources for large-scale agriculture is a critical component of sound environmental management to achieve sustainable and productive farm systems. The crop water requirement for irrigation scheduling depends on the ET. In this research, the ET was highest in the months of May to July, signifying that the irrigation water applied was satisfactory to meet the full crop water requirement. This is helpful in decision making for water allocation and management. Inadequate and irregular irrigation could affect the yield and thereby agricultural economics. Environmental management implications focus on the following issues:

1. The impact of drought and increased arid lands resulting in rising greenhouse gases is important to study climate change and future prediction of global warming.
2. Protection of watersheds and recharge areas.

3. Important role of decision-making regarding water allocation, water quantity management, source protection, and the protection of water dependent ecosystems

This work used an integrated approach to study hydrologic modeling and water resource using hydro-geological methods and remote sensing. This research will be beneficial to water resources planner for managing and predicting supply and demand of groundwater for agricultural needs and by analyzing the aquifer fluctuations, flows, soil moisture status and its implications including:

- Effect of land-use and land-cover changes on water resources.
- The remotely sensed infrared crop water stress index (CWSI) provided a useful tool for the evaluation of crop water status especially in arid agricultural land.
- Effects of climate change on water resources on the aspect of energy budget and its influence in crop evapotranspiration.
- Assessment of water balance is very helpful for the local population for decision making on irrigation scheduling and planning crop calendar especially for the drought prone region.

This research can be extrapolated to pistachios farm adjacent to almond orchards (see MASTER land use/cover classification map shown in Figure 2-3a). Ground data such as thermal data of canopy, soil, and water are required in the pistachios orchards for calibration with the MASTER data. Vegetation characteristics (albedo, soil emissivity and canopy conductance) of pistachios crops are also required to estimate ET and CWSI. In addition, weather data (solar radiation, air temperature, humidity, wind speed) are



required to estimate vapor pressure deficit and crop baseline parameters for calculating water stress index. The hydrological modeling can be done by taking into account, the observation wells located in Paramount farm to simulate the groundwater flow. Water Budget analysis of the pistachios orchards requires rooting depth of pistachios as well as soil characteristics such as albedo, soil emissivity and soil moisture capacity. In addition, biophysical properties of pistachios crop such as length of growing period, growth stage, and chlorophyll content can be measured in field using SPAD meter to estimate greenness or plant health. This is helpful in delineating plants from soils in remote sensing image and, also used for calibrating remotely sensed Normalized Difference Vegetation Index (NDVI). Therefore, it is possible to generalize the outcome by employing an integrated hydrologic modeling to compute water balance of pistachios farms executing the same techniques used for almond farm. The application of this dissertation study to other arid or semi-arid regions is more difficult due to extreme hydrological conditions along with spatial heterogeneity of soil, vegetation, and climatic characteristics. Such areas need new sets of variables from a high-resolution satellite image data along with weather data. However, scarcity of weather data for inaccessible regions can hinder the model output. Therefore, for such studies, a distributed hydrological model with remote sensing methods is perhaps recommended to study limited water resources.

**Future studies:**

1. The SEBAL approach used in this study assumes a sensible heat ( $H$ ) from dry pixel. A further modification may consist of cold pixel to compute the  $H$  values in well-irrigated areas.
2. The soil moisture condition of the root zone can be determined from the evaporative fraction. This will be appended in the model for computing soil moisture surplus and storage for water balance study.
3. Crop coefficient ( $K_c$ ) corresponds to particular crop, growth stage and management, which is required to estimate actual ET possibly estimated real-time throughout the season using NDVI (Choudhury et al., 1994) and Soil Adjusted Vegetation Index (SAVI) (Moran et al., 1994; Bauch, 1995; Ray & Dadhwal, 2001) will be considered in future studies.
4. In CWSI method, the baseline parameters depend on the type of crop, soil, location, and weather parameters to calculate water stress index. Therefore, a further improvement of this method can perhaps be executed using sub-pixel analysis of remote sensing imagery using spectral un-mixing methods. Depending on the canopy cover, Water Deficit Index (WDI) (Moran et al., 1994) or CWSI will be determined.
5. An extension of the study will include snowmelt runoff from the snow-covered mountain adding to the system. This contributes to groundwater and surface water runoffs resulting in recharge and discharge from the farm.

The study has established the potential for using remote sensing data in hydrological modeling to derive various parameters to study farm water management in arid

regions. Integration of remote sensing data into other surface parameters (e.g. vegetation height or stomata resistance) may contribute to improvements of the hydrological simulations. Result obtained from this study will help the water managers to plan the irrigation scheduling, understand how water moves through the aquifer system, and predict water supply scenarios based on water balance computations. Singh et al., (2004) suggested that such water balance studies are useful for local population for dealing with water conservation techniques, deciding crop calendar and irrigation requirements by identifying the period of soil moisture deficit or surplus. This research work also aspires to educate agronomy workers, agricultural cooperative services and county water management agencies. The translation of the work will be carried out using computerized coded interface in future studies for easy accessibility and to communicate the scientific methods and field level understanding to farmers.

### **1.1 Research Objectives**

The overall objectives of this research were to:

1. Apply remote sensing for land use land cover classification and estimate crop evapotranspiration (ET<sub>a</sub>);
2. Compute water stress index in the time of drought;
3. Develop three-dimensional (3-D), finite-difference numerical model of the Paramount Farm regional groundwater-flow system;
4. Quantify annual water balance using Thornthwaite and Mather model.

## **1.2 Organization of Thesis**

The thesis has been organized into five main chapters, the Introduction followed by chapters two through five, which have been prepared as distinct chapters.

Chapter two, titled “Estimation of Actual Evapotranspiration using Surface Energy Balance Algorithms for Land Model : A Case study in San Joaquin Valley, California”, estimates ET of almond orchards over the large area of Paramount Farm using remote sensing with a customized SEBAL model.

Chapter three, titled “Estimation of Crop Water Stress Index in Almond Orchards using Thermal Aerial Imagery”, quantifies crop stress associated with water deficit under field conditions.

Chapter four, titled “Simulation of Regional Groundwater Flow using MODFLOW in southern San Joaquin Valley, California”, addresses the groundwater flow and potential area of recharge from percolation of irrigated water. This study also illustrates that the groundwater table has increased from percolation of irrigated water.

Chapter five, titled “Assessment of water balance of the semi-arid region in Southern San Joaquin Valley California using Thornthwaite and Mather’s model”, examines the water budget of Paramount farm. It was used to study the period of moisture deficit, soil moisture recharge and soil moisture utilization in the farm. This chapter also investigates the monthly variation of precipitation, potential evapotranspiration, actual evapotranspiration, and runoff in the area for computing water balance.

### 1.3 References

- Bausch W. C., 1995. Remote sensing of crop coefficients for improving the irrigation scheduling of corn, *Agricultural Water Management*. Vol. 27, pp. 55-68.
- Bastiaanssen W. G. M., M. Menenti, R. A. Feddes and A. A. M. Holtslag, 1998. A remote sensing surface energy balance algorithm (SEBAL) 1. Formulation, *Journal of Hydrology*. Vol. 212-213, pp. 198-212.
- Burow , Karen R., Jennifer L., Shelton, Joseph A., Hevesi, and Gary S. Weissmann, 2004. Hydrogeologic Characterization of the Modesto Area, San Joaquin Valley, California, *U.S. Geological Survey, Scientific Investigations Report 2004-5232*
- California Department of Food and Agriculture. 2009.  
[http://www.cdfa.ca.gov/egov/Press\\_Releases/Press\\_Release.asp?PRnum=09-009](http://www.cdfa.ca.gov/egov/Press_Releases/Press_Release.asp?PRnum=09-009)
- Choudhury B. J., N. U. Ahmed, S. B. Idso, R. J. Reginato and C. T. S. Daughtry, 1994. Relations between evaporation coefficients and vegetation indices studied by model simulations, *Remote Sensing of Environment*. Vol. 50, pp. 1-17.
- Davis, G.H., Green, J.H., Olmsted, F.H., and Brown, D.W., 1959. Ground-water conditions and storage capacity in the San Joaquin Valley, *California: U.S. Geological Survey Water-Supply*. Paper 1469, pp. 287
- Hook Simon J., Jeffrey J. Myers, Kurtis J. Thome, Micheal Fitzgerald, and Anne B. Kahle, 2001. The MODIS/ASTER airborne simulator (MASTER) a new instrument for earth science studies. *Remote Sensing of Environment*. Vol. 76, pp. 93-102

- Idso, S.B., 1982. Non-water-stressed baseline: a key to measuring and interpreting plant water stress, *Agric. Meteorol.* Vol. 27, pp. 59–70.
- Jackson, R.D., 1982. Canopy temperature and crop water stress. *Advances in Irrigation, New York, Academic Press.* Vol. 1, pp. 43–85
- Michael, J., R. Howitt, J. Medellín-Azuara, and D. MacEwan, 2010. A Retrospective Estimate of the Economic Impacts of Reduced Water Supplies to the San Joaquin Valley in 2009. Retrieved on November 19, 2010 from [http://forecast.pacific.edu/waterjobs/SJV\\_Rev\\_Jobs\\_2009\\_092810.pdf](http://forecast.pacific.edu/waterjobs/SJV_Rev_Jobs_2009_092810.pdf)
- Moran M. S., R. Clarke, Y. Inoue and A. Vidal, 1994. Estimating crop water deficit using the relation between surface-air temperature and spectral vegetation index, *Remote Sensing of Environment.* Vol. 49 (2), pp. 246-263.
- Moran M. S., 1994. Irrigation management in Arizona using satellites and airplanes, *Journal of Irrigation Science.* Vol. 15, pp. 35-44.
- National Climatic Data Center, 2009. Drought: A Paleo Perspective – 20th Century Drought. California Department of Water Resources. Retrieved April 05, 2009.
- Ray S.S., and V. K. Dadhwal, 2001. Estimation of crop evapotranspiration of irrigation command area using remote sensing and GIS, *Agricultural Water Management.* Vol. 49, pp. 239-249.
- <http://hydrology1.nmsu.edu/teaching/soil698/CWSI.html>
- R. K. Singh , V. Hari Prasad & C. M. Bhatt. 2004. Remote sensing and GIS approach for assessment of the water balance of a watershed, *Hydrological Sciences Journal,* Vol. 49:1, pp. 131-141.

**CHAPTER 2**

**ESTIMATION OF ACTUAL EVAPOTRANSPIRATION USING SURFACE  
ENERGY BALANCE ALGORITHMS FOR LAND MODEL: A CASE  
STUDY IN KERN COUNTY, CALIFORNIA**

[This chapter was published in Journal of Environmental Hydrology (2013)]

Abstract:

Almond is an important cash crop in semi-arid southern San Joaquin Valley, California. Estimating almond water use is an important research objective in the arid area of Paramount farm. A Surface Energy Balance Algorithm for Land (SEBAL) model spatially estimates actual evapotranspiration (ET<sub>a</sub>) in the southern San Joaquin Valley in California from available MASTER airborne data. The objectives of the study are: (1) to study the spatial distribution property of canopy surface temperature (T<sub>c</sub>), Normalized Difference Vegetation Index (NDVI), and ET<sub>a</sub> over the San Joaquin Valley, (2) estimate ET<sub>a</sub> of almond class on pixel-by-pixel basis in the Central Valley, California, and (3) to compare ET<sub>a</sub> obtained from SEBAL model with Penman- Monteith method. The results show that the regression between ET<sub>a</sub>, and T<sub>c</sub> show negative (-) correlation. The correlation coefficient (R<sup>2</sup>) of ET<sub>a</sub> from remote sensing with Penman Monteith was 0.85 with bias of 0.77 mm and mean percentage difference is 0.10%. These results indicate that a combination of MASTER data with surface meteorological data could provide an efficient tool for the estimation of regional actual ET used for water resources, irrigation scheduling and management.

Keywords: Evapotranspiration, hydrologic cycle, SEBAL, actual evapotranspiration, net surface radiation flux, MASTER, NDVI, Penman Monteith, CIMIS, correlation.



## 2. Introduction

Ground measurement of ET is very time consuming and cannot obtain accurate spatial ET estimation. Therefore, the complexity involved with the estimation of ET manually resulted in development of various spatial methods using remote sensing over the period of time (Allen et al., 1998). Several studies shows the progress of estimating ETa using remote sensing techniques (Kustas and Norman, 1996, Bastiaanssen et al., 1998 and Kustas et al., 2003, Courault et al, 2003, Engman & Gurney, 1992). Wang (2008) mentioned “there are two main methods for remote sensing ET estimations: direct and indirect. Direct methods use thermal infrared data (TIR) and energy budget equations. Whereas, an indirect method uses Soil-Atmosphere Transfer model”. Both of these estimations requires albedo, emissivity and leaf area index under different wavelength (Courault et al., 2003). In this study, direct measurement of ET using the Surface Energy Balance Algorithm for Land (SEBAL) is applied in the agricultural land of southern San Joaquin Valley in California. Bastiaanssen et al. (1998) developed SEBAL method, which is one-layer energy balance model. The model uses energy budget equations to estimate instant evapotranspiration for each pixel. Wang (2008) suggested that from the input data (incoming radiation , wind speed and spectral radiance), the output data such as NDVI (normalized difference vegetation index), albedo, roughness length, and soil heat flux (G) can be calculated. The study area was irrigated under CVP, which supplies water from the Sacramento-San Joaquin river system. Therefore, the quantification of ET is necessary to understand the crop water use.

The objective of this study is to (1) investigate the spatial distribution property of canopy surface temperature ( $T_c$ ), Normalized Difference Vegetation Index (NDVI), and  $ET_a$  over the San Joaquin Valley. (2) Estimate actual evapotranspiration of the almond class on a pixel-by-pixel basis in the study area using image classification and mask, (3) and to compare actual evapotranspiration obtained from SEBAL model with reference evapotranspiration ( $ET_o$ ) using Penman Monteith method (PM) obtained from California Irrigation Management Information System (CIMIS) station.

## **2.1 Materials and Method**

### **2.1.1 Study Area**

The 402 km<sup>2</sup> Paramount Farm is located at the Lost Hill of Kern County in southern San Joaquin Valley, California (35°30'N, 119°39'W) (Figure 2-1). The total annual rainfall in 2009 drought year of the farm was 98.5 mm. The valley occupies two-thirds of the southern Central Valley in California. San Joaquin River flows in the northern part of the San Joaquin Valley and drains to the San Francisco Bay. About 4 percent of the basin area is urban. Most of the basin's population is focused on agricultural activities. Southern San Joaquin is the world's largest supplier of almonds with more than 4,000 acres of almond orchards. Geographically, the southern part of the San Joaquin Valley is the Tulare Basin, bordered by the Sierra Nevada on the east, the Tehachapi Mountains on the south, and the Coast Ranges on the west. The northern extent corresponds to the Kings River. Significant geographic features include the Tulare Lake Basin and the Kettleman Hills. The main land use is agriculture.

### 2.1.2 Data

An airborne image was obtained from MODIS/ASTER airborne simulator (MASTER). This simulator has the characteristics of both the EOS Terra Advanced Space borne Thermal Emission Reflection Radiometer (ASTER) and Moderate Resolution Imaging Spectro-radiometer (MODIS) sensors (Hook et al., 2000). This sensor has 50 spectral bands over the spectral range 0.4 to 12  $\mu\text{m}$  (visible through thermal infrared) at a variety of spatial resolutions. An image was taken on July 24, 2009. Field data was also available for calibrating land surface heat fluxes in the study area. SEBAL model was applied to MASTER level 1-B dataset of visible, near infrared and thermal infrared radiation channels of airborne MASTER instrument onboard the NASA DC-8 aircraft. Meteorological data such as incoming solar radiation, relative humidity, air temperature, and wind speed are available from the California Irrigation Management Information System (CIMIS) located in Belridge, California (station no. 146). CIMIS is a program governed by the Department of Water Resources (DWR) in California. DWR manages a network of 120 weather stations to collect, store and process weather data. These data are useful for irrigator to manage water resources efficiently ([www.cimis.water.ca.gov](http://www.cimis.water.ca.gov)).

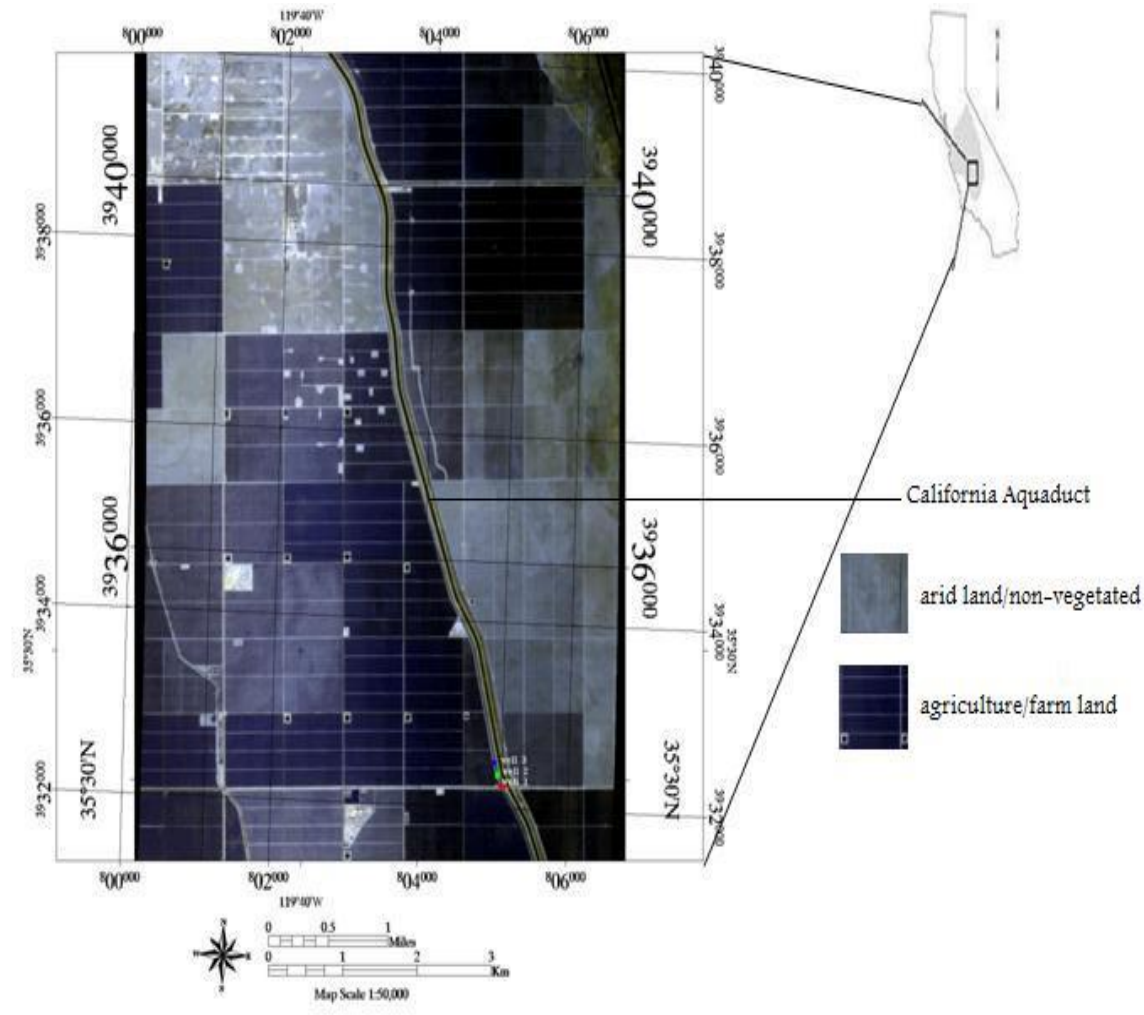


**Figure 2-1.** Remotely sensed false color composite (Band 1, Band 2 and Band 6) of MASTER image showing Paramount farm in Southern San Joaquin Valley, California. Blocks shows reflectances of various types of crops in dark tone. Bright tone shows reflectances of non-vegetated/arid areas (Land cover classification of this image shown in Figure 2-3a).

### 2.1.3 SEBAL Model Description

The SEBAL model does not only calculate an entire radiation and energy balance, but also computes resistances for momentum, heat, and water vapor for each pixel (Bastiaanssen et al., 1998 and Bastiaanssen et al., 2000). SEBAL model requires inputs such as weather parameters (wind speed, humidity, incoming solar radiation, and temperature), remote sensing images, and spectral radiance (visible, near infrared and thermal infrared) of electromagnetic spectrum (Allen et al., 1998, Gamage et al., 2009). When considering instantaneous conditions, the energy balance for a land surface is given as:

$$R_n = G_0 + H + LE \quad (\text{W m}^{-2}) \quad (2-1)$$

Where  $R_n$  is the net radiation [ $\text{W m}^{-2}$ ],  $G_0$  is the soil heat flux [ $\text{W m}^{-2}$ ],  $H$  is the sensible heat flux [ $\text{W m}^{-2}$ ] and  $LE$  is the latent heat flux [ $\text{W m}^{-2}$ ], which is equal to AET. Other factors affecting the energy balance such as heat stored by the vegetation and photosynthesis are usually neglected, because they are considered a small fraction of net radiation when compared with the other four components (Allen et al., 1998). Equation (2-1) can also be expressed in terms of latent heat flux.

$$LE = EF (R_{n24} - G_0) \quad (\text{W m}^{-2}) \quad (2-2)$$

Where  $EF$  is the evaporative fraction. The instantaneous evaporative fraction ( $EF$ ), and the daily averaged net radiation,  $R_{n24}$  is used to calculate evaporation. The  $EF$  is defined as the ratio of evapotranspiration to the available energy.

$$EF = \frac{LE}{H + LE} \quad (\text{W m}^{-2}) \quad (2-3)$$

The EF is supposed to be constant during daytime hours, even though H and LE differ considerably (Crago, 1996). When the atmospheric moisture and soil moisture are in equilibrium, then the EF expresses the ratio of the actual to the crop evaporative demand. The incoming solar radiation is measured using a pyranometer. The instantaneous net radiation ( $R_n$ ) was calculated between ( $\downarrow$ ) and outgoing fluxes ( $\uparrow$ ) of shortwave  $R_s$  and long wave  $R_L$  radiation. Negative fluxes are considered those leaving the surface and positive for those incoming to the surface. Further, to solve for equation 2-2, the values of  $R_n$ , EF and  $G_0$  are computed using the surface radiation balance equations:

$$R_n = R_{s\downarrow} - aR_{s\downarrow} + R_{L\downarrow} - R_{L\uparrow} - (1 - \epsilon_0) R_{L\downarrow} \quad (\text{W m}^{-2}) \quad (2-4)$$

Where  $R_{s\downarrow}$  is the incoming short-wave radiation ( $\text{W/m}^2$ ),

$a$  is the surface albedo (dimensionless),

$R_{L\downarrow}$  is the incoming long wave radiation ( $\text{W/m}^2$ ),

$R_{L\uparrow}$  is the outgoing long wave radiation ( $\text{W/m}^2$ ), and

$\epsilon_0$  is the surface thermal emissivity (dimensionless)

The amount of energy absorbed to sustain crop evaporation rate describes the latent heat flux. The surface temperature, vegetation index and surface albedo are derived from remote sensing measurements, and used together to solve for  $R_n$ ,  $G_0$  and H. Surface emissivity is obtained according to the relationship proposed by Van de Griend y Owe, (1993)

$$\varepsilon_s = 1.0094 + 0.047 \cdot \ln(\text{NDVI}) \quad (2-5)$$

where  $\varepsilon_s$  the surface emissivity and NDVI is is Normalized Difference Vegetation Index. Sensible heat flux (H) is computed in an alternate way in SEBAL. It is called “self calibration” procedure. It was based on the manual identification of wet (well irrigated) and dry (dry ground) pixels in the image. H can be calculated as follows (Bastiaanssen et al., 2005).

$$H = \rho_a C_p T^* u^* \quad (\text{Wm}^{-2}) \quad (2-6)$$

$\rho_a$  is density of air ( $\text{Kgm}^{-3}$ ),  $C_p$  is Specific heat at constant pressure ( $\text{J} \cdot \text{kg}^{-1} \cdot \text{K}^{-1}$ ),  $T^*$  (K) is the temperature scale and  $u^*$  ( $\text{m} \cdot \text{s}^{-1}$ ) the friction velocity. The temperature scale can be formulated as

$$T^* = \Delta T / [\ln(z_2/z_1) - \gamma_h(z_2, L) + \gamma_h(z_1, L)] \quad (\text{K}) \quad (2-7)$$

Where  $\Delta T$  = the vertical air temperature difference between the heights  $z_1$  and  $z_2$ ; L is the Monin-Obukhov length; and  $\gamma_h$  is the stability correction for heat transport which is affected by wind speed, atmospheric stability, and surface roughness. Heights  $z_1$  and  $z_2$  are considered predetermined in SEBAL at 0.1 and 200 m elevation respectively because it is considered that wind speed is spatially constant at height 200 m above the ground. By model inversion method,  $\Delta T$ , which is required to match between wet & dry pixel

under turbulence condition, follows the standard Monin-Obukhov theorem for turbulence exchange processes and thermal convection (Brutsaert 1982). A significant feature of SEBAL is that  $\Delta T$  or  $T(z_1) - T(z_2)$  at  $z_1$  and  $z_2$  is determined from hot and cold pixel where  $H = \text{zero}$  for wet pixel and  $H = R_n - G_0$  for dry pixel. The friction velocity  $u^*$  is determined from a single-layer wind speed. The sensor buried in the soil usually measures the soil heat flux, although the remote sensing of  $G$  is possible by taking the daytime ratio of  $G/R_n$  with canopy temperature ( $T_c$ ), albedo, and Normalized Difference Vegetation Index (NDVI). Soil heat flux perhaps estimated from  $R_n$ , albedo, temperature. The equation for soil heat flux (Singh et al., 2008):

$$G_0 = [0.3811 \exp(-2.3187\text{NDVI})] R_n \quad (\text{W m}^{-2}) \quad (2-8)$$

NDVI is calculated as following:

$$\text{NDVI} = \frac{r_{\text{NIR}} - r_{\text{red}}}{r_{\text{NIR}} + r_{\text{red}}} \quad (2-9)$$

Where  $r_{\text{NIR}}$  and  $r_{\text{red}}$  are the reflectance data of near infrared (band 7) and red (band 5) respectively in MASTER image.

The ET<sub>a</sub> in 24 hours is estimated using instantaneous EF and the daily averaged net radiation  $R_{n24}$ . For the time scales of 1 day or longer,  $G_0$  was ignored and net available energy ( $R_n - G_0$ ) reduced to net radiation ( $R_n$ ). The daily timescales, ET<sub>24</sub> (mm/day) can be computed as:

(Bastiaanssen et al., 2005, Singh et al., 2008, Mutiga 2010):



$$ET_{24} = 86400 \times 10^3 \times EF \times R_{n24} / \lambda \rho_w \quad (\text{mm/day}) \quad (2-10)$$

Where:  $R_{n24}$  ( $\text{W/m}^2$ ) is the 24-h averaged net radiation,  $\lambda$  ( $\text{J/kg}$ ) is the latent heat of vaporization, and  $\rho_w$  ( $\text{kg/m}^3$ ) is the density of water, EF is the evaporative fraction.

#### **2.1.4 Program Model and Flowchart**

The SEBAL equations were coded instead of procuring the original software developed by Bastiaanssen et al (1995). It follows the energy balance equations given in Bastiaanssen et al. (1995, 1998). The SEBAL model was coded in Interactive Data Language (IDL) programming language incorporated in ENVI 4.0 version with some assumptions going into the model. The model estimated ETa in  $90 \text{ m} \times 90 \text{ m}$  resolution using MASTER image. This program uses imported data from MASTER images ( $112 \times 455$  pixels) of four blocks of the almond orchards. The flowcharts representing the steps for estimation of ETa are shown in Figure 2-2. This model inputs MASTER airborne data (ground surface reflectance and temperature) and local weather data (solar radiation and wind speed) to calculate the soil heat flux (G) and sensible heat flux (H). Finally, it outputs the spatial ETa (mm/day).

#### ***Inputs***

The inputs include wind speed, humidity and solar radiation data at the local weather station and airborne data from MASTER including ground surface reflectance and temperature. The reflectance has a resolution of  $15 \text{ m} \times 15 \text{ m}$  for the bands 1 to 3 (Visible and Near-infrared bands) and  $30 \text{ m} \times 30 \text{ m}$  for the bands 4 to 9 (Shortwave

Infrared bands). The MASTER thermal IR bands have a resolution  $90\text{ m} \times 90\text{ m}$ . The reflectance data were averaged over  $90\text{ m} \times 90\text{ m}$  to fit the temperature data resolution. This model does not calculate solar radiation, ground surface temperature and reflectance. Instead, those data are obtained from CIMIS weather station located at Belridge, California. This simplified the model complexity, which reduced the program work and time.

### ***Output***

The spatial ETa (mm/day) of almond orchards is the output from the model. The resolution is  $30\text{ m} \times 30\text{ m}$ .

### **Assumptions in the Model:**

1. The most major simplification involved prescribing the temperature gradient between 0.1 and 200 meters above the surface to be 1.96 K.
2. The albedo value of almonds obtained from Guo et al., (1995), using spectral data on an airplane flight over California's Central Valley.
3. Evaporative fraction remains constant during daytime.
4. All raster cells/pixels are pure and can be assigned to a unique land cover/use class.

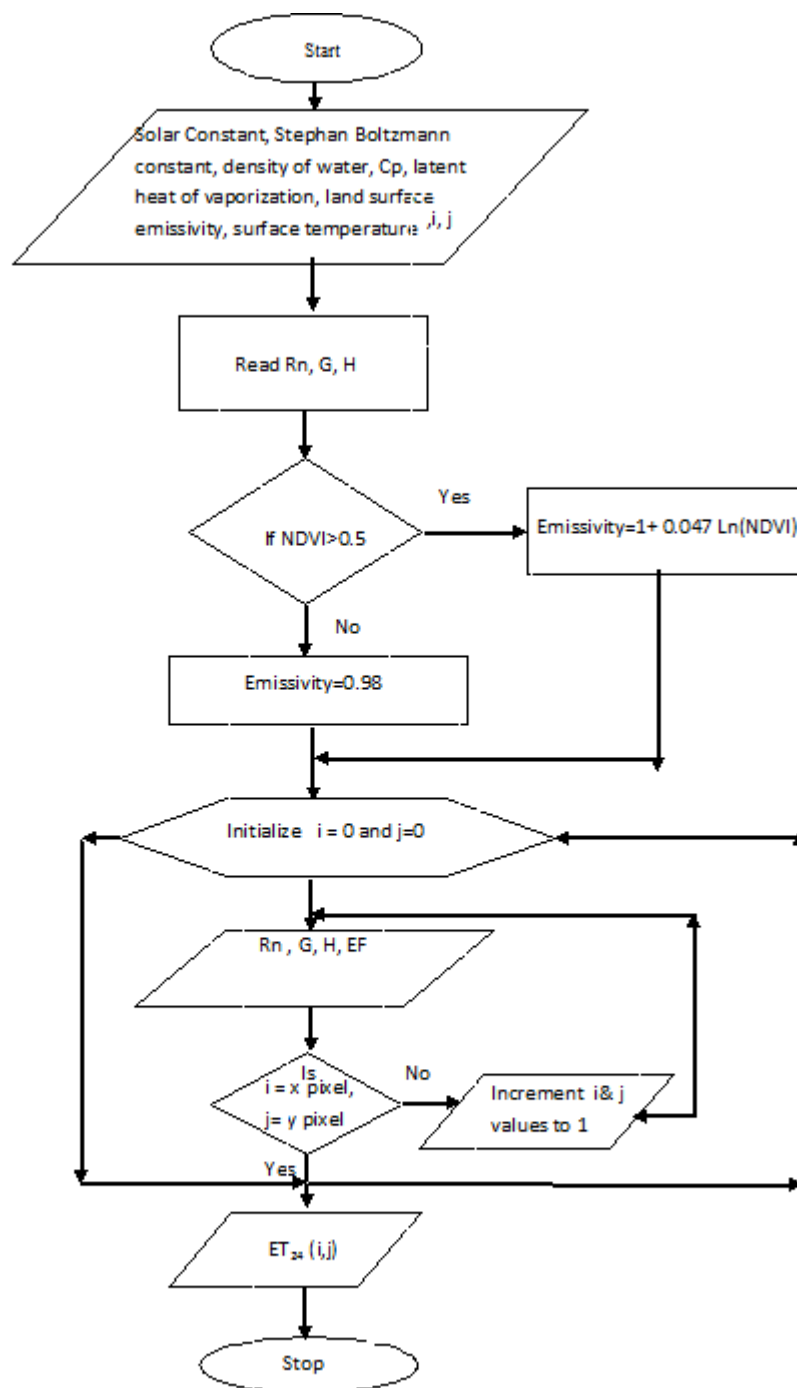


**Figure 2-2.** Flow chart representing the steps included in the ENVI+IDL programming for coding SEBAL algorithm in IDL.

## **2.1.5 Image Classification and Masking**

### **2.1.5.1 Land Use Land Cover Classification**

With supervised classification using Maximum Likelihood criterion, the training sites were selected for the region of interest (ROI) of each land cover class. Different ROIs such as almonds, urban, water soil, pistachios, non-photosynthesis plants (NPV) and other green vegetations are selected to analyze statistics for classification, and masking (Figure 2-3a). Supervised classifications are required to select training areas to define each class. Pixels are compared to the training data for calibration. Based on spectral reflectance, they are assigned to the most appropriate class. The statistical characterization of the spectral reflectance for each information class is developed from ENVI image processing software system. According to Singh et al., (2012) “Maximum Likelihood Classification is a statistical decision criterion to assist in the classification of overlapping signatures; pixels are assigned to the class of highest probability”. After achieving the statistical characterization for each information class, the classification is made based on the reflectance of each pixel image. The maximum likelihood classifier gave more accurate results than Spectral Angle Mapper; however, it is much slower due to extra computations. Classification accuracy assessment are prepared by selecting testing sites in the image for all the corresponding land cover classes, and confusion matrix was built using ground truth ROIs. A statistical test was performed using the kappa index of agreement for classification accuracy of the image or individual cells (Table 2-1).

### **2.1.5.2. Masking**

Post-processing of classified image was required to estimate accuracy to generalize classes by exporting image-maps and vector GIS. Masking reduces the spatial extent of the analysis by masking out areas of the image that do not contain data of interest. The almond class map is obtained by masking all other land cover classes, which do not have same spectral reflectance characteristics of an almond pixel. This is required for the estimation of evapotranspiration of almond orchards (Figure 2-3b). Confusion matrix function in ENVI imaging allows comparison between the classified image and the ground-based image or with ROIs ([www.ltid.inpe.br/tutorial/tut2.htm](http://www.ltid.inpe.br/tutorial/tut2.htm)). The truth image can be another classified image, or an image created from actual ground based measurements. Since there were no ground reference data for this scene, it was achieved by comparing two of the classifications to each other, and there was comparison between classifications of testing ROIs with training ROIs, although this will not provide an unbiased measure of accuracy (Table 2-1).

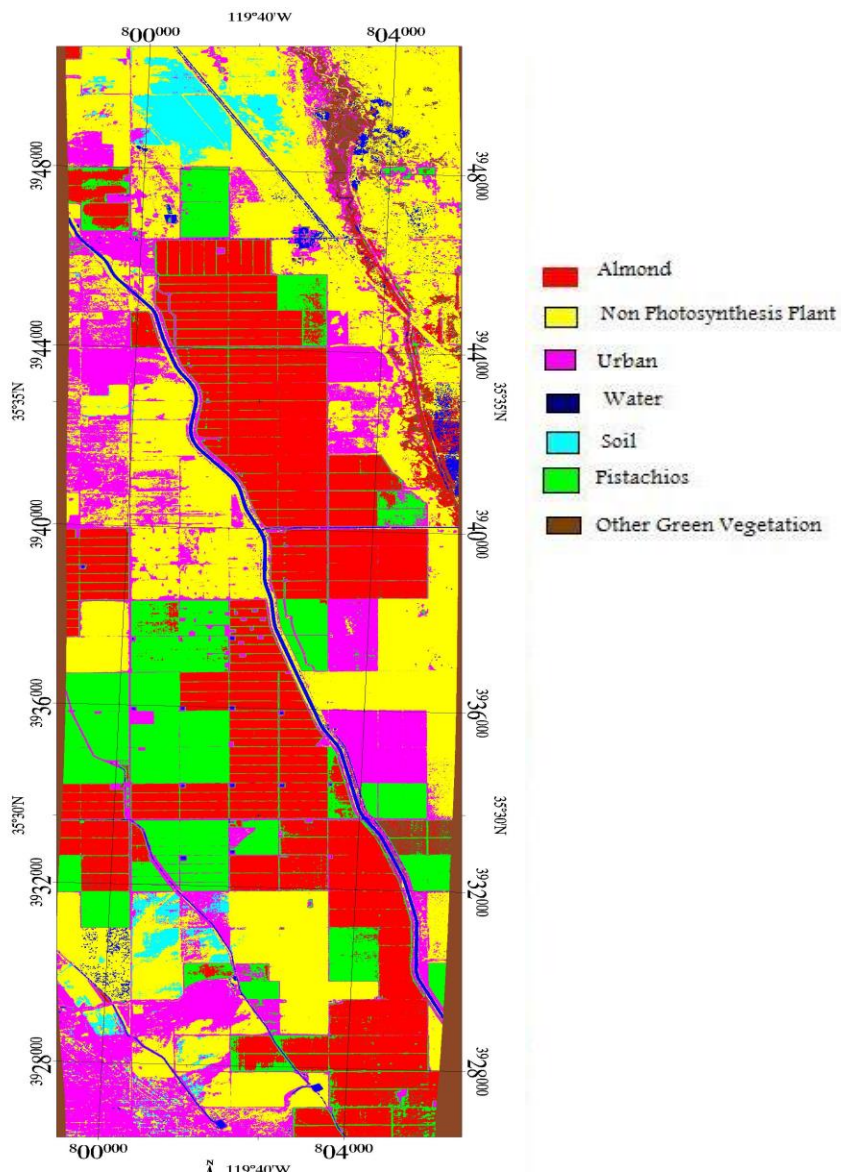


**Figure 2-3a:** Supervised classification using maximum likelihood for almond orchards, non-photosynthetic plant (NPV), urban, water, soil, pistachio orchards, and other green vegetations.

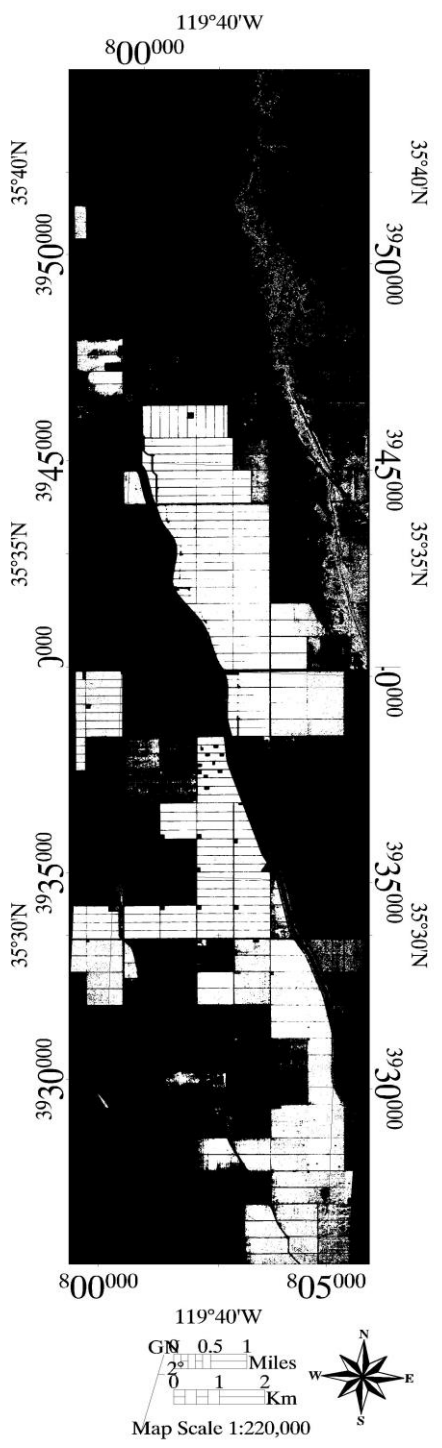


**Figure 2-3b.** Post classification: Building Mask. White scale shows the almond class pixel. Other land cover classes are assigned black color using Masking technique.

**Table 2-1.** A confusion matrix generated from the classification between training data and testing data.

Classified Category (Training data)	Testing data							Total	User's Accuracy
	Almond	NPV	Urban	Soil	Water	Pistachios	Green Veg		
Almond	387	0	0	0	0	1	0	389	99.4%
NPV	0	252	0	1	1	0	1	253	99.6%
Urban	0	0	69	0	1	1	0	70	98.5%
Soil	0	1	0	221	0	0	0	221	100%
Water	0	0	0	0	267	543	0	267	100%
Pistachios	0	0	0	0	0	7	0	543	100%
Green Veg	0	0	0	0	0	0	71	71	100%
Total	387	252	69	222	267	545	72	1814	
Producer's Accuracy	100.00%	100%	100.00%	99.50%	100%	99.63%	98%		
Overall accuracy = 99.77 %. Overall Kappa = 0.9973									



## 2. 2 Results and Discussion

### 2.2.1 ET estimation result

Actual evapotranspiration (ET<sub>a</sub>) in mm/h for July 24, 2009 was computed by solving the surface energy balance using eq. 2-1, eq. 2-3, and eq. 2-6. The spatial variation of ET for the almond class was shown in the Figure 2-4. It ranges from 0.63 mm/h to 0.70 mm/h for the almond canopy. The average reference evapotranspiration (ET<sub>o</sub>) on July 24, 2009 was calculated based on Penmen-Monteith equation as 0.73 mm/h using CIMIS data. The almond crop coefficient K<sub>c</sub> at this time of the year was calculated at 1.05-1.15 in the field. Therefore, the mean empirical estimation of actual evapotranspiration of almond was 0.7519 mm/h. Real time crop evapotranspiration was calculated from the MASTER images. The ET<sub>a</sub> distribution was plotted pixel by pixel in Figure 2-4. The daily time-scale of ET<sub>24</sub> was estimated from SEBAL using eq. 2-10 as 16.19 mm/day, whereas CIMIS-PM estimation of ET<sub>24</sub> is 17.76 mm/day.

There are two types of ET<sub>o</sub> data use for irrigation scheduling: 1) historic ET<sub>o</sub> 2) real time ET<sub>o</sub>. Historic ET<sub>o</sub> represents long-term daily average for 30 years of data. Table 2-3 illustrates the historical ET from 2000-09 with estimated ET for the month of July. The average of estimated ET for July from 2000 to 2009 is 17.36 mm/day; consequently, the maximum ET had occurred in the year 2003 of 19.5 mm/day. This implied that in the non-drought event, water supply exceeds the crop water use and resulted in ET loss. Real time ET<sub>o</sub> is updated daily for scheduling irrigation. Real Time ET<sub>o</sub> has advantage over historical ET<sub>o</sub>-based approach because it accounts for daily variations of weather conditions.

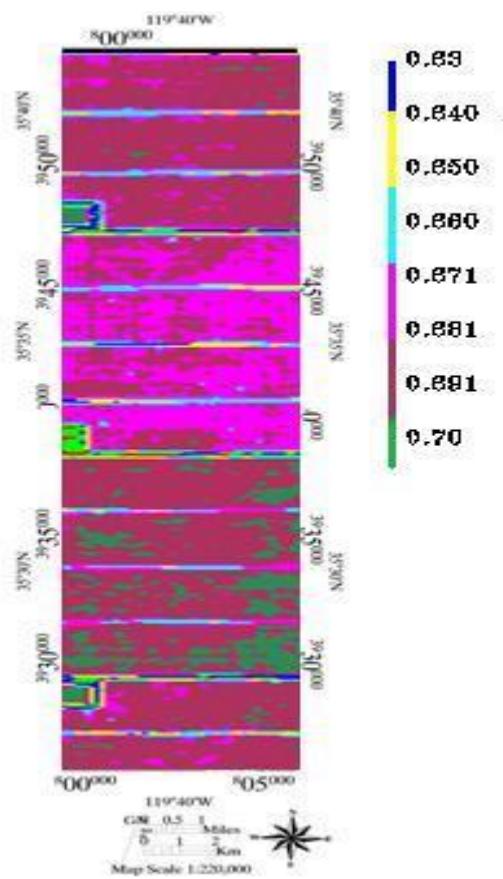


**Figure 2-4.** The actual evapotranspiration map of almond crop distribution

The ET<sub>a</sub> obtained from SEBAL was estimated by multiplying crop coefficient with reference evapotranspiration (ET<sub>o</sub>). Figure 2-9 shows the comparison between estimated ET with previous year ET and historical ET. CIMIS-PM estimated ET value that was higher in 2000, 2001 and 2003 when compared with historical ET data. However, historical ET value is high in the year 2007 when compared to estimated ET. This suggests that the water loss to the atmosphere is less because of stringent supply of CVP deliveries.

### **2.2.2 Spatial analysis of ET<sub>a</sub>, NDVI and T<sub>c</sub>**

Figures 2-5 and 2-6 show a positive relationship of evapotranspiration with vegetation indices ( $y = 0.25x + 0.52$ ;  $R^2 = 0.96$ ), and a negative relationship of ET<sub>a</sub> with canopy temperature ( $y = -0.0049x + 2.22$ ;  $R^2 = 0.86$ ) in the study area. This relationship related to the surface moisture conditions in the arid and semi-arid region. There is a negative relationship of canopy temperature with vegetation Indices ( $y = -47.1x + 343.17$ ;  $R^2 = 0.93$ ) in Figure 2-7. That explains why with increase in NDVI, the canopy temperature decreases.

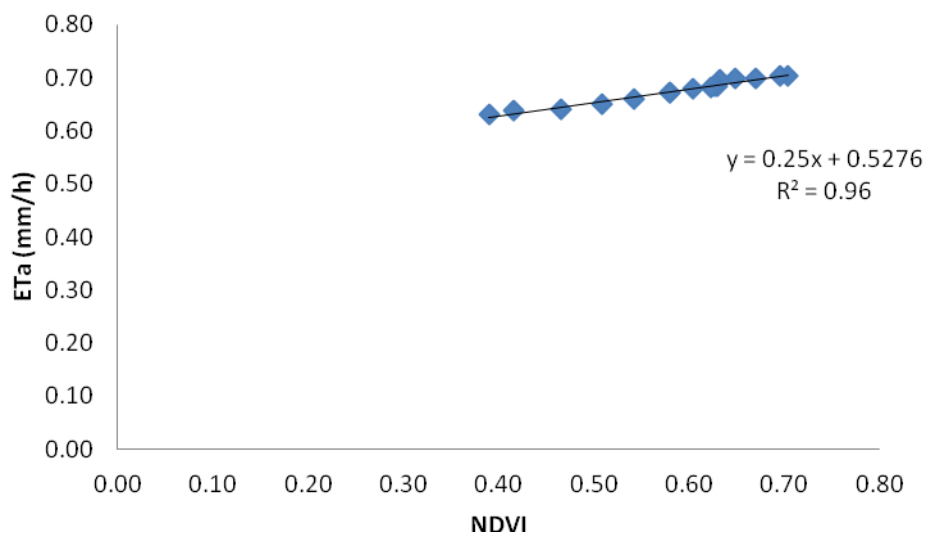


**Figure 2-5.** Curve of relationship of hourly evapotranspiration (ETa) with vegetation Index (NDVI) for almond orchards.

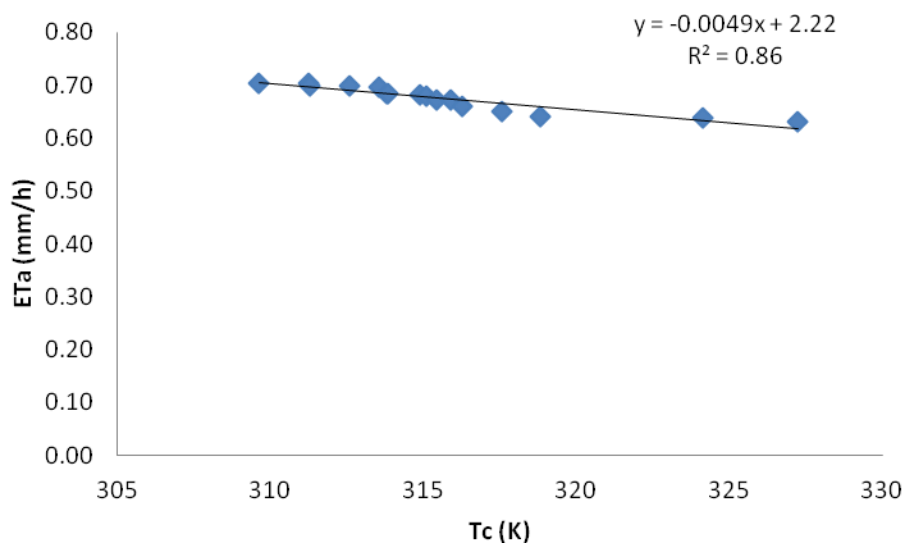


**Figure 2-6.** Curve of relationship of hourly actual evapotranspiration (ETa) with canopy temperature (Tc) for almond orchards.

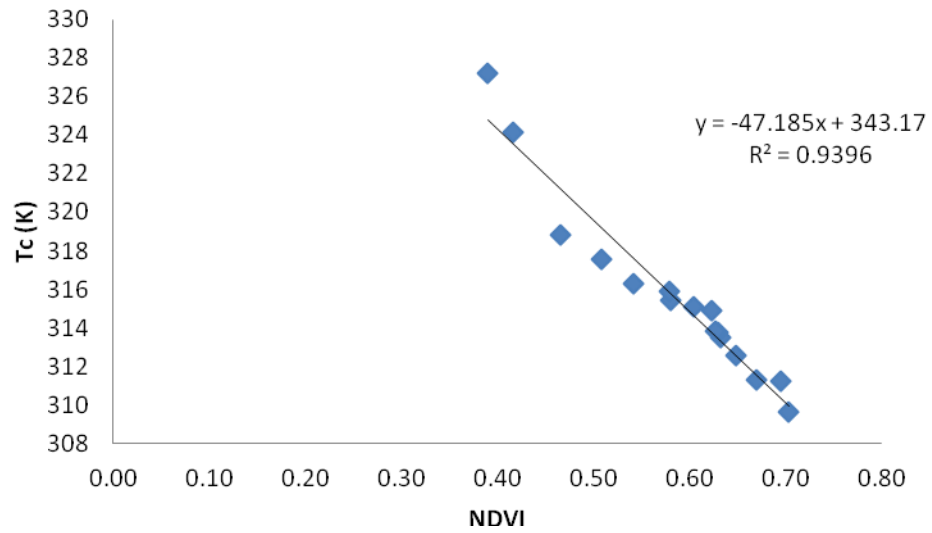


**Figure 2-7.** Curve of relationship between Vegetation Index (NDVI) canopy temperatures (Tc)

### 2.2.3 Validation of SEBAL model with Penman-Monteith

The validation of these remotely sensed actual ETa estimates of almond crop from SEBAL compared with the actual ETa obtained from the Penman-Monteith method. The measured and simulated ET was compared to establish correlation relationship (Figure 2-8). The relative error (mean percent difference) was calculated as:

$$\text{RelativeError}(\%) = \frac{| \text{simulation} - \text{observation} |}{\text{observation}} \quad (2-11)$$

The absolute error (mean difference) is calculated as (mm/h):

$$\text{AbsoluteError} = | \text{simulation} - \text{observation} | \quad (2-12)$$

The average of daily ETa of remote sensing image is compared with ETa from CIMIS website located at the study area. Figure 2-8 shows a positive correlation of ETa from Penman-Monteith with SEBAL estimated ETa. The correlation coefficient of ETa estimates from remote sensing with PM was 0.93. The mean difference between actual ETa from SEBAL in almond and Penman-Monteith for over all observations associated with ETa was 0.77 mm/h. Table 2-2 compares ET between the field data used by CIMIS and remote sensing method. The mean percent difference for ETa from SEBAL and CIMIS Penman-Monteith (PM) is calculated as  $(\text{PM} - \text{SEBAL}) / \text{SEBAL}$  was 0.109%.

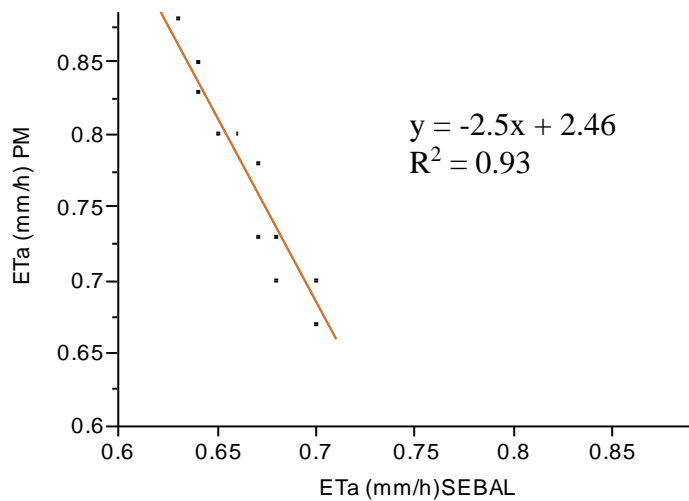


**Figure 2-8.** Comparison of remotely sensed ETa (SEBAL) with Penman-Monteith (PM) method ( $p < 0.0001$ )

**Table 2-2.** Comparison of ETa among SEBAL, PM and Field data

<b>ET Estimation Approach (mm/h)</b>	<b>Crop Coefficient</b>	<b>Average actual ET(mm/h)</b>
SEBAL (ETa)	2.29	0.6745
PM-CIMIS (ETa)	1.02	0.7519
Field (ETa)	1.15	1.26

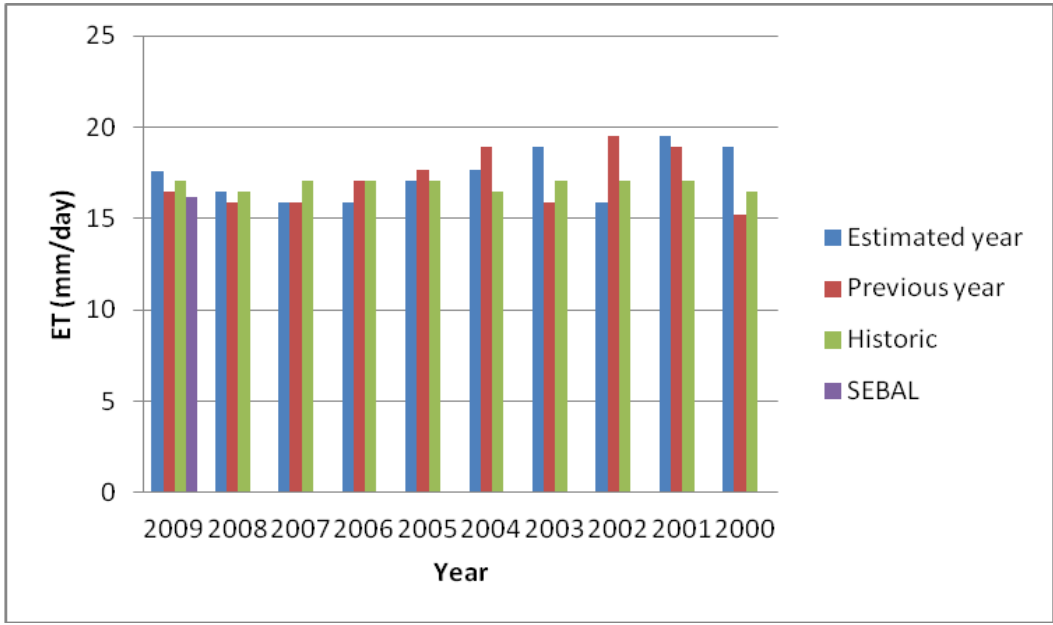


**Figure 2-9.** Histogram show ET (mm/day) estimates from 2000 to 2009

**Table 2-3.** ET (mm/day) estimates for current year, previous year and historic data for the month of July.

ET (mm/day)			
Year	Estimated Year	Previous year	Historic
2009	17.6	16.4592	17.0688
2008	16.4592	15.8496	16.4592
2007	15.8496	15.8496	17.0688
2006	15.8496	17.0688	17.0688
2005	17.0688	17.6784	17.0688
2004	17.6784	18.8976	16.4592
2003	18.8976	15.8496	17.0688
2002	15.8496	19.5072	17.0688
2001	19.5072	18.8976	17.0688
2000	18.8976	15.24	16.4592



### 2.3 Conclusion

Cloud free aerial MASTER image obtained during the almond pre-harvesting season on July 24, 2009 is processed for Paramount farm in California using a remote sensing based SEBAL model. The modified SEBAL is capable of computing the spatial almond hourly water use with resolution of 30 m x 30 m. The average actual evapotranspiration (ET<sub>a</sub>) estimated from SEBAL is 0.67 mm/h. The simulated ET is compared with that from ground measured PM method. The mean percent difference (relative error) was 0.10% and the mean difference (absolute error) was 0.77mm/h.

The result shows a positive relationship of ET<sub>a</sub> with vegetation indices ( $y = 0.25x + 0.52$ ;  $R^2 = 0.96$ ), and a negative relationship of ET<sub>a</sub> with canopy temperature ( $y = -0.0049x + 2.22$ ;  $R^2 = 0.86$ ) in the study area. This relationship is related to the surface moisture conditions in the arid and semi-arid region. There is a negative relationship of canopy temperature with vegetation Indices ( $y = -47.1x + 343.17$ ;  $R^2 = 0.93$ ) which explains with increase in NDVI, the canopy temperature decreases.

## 2.4 References

- Allen, R.G., L.S. Pereira, D. Raes, and M. Smith, 1998. Crop Evapotranspiration. Irrigation and Drainage. *Food and Agriculture Organization of the United Nations. Rome, Italy.* pp. 56.
- Bastiaanssen, W.G.M., M. Menenti, R.A. Feddes, and A.A.M Holtslag, 1998. A Remote Sensing Surface Energy Balance Algorithm for Land (SEBAL). Part 1: Formulation, *Journal of Hydrology*, Vol. 212/213, pp. 198-212.
- Bastiaanssen, W.G.M., D.J. Molden, and I.W. Makin, 2000. Remote sensing for irrigated agriculture: examples from research of possible applications, *Agricultural Water Management*, Vol. 46(2), pp. 137-155.
- Bastiaanssen, W. G. M., 2000. SEBAL based sensible and latent heat fluxes in the irrigated Gediz Basin, Turkey. *J. Hydrol.*, Vol. 229, pp. 87–100.
- Bastiaanssen, W.G.M., E.J.M. Noordman, H. Pelgrum, G. Davids, and R.G. Allen, 2005. SEBAL for spatially distributed ET under actual management and growing conditions, *Journal of Irrigation and Drainage Engineering*, Vol. 131(1), pp. 85-93.
- Bastiaanssen W. G. M., E. J. M. Noordman; H. Pelgrum; G. Davids; B. P. Thoreson, and R. G. Allen, 2005. SEBAL Model with Remotely Sensed Data to Improve Water-Resources Management under Actual Field Conditions. *Journal of Irrigation and Drainage Engineering*, Vol. 131, pp. 85-93.

Brutsaert, W., 1982. *Evaporation into the Atmosphere*. Reidel, Dordrecht, The Netherlands

California Dept. of Food and Agriculture. 2009.

[http://www.cdfa.ca.gov/egov/Press\\_Releases/Press\\_Release.asp?PRnum=09-009](http://www.cdfa.ca.gov/egov/Press_Releases/Press_Release.asp?PRnum=09-009)

California Department of Water Resources Revised June 18, 2009.

Courault, D., B. Seguin, and A. Olioso, 2003: Review to estimate evapotranspiration from remote sensing data: some examples from the simplified relationship to the use of mesoscale atmospheric models. ICID workshop on remote sensing of ET for large regions, 17th September, 2003.

"Drought: A Paleo Perspective – 20th Century Drought". National Climatic Data Center.

[http://www.ncdc.noaa.gov/paleo/drought/drght\\_history.html](http://www.ncdc.noaa.gov/paleo/drought/drght_history.html).

<http://www.cimis.water.ca.gov/>

Davis, G.H., J.H. Green, F.H. Olmsted, and D.W. Brown, 1959. Ground-water conditions and storage capacity in the San Joaquin Valley, California. *U.S. Geological Survey Water-Supply*, Vol. 1469, pp. 287.

Daughtry, C. S. T., W. P. Kustas, M. S Moran, P. J. Pinter, R. D. Jackson, P. W. Brown, W. D. Nichols, and L. W. Gay, 1990. Spectral estimates of net radiation and soil heat flux. *Remote Sens. Environment*, Vol. 32, pp. 111–124.

Engman , E.T., and R. J. Gurney, 1991. *Remote sensing in hydrology*, Chapman and Hall, London.

- Gamage, N et al., 2009. 18th World IMACS / MODSIM Congress, Cairns, Australia 13-17 July <http://mssanz.org.au/modsim09>, p3699.
- Hook Simon J., Jeffrey J. Myers, Kurtis J. Thome, Micheal Fitzgerald, and Anne B. Kahle, 2001. The MODIS/ASTER airborne simulator (MASTER) a new instrument for earth science studies. *Remote Sensing of Environment*. Vol. 76, pp. 93-102
- Kustas, W. P., and C. S. T. Daughtry, 1990. Estimation of the soil heat flux/net radiation ratio from spectral data. *Agricultural and Forest Meteorology*. Vol. 49, pp. 205-223.
- Kustas, W. P., E. M. Perry, P. C. Doraiswamy, and M.S. Moran, 1994a. Using satellite remote sensing to extrapolate évapotranspiration estimates in time and space over a semiarid rangeland basin. *Remote Sens. Environ.* Vol. 49, pp. 275-286.
- Kustas, W. P., M. S. Moran, K.S. Humes, D.I. Stannard, P.J. Pinter, L.E. Hipps, E. Swiatek, and D.C. Goodrich, 1994a. Surface energy balance estimates at local and regional scales using optical remote sensing from an aircraft platform and atmospheric data collected over semiarid rangelands. *Water Resour. Res.* Vol. 30(5), pp 1241–1259.
- Kustas, W.P and J.M. Norman, 1996, Use of remote sensing for Evapotraspiration monitoring over land surfaces. *IAHS Hydrological Science Journal*. Vol. 41, pp 496-526.

- Kustas, W. P., M.C. Anderson, J.N. Norman, and A.N. French, 2003. Estimating subpixel surface temperatures and energy fluxes from the vegetation index-radiometric temperature relationship. *Remote Sensing of Environment*. Vol. 85, pp. 429-440.
- Mutiga Jeniffer Kinoti, Zhongbo Su, Tsahaei Woldai. 2010. Using satellite remote sensing to assess evapotranspiration: Case study of the upper Ewaso Ng'iro North Basin, Kenya. *International Journal of Applied Earth Observation and Geoinformation* 12, S100-S108.
- Singh, Ramesh K, Ayse Irmak, Suat Irmak, Dareel L Martin, 2008. Application of SEBAL Model for Mapping Evapotranspiration and Estimating Surface Energy Fluxes in South-Central Nebraska. *Journal of Irrigation and Drainage Engineering*. Vol. 134(6), pp. 722-729.
- Singh A Thakur, S., Suraiya S., 2012. Comparison of Different Image Classification Techniques for Land Use Land Cover Classification: An Application in Jabalpur District of Central India, *International Journal of Remote Sensing and GIS*, Volume 1, Issue 1. pp. 26-31.
- Wang, Junming, TW Sammis CA Meier, LJ Simmons (2008) "A Modified SEBAL Model for Spatially Estimating Pecan Consumptive Water Use for Las Cruces, New Mexico" Article 7.13 J. IEEE

## CHAPTER 3

### ESTIMATION OF CROP WATER STRESS INDEX IN ALMOND ORCHARDS USING THERMAL AERIAL IMAGERY

[This chapter was accepted in Journal of Spatial Hydrology (2013)]

#### **Abstract**

An important method for estimating Crop Water Stress Index (CWSI) is by measuring surface temperature of the canopy. A remote sensing method was used to estimate CWSI of an almond orchard in Paramount farm, California. An aerial remote measurement using MASTER (MODIS/ASTER) thermal band data is used to measure canopy temperature ( $T_c$ ). The empirical relationship for canopy - air temperatures difference ( $T_c - T_a$ ) versus Vapor Pressure Deficit (VPD) represents the crop water stress quantitatively. The results implied that the average value of CWSI for well-irrigated (non-stressed) almonds is 0.24 while the almond yield is affected when the average CWSI values for stressed crop is greater than 0.5. The difference in crop canopy to air temperature ( $T_c - T_a$ ) was negatively related to the VPD [ $R^2=0.96$  and  $p<0.0001$ ]. However, the relationship between ( $T_c - T_a$ ) and VPD was used to develop a non-stressed baseline equation for almonds, which estimates CWSI. Determination of CWSI is useful for irrigation scheduling and water management.

Keywords: Crop Water Stress Index, MASTER, canopy, vapor pressure deficit, almond

### 3. Introduction

Traditional method for monitoring water stressed crop carried out by calculating plant biomass that gives plant water content. This method fails to give spatial and temporal estimation of crop water stress. The widely used method developed by Idso et al. (1981) and Jackson et al. (1981), suggested that the energy balance isolates net radiation from the sun into sensible heat (that heats the air) and latent heat (used for transpiration). These widely used methodologies are analyzed for detecting crop water requirement, which is an important part to study spatial and temporal extent of crop health, crop water stress. The canopy-air temperature difference was explained by the energy balance method on the plant surface (Jackson, 1982, Guyot, 1998, Alves et al., 1998 and Al-Faraj et al., 2001). This is important for estimating Crop Water Stress Index (CWSI) by measuring canopy temperature ( $T_c$ ) and air temperature ( $T_a$ ). Factors such as water stress, stomata conductivity, heat flux, transpiration and the cooling causes plants to close their stomata, as a result, evaporation decreases and the canopy temperature increases, when compared to non-stressed plants (Stokcle and Dugas, 1992).

The surface temperature and crop water stress are associated for the reason that as a crop transpires, the evaporated water cools the canopy below the air temperature. Moreover, as a crop becomes water stressed, the transpiration will decrease and the crop surface temperatures will then increase sometimes more than the air temperature (Jackson 1982). In water stressed conditions, the plants close their stomata as a result, evaporation decreases, and the canopy temperature increases when compared to non-stressed plants. Therefore, the concept of canopy temperature was implemented to determine plant water

status (Stokcle and Dugas, 1992). The empirical relationship for canopy- air temperatures difference ( $T_c - T_a$ ) versus vapor pressure deficit (VPD) represented to quantify the crop water stress. Reginato and Howe (1985) found that cotton yield was declined when the average CWSI during the season was greater than 0.2. A model was developed by Kjelgaard et al. (1996) for evaluating daily ET rates and CWSI measurement to plan irrigation scheduling such as how much to irrigate and when to irrigate. Both ET and CWSI techniques use much of the same data.

Jackson et al. (1981) and Idso et al. (1981) used soil moisture content, bio-physical properties of plants or meteorological data to detect water stress in plants. Such Ground measurements are difficult and time consuming for each point scale and cannot obtain accurate spatial estimation. Indirect measurement of canopy temperature radiance using thermal band of the MODIS/ASTER simulator (MASTER) sensor is related to crop water stress because under non-stressed condition the transpiration cools the leaves, therefore,  $T_c - T_a$  is negative. For partial canopy cover, Water Deficit Index (WDI) is applied (Moran et.al., 1994). WDI employs the combination of spectral vegetation indices and surface temperature based on the same theory as CWSI. Albeit, CWSI is applied for full canopy cover. In this study, it is assumed that the almond orchards have full canopy cover and soil heat flux is negligible (Figure 3-1b) To understand crop water use and irrigation requirement, the analysis of CWSI are based on three main environmental variables: plant canopy temperature ( $T_c$ ), air temperature ( $T_a$ ) and atmospheric vapor pressure deficiency (VPD).



The objective of this study is to integrate meteorological data and remote sensing to obtain spatial water stress using the baseline parameters of almond for calculating CWSI.

### **3.1. Materials and Method**

#### **Study area and Data**

This study focused on calculating the CWSI for an almond field in Paramount Farm (35°30'N, 119°39'W), California (Figure 3-1a). The valley occupies two-thirds of the southern Central Valley in California. San Joaquin River flows in the northern part of the San Joaquin Valley and drains to the San Francisco Bay. Southern San Joaquin Valley is the world's largest supplier of almonds with more the 4,000 acres of almond orchards which is over a 4-billion dollar industry. Geographically, the southern part of the San Joaquin Valley is the Tulare Basin, bordered by the Sierra Nevada on the east, the Tehachapi Mountains on the south, and the Coast Ranges on the west. The northern extent corresponds to the Kings River. The main land-use is agriculture.

The remote sensing data was obtained from the airborne MODIS/ASTER simulator (MASTER) at an altitude of 11,500 m on July 24, 2009 with a spatial resolution of 7.2 m. This sensor has 50 spectral bands over the spectral range 0.4 to 12  $\mu\text{m}$  (visible through thermal infrared) at a variety of spatial resolutions. The platform was NASA's DC-8 aircraft and the images were acquired at 12:00 PM PST. Canopy surface temperature was measured with Infrared Thermometer (IRT) and calibrated using thermal infrared band of MASTER image. The thermal data obtained from MASTER was used for computing canopy temperature of the almonds. Meteorological data such as air temperature, relative

humidity, vapor pressure, wind speed, and solar radiation were obtained from the California Irrigation Management Information System (CIMIS) station in Belridge (station number 143) at Kern County, California. Figure 3-2 shows the experimental design to estimate  $T_c$ ,  $T_a$ ,  $T_c - T_a$ , VPD and CWSI for the almond orchards in the study area.

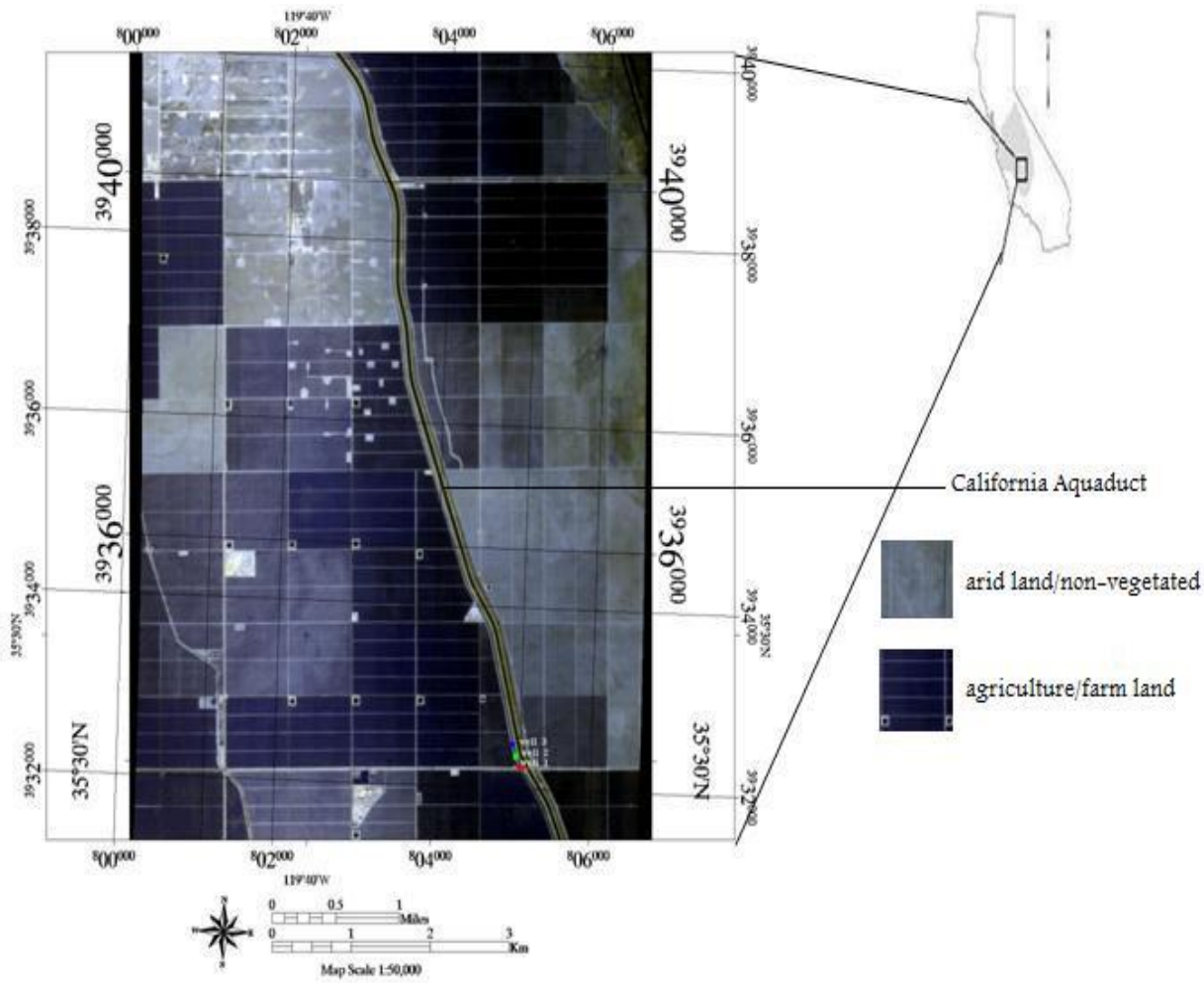


**Figure 3-1a.** Remotely sensed false color composite (Band 1, Band 2 and Band 6) of MASTER image showing Paramount farm in Southern San Joaquin Valley, California. Blocks show reflectance of various types of crops in dark tone. Bright tone shows reflectance of non-vegetated/arid areas.



**Figure 3-1b.** Aerial photograph of the almond orchards in Paramount farm taken from the flight NASA DC 8 (Above). Field photograph of the almond orchard in Paramount farm in California (Below)

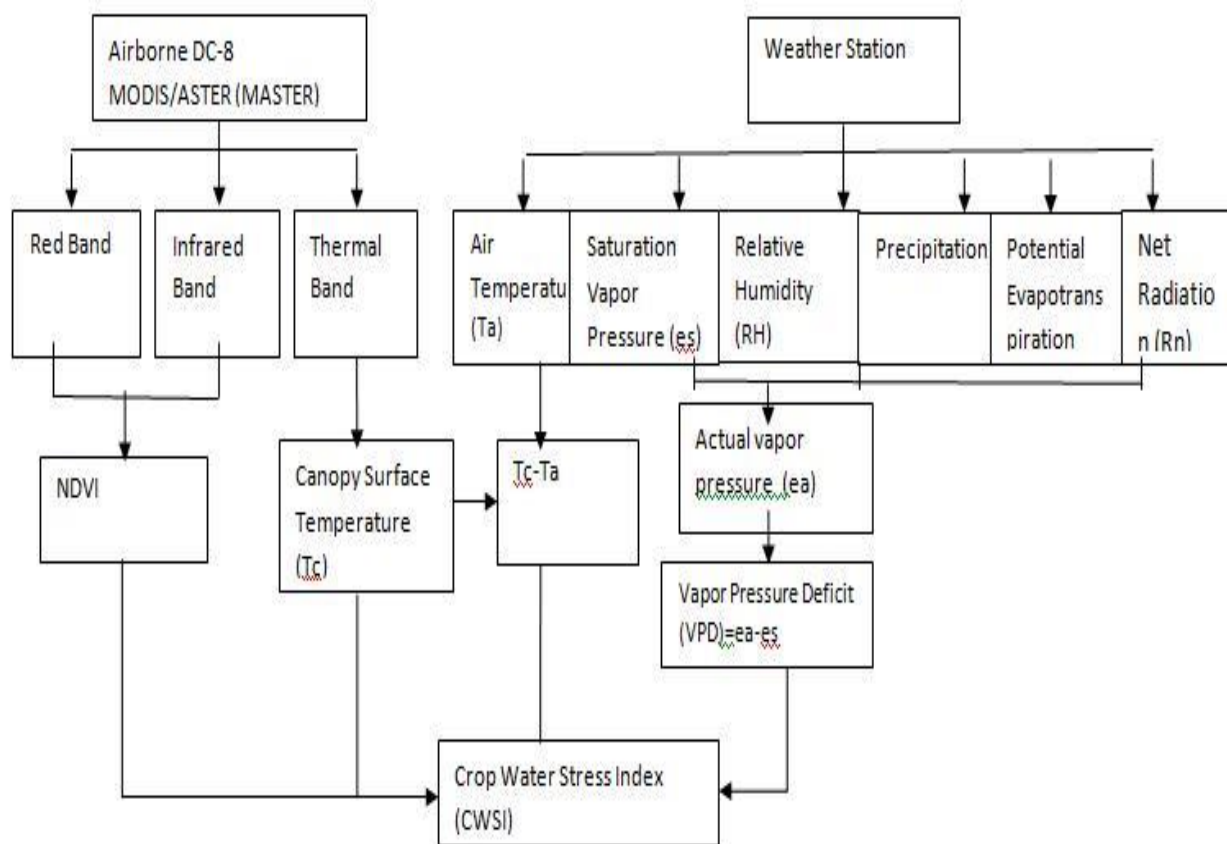


**Figure 3-2.** Experimental design to compute CWSI

Idso et al. (1981) developed empirical linear relationships between canopy and air temperature difference  $dT$  ( $T_c - T_a$ ) and Vapor Pressure Deficit (VPD). The lower limit of  $dT$  versus VPD represents that the crop is well-watered (minimum stress). Upper limit of  $dT$  versus VPD means the crop is not transpiring and dry (maximum stress) (Reginato, 1983; Stegman and Soderlund, 1992; Stockle and Dugas, 1992). Since CWSI is applied to full-canopy cover for remote sensing based measurements of surface temperature. Such measurement consider the land surface temperature equal to canopy temperature. Kustas et al., (2003). Decreased water uptake closes stomata of the leaves resulting in reduction of transpiration. The leaf or canopy temperature is used to quantify plant water stress.

The Crop Water Stress Index is calculated using the procedure of Idso et al. (1981)

$$CWSI = \frac{(dT - dT_l)}{dT_u - dT_l} \quad (3-1)$$

*Where*  $dT$  is the difference between air temperature ( $T_a$ ) and canopy temperature ( $T_c$ ) which is  $T_c - T_a$ .  $dT_u$  is the upper limit of the air temperature and canopy temperature difference (non-transpiring, dry), and maximum stress baseline.  $dT_l$  is the lower limit of the air temperature and canopy temperature difference (transpiring, well watered). The values for the CWSI are within zero and one. Value of zero indicates minimum stress while a value of one indicates maximum stress. The thermal data from IR radiometer was used to calibrate thermal IR band (band 42) of MASTER image. This was used to measure the surface canopy temperature of the almonds in the MASTER image using the algorithm obtained from Vicente et al., 1992.

$$T_c = \frac{hc}{\lambda k [\ln(\frac{2hc^2}{\lambda^5} + L_{BB}) - \ln(L_{BB})]} \quad (3-2)$$

Where  $T_c$  is surface temperature of canopy (K),  $\lambda$  is wavelength of band 42 (m),  $h$  is the plank constant ( $6.626068 \times 10^{-34}$  m<sup>2</sup>kg/s),  $c$  is the speed of light,  $k$  is the Boltzmann's constant ( $1.3806503 \times 10^{-23}$  m<sup>2</sup>kg/s<sup>2</sup>/K),  $L_{BB}$  is the radiance of blackbody at same temperature as surface (W/m<sup>2</sup>/sr/m).

The main computation of CWSI is the measurement of upper and lower limit equations. Idso et al., (1981) and Jackson et al., (1982) suggested that the changes in the upper limit and lower limit are due to variation in Vapor Pressure Deficit (VPD). Therefore, VPD is calculated as

$$VPD = VP_{sat} - VP \quad (3-3)$$

where  $VP_{sat}$  is the maximum vapor pressure at the given temperature and pressure and  $VP$  is the actual vapor pressure.

Thermal IR radiometer was used to measure surface temperature of bare land, water, and the canopy. This is required to calibrate MASTER data in the thermal infrared band. The air temperature and RH measurements are used to calculate the VPD of the air as (Allen et al. 1998):

$$e_s = 0.6108 \times \exp [17.27 T_a / (T_a + 237.3)] \quad (3-4)$$

$$e_a = e_s \times (RH/100) \quad (3-5)$$

$$VPD = e_s - e_a \quad (3-6)$$

Where  $e_s$  is the saturation vapor pressure at the given temperature (kPa),  $e_a$  is the actual vapor pressure (kPa),  $T_a$  is the air temperature (K), RH is the relative humidity (%) and

VPD is the vapor pressure deficient (kPa). The key input for CWSI measurement are humidity, air temperature, and canopy temperature. The canopy-air temperature difference for a well-watered crop (lower limit) and severely stressed crop (upper limit) is calculated using equation 3-1 as outline by Idso et al., (1981) Jackson et al., (1982):

$$dT_i = \text{Intercept} + \text{Slope (VPD)} \quad (3-7)$$

$$dT_u = \text{Intercept} + \text{Slope [es (Ta) - es (Ta + Intercept)]} \quad (3-8)$$

Where  $es(T_a)$  is the saturation vapor pressure at air temperature (kPa), and  $es(T_a + \text{Intercept})$  are the saturation vapor pressure at air temperature plus the Intercept value for the crop. Thus, with a measure of humidity, air temperature, and canopy temperature, it is now possible to determine CWSI. Figure 3-3 illustrates an example of a VPD baseline for alfalfa (Idso and Jackson, 1981). Jackson et al., (1982) studied that the upper line represents maximum water stress. All measurements should lie between these two lines. The position of baseline parameters assumed between these two lines for computing crop water stress. CWSI value is allocated between zero and one, where zero is on the baseline and one is on the upper line. The blue line is the baseline of lower limit of  $T_c - T_a$  (i.e., non water-stressed baseline or  $dT_i$ ). The red line is the canopy-air temperature difference for a non-transpiring crop or  $dT_u$ . Figure 3-3 illustrates slopes and intercept values for alfalfa that is -1.92 and 0.51 respectively. Slope and intercept values have been determined for a number of crops as shown in the Table 3-1. Although, the slope and intercept values for almond are not calculated. Consequently for a given vapor pressure deficit, the CWSI can be calculated if the slope and intercept values are known.



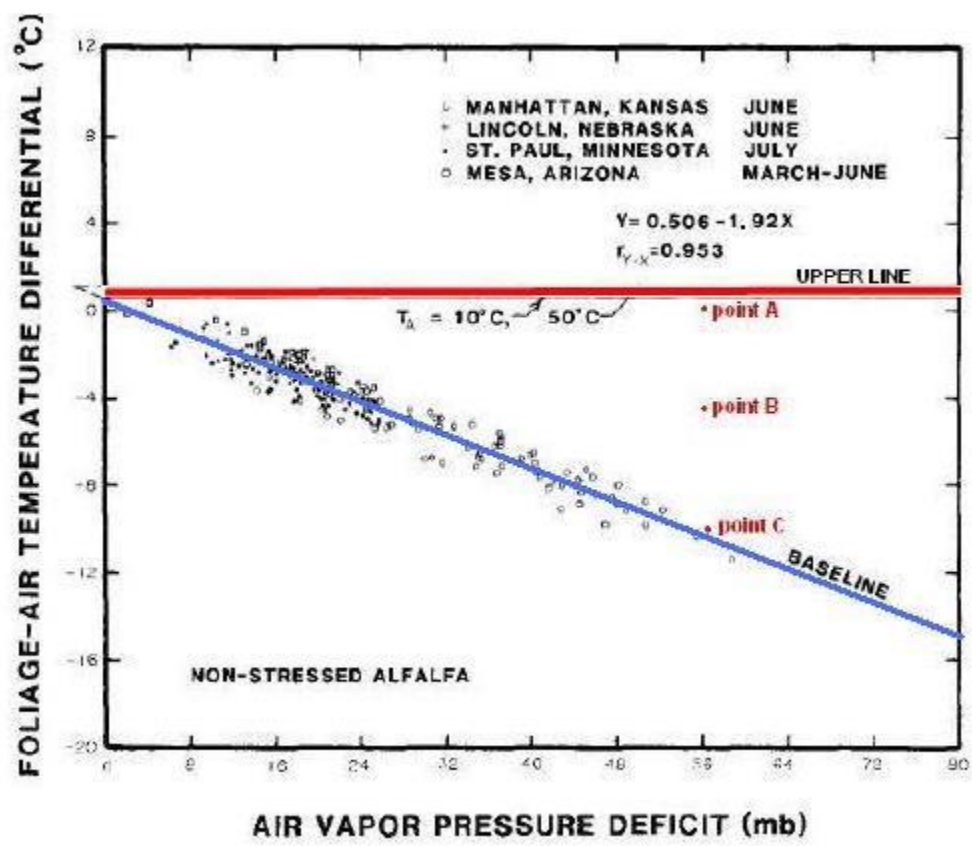


**Figure 3-3.** Figure 3-3. The red line shows the maximum water stress baseline where the CWSI of point A is approximately 1. The blue line is non water-stress shows the crop is well- watered with CWSI is 0 at point C. Whereas at Point B, the crop is moderately stressed with CWSI 0.5. Figure adapted from Idso and Jackson et al., 1981.

**Table 3-1.** Baseline parameters for various crops – sunlit conditions (Idso, 1982)

<b>Crop</b>	<b>Intercept</b>	<b>Slope</b>
Alfalfa	0.51	-1.92
Barley (pre-heading)	2.01	-2.25
Barley (post-heading)	1.72	-1.23
Bean	2.91	-2.35
Beet	5.16	-2.3
Corn (no tassels)	3.11	-1.97
Cowpea	1.32	-1.84
Cucumber	4.88	-2.52
Lettuce, leaf	4.18	-2.96
Potato	1.77	-1.83
Soybean	1.44	1.34
Tomato	2.86	-1.96
Wheat (pre-heading)	3.38	-3.25
Wheat (post-heading)	2.88	-2.11

### 3.2 Results and Discussions

The canopy-air temperature difference for lower limit (well irrigated) and upper limit (stressed crop) is calculated using intercept and slope values. These values are used to calculate the CWSI that is often referred to as the “empirical” CWSI. In the first calibration,  $T_c - T_a$  of MASTER imagery was positive, and the average temperature difference is  $\pm 5.02$  °C. This is a problem because the test field was well watered and the transpiration occurring should cause a canopy temperature lower than the air temperature. On the contrary, the ground based thermal IR radiometer measurements of  $T_c - T_a$  was negative. Therefore, another calibration was applied. In this calibration, the canopy temperatures measured by the thermal IR radiometer were averaged for three different trees to get representative temperature for those almond trees. The locations of these trees are identified in the MASTER image, so the temperatures from the nine surrounding pixels were averaged in the MASTER data (Figure 3-4). The difference between the MASTER temperatures and the thermal IR radiometer temperatures were calculated and then averaged. The average difference of 7.87 °C applied to the MASTER data. This sufficiently reduced the canopy temperatures to allow for the calculation of CWSI.

There are no studies on baseline parameters for almond crop. Therefore, in this study, slope and intercept parameters are computed using thermal remote sensing. A linear regression was executed to determine the relationship between  $T_c - T_a$  and VPD. The baseline equation was developed for almond orchards. The upper and lower baselines required to compute CWSI are depicted in Figure 3-5. The value for the upper line is created above the plot that appeared to be in the most water stressed areas. The

upper limit is  $dT_u = (T_c - T_a) u$ , was 274 °K (~1°C) when the air temperature at solar noon was 298 °K. . In a similar study, Throssell et al. (1987) determined that the upper limit for Kentucky bluegrass, cool season grass was 12.71 °C. The equation that defines the lower baseline is:  $dT_l = (T_c - T_a) = -1.16 \text{ VPD} + 31.6$  ( $R^2 = 0.96$ ,  $p < 0.0001$ ) as shown in Figure 3-5. The slope and intercept values of almond is -1.16 and 31.6 respectively.

The average value of CWSI for well-irrigated (non-stressed) almonds is 0.24 while the average CSWI values for water-stressed crops is greater than 0.5. Bare land shows white color in the image, illustrating the absence of vegetation and hence it is maximum dry with CWSI appearing between 0.8 to 1 as shown in Figure 3-6.

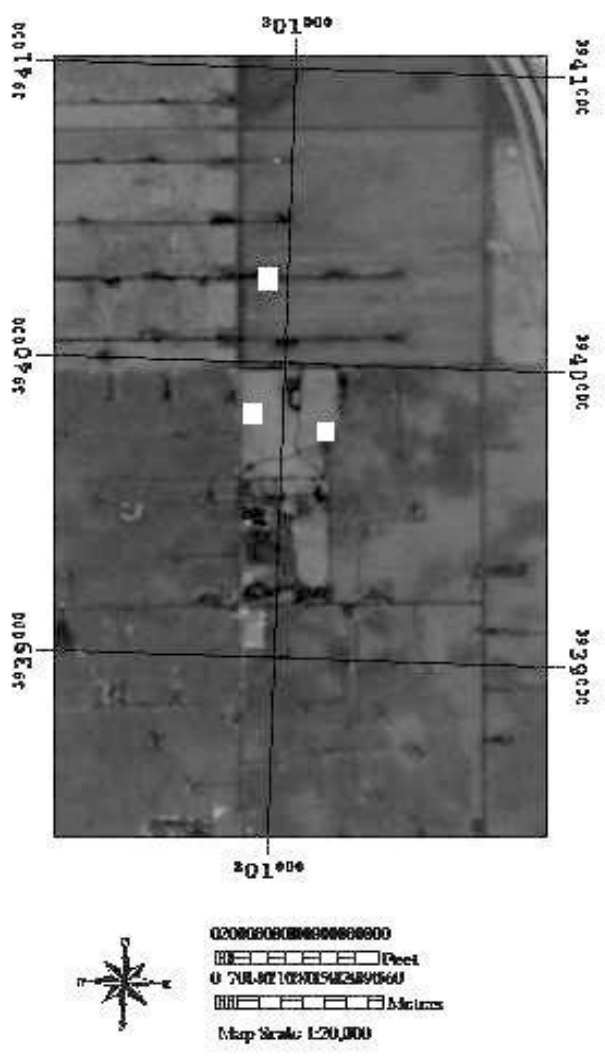


**Figure 3-4.** The image shows the location of the thermal IR radiometer measurements represented in white color, which is used for Tc-Ta calibration.

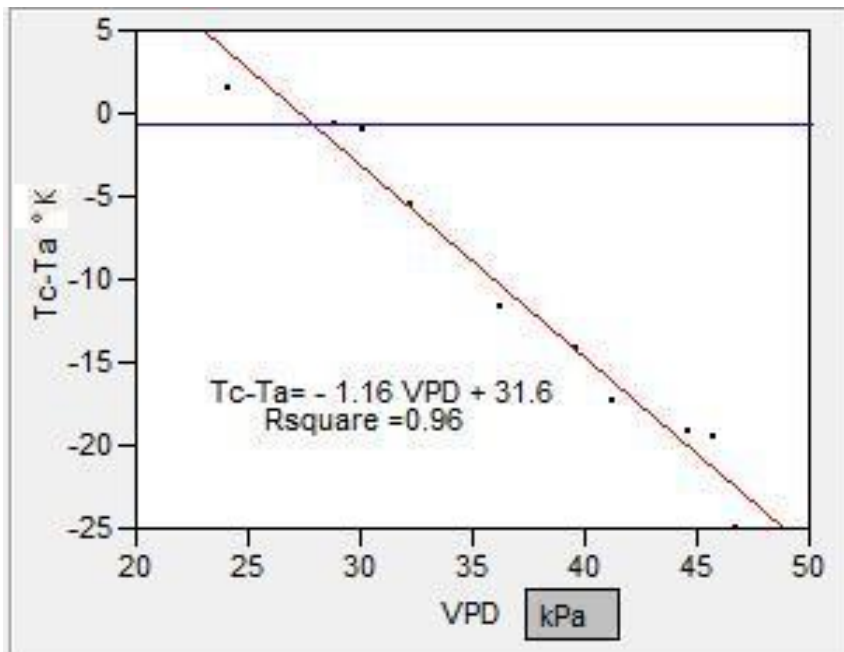


**Figure 3-5.** Non-stressed baselines for CWSI calculation of almond orchards ( $p < 0.0001$ ).

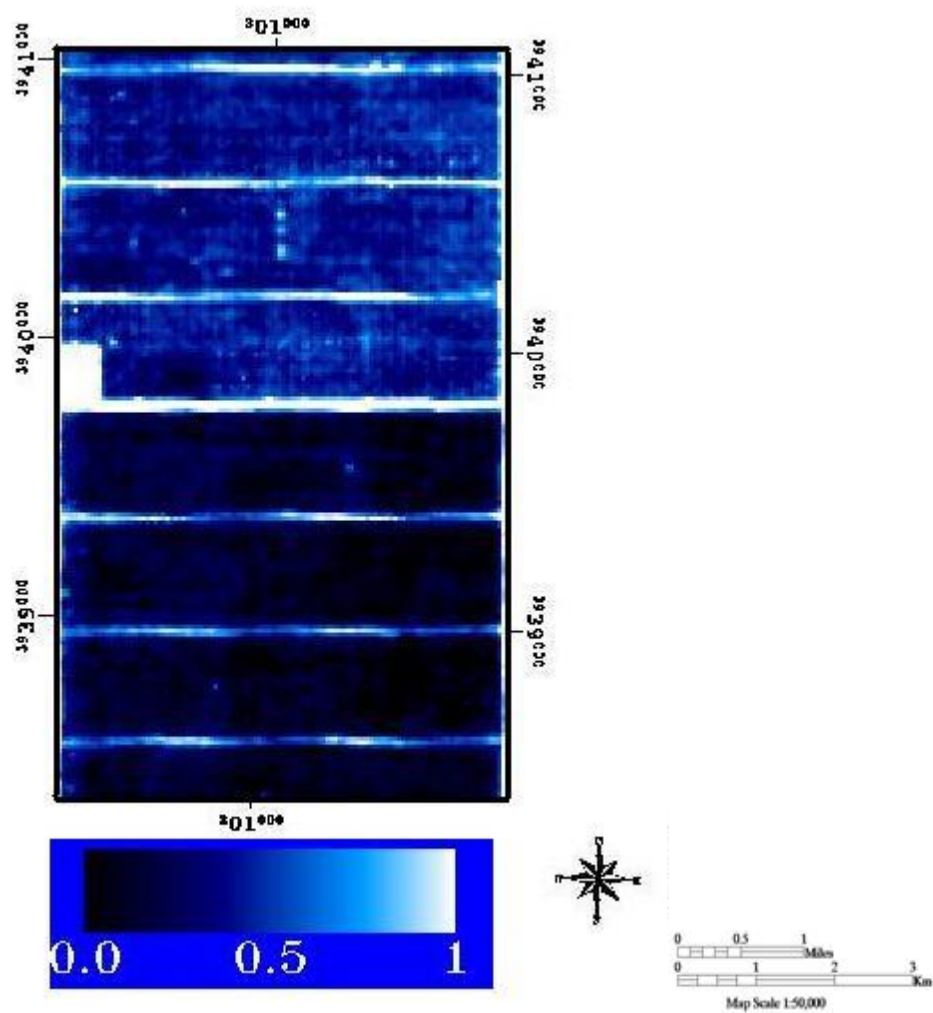


**Figure 3-6.** CWSI value of almond orchards. The darker color represents well-irrigated crops with  $CWSI < 0.5$  whereas lighter tone represents high water stress crops with  $CWSI > 0.5$ .

### 3.3 Conclusion

Remote sensing thermal infrared crop water stress provides a useful tool for understanding crop water requirements. Jackson et al. (1981) suggested that the incoming net radiation is dissipated into sensible heat flux (H) and latent heat flux (LE). These outgoing fluxes H and LE are responsible for heating the air and evapotranspiration respectively. They used classical methods to study situ measurement of soil water content, plant properties or meteorological variables to estimate water lost from the plant-soil system during a given period. In this study, calibration of in-situ thermal data was done by taking the difference between the temperature of MASTER image and the ground based thermal IR radiometer for each tree. The difference was to be 7.87 degrees. It was found that the upper limit of  $dT_u = (T_c - T_a) u$ , was 274 °K (~1°C) when the air temperature at solar noon was 298 °K. The analysis shows that the average value of CWSI for well-irrigated (non-stressed) almond crop was 0.24 while the almond yield is affected when the average CSWI values was greater than 0.5, indicating a major water stress.

CWSI helps in detecting crop water stress for arid agricultural land for guiding the farmers when to irrigate and where to irrigate



### 3.4 References

- Alves, A. Perrier, and L.S. Pereira. 1998. Aerodynamic and surface resistances of complete cover crops: how is the “Big Leaf”? *Trans. ASCE*. Vol.1, pp. 345–351
- Al-Faraj, A., G.E. Meyer, and G.L. Horst. 2001. A crop water stress index for tall fescue (*Festuca arundinacea* Schreb.) irrigation decision-making: a traditional method, *Comput. Electron. Agric.* Vol. 31, pp. 107–124.
- Guyot, G., 1998. *Physics of the Environment and Climate*. Wiley-Praxis Series in Atmospheric Physics and Climatology. *John Wiley and Sons-Praxis Publishing Association*, pp 632.
- Idso, S.B. ,1982. Non-water-stressed baseline: a key to measuring and interpreting plant water stress. *Agric. Meteorol.* Vol. 27, pp. 59–70.
- Jalali-Farahani H.R., D.C. Slack, D.M. Kopec and A.D. Matthias, 1993. Crop water-stress index models for Bermuda grass turf—a comparison. *Agron. J.*, Vol. 85 (6), pp. 1210–1217.
- Jackson, R.D., S.B. Idso, R.J. Reginato, and P.J. Pinter Jr.,1981. Canopy temperature as a crop water stress indicator. *Water Resources Research*, Vol. 17, pp. 1133.
- Jackson R.D., 1982. Canopy Temperature and Crop Water Stress Index. *Advances in Irrigation Journal*, Vol. 1, pp. 43–85.
- Kustas W et al., 2003. Remote Sensing Research in Hydrometeorology, *Photogrammetric Engineering & Remote Sensing*. Vol. 69, pp. 631–646.

- Moran M.S., T.R. Clarke, Y. Inoue and A. Vidal, 1994. Estimating crop water deficit using the relation between surface-air temperature and spectral vegetation index. *Remote Sens. Environ.* Vol. 49, pp. 246–263
- Reginato, R.J., 1983. “Field quantification of crop water stress”. *ASAE*. Vol. 26, pp. 772–775.
- Stokcle C.O., and W.A. Dugas, 1992. Evaluating canopy temperature-based indices for irrigation scheduling. *Irrig. Sci.* Vol. 13, pp. 31–37.
- Stegman, E.C., M. Soderlund. 1992. Irrigation scheduling of spring wheat using infrared thermometry. *ASAE*. Vol. 35, pp. 143–152.
- Throssell, R.N., Carrow, and G.A. Milliken, 1987. Canopy temperature based irrigation scheduling indices for Kentucky bluegrass turf. *Crop Sci.*, Vol. 27, pp. 126–131.
- Vicente Caselles, Jose A Sobrino, and Cesar Coll. 1992. A Physical model for interpreting the land surface temperature obtained by remote sensors over incomplete canopies. *Remote Sensing of Environment*. Vol 39, pp. 203-211.
- <http://www.uswcl.ars.ag.gov/epd/remsen/irrweb/thindex.htm>)

**CHAPTER 4**

**SIMULATION OF REGIONAL GROUNDWATER FLOW IN SOUTHERN SAN  
JOAQUIN VALLEY, CALIFORNIA.**

[This chapter was accepted in Journal of Environmental Geology (2013)]

**ABSTRACT**

A mathematical groundwater flow model is developed for Paramount Farm located in southern San Joaquin Valley in California. The groundwater flow model was constructed using available hydro-geological data. The objective was to simulate the flow direction and assess the potential recharge areas for water stressed areas. A finite difference grid of 20 rows and 35 columns was spaced with 700 active cells in X and Y directions and five layers in Z direction. The boundary conditions were selected from the USGS topographic map. MODFLOW- 2000 integrated in Groundwater Modeling Software (GMS) was used to simulate 3-D flow. There are five observational wells in the study area monitored by U.S.G.S California Water Science Center (CAWSC) and California Department of Water Resources (DWR). Available meteorological, geological and hydro-geological data were used to characterize the existing groundwater conditions and to simulate the equi-potential surface. The model was calibrated using groundwater elevation data against the historical water level data in 1955 under steady state conditions. A transient simulation was carried out from the year 2006 to 2011 for 5 stress periods. Results showed that the groundwater flows from west to east of the study area. The average water surface elevation (WSE) in 1955 for the growing season (May to July)

was 161.04 m. This value is low when compared to those of 2009, 2010, and 2011, which are 237.14 m, 236.28 m, and 235.74 m respectively.

Keywords: MODFLOW, GMS, finite difference, equi-potential, modeling, Paramount Farm.

#### **4. Introduction**

Understanding groundwater dynamics is of primary importance in water resources planning and management in extensively irrigated fields. Mining groundwater for agriculture and domestic purposes has led to the depletion of natural resources for years. In southern San Joaquin Valley, California, an intensive exploitation of groundwater for domestic and irrigation supply exists to provide abundant irrigation to one of the most productive agricultural districts. The surface water diverted from San Joaquin River provides enough water for irrigation in the southern San Joaquin Valley. The State and Central Valley Projects diverted it mainly from the Sacramento-San Joaquin Delta, San Joaquin, Kings, Kern and Feather Rivers (Devin Galloway and Francis S. Riley, USGS). About one-fifth of the state's groundwater discharge is from the Central Valley aquifer system, and as a result, the groundwater in southern San Joaquin Valley is below drought period water level. It has Mediterranean climate, with hot and dry summer and wet winter. It rains in winter months (December to February) with an annual rainfall of 98.5 mm and remains arid during the growing season of orchards. Therefore, the optimal use of limited groundwater resources in the region is of primary importance and hence proper water management is of extreme economic importance.

The study area is located in the Central Valley aquifer system in California. The groundwater abstraction in California is known to be the second largest withdrawal in United States (Maupin and Barber, 2005). Under pre-development condition (prior to development of surface water diversions), the total recharge and discharge was observed to be under steady state. Due to the population growth in late 1900, and massive

agricultural water demand, the estimated recharge and discharge observed was 13300000 and 14600000 acre-ft/yr respectively. Therefore, the change in the storage is -1300000 acre-ft/yr (Williamson et al., 1989). The natural pattern of groundwater flow and the rate of recharge-discharge were significantly altered by pumping, and by surface water diversion for irrigation especially during drought periods.

Recharge from irrigation water and discharge from wells averaged about 9200000 and 9300000 acre-ft/yr from 1962 to 2003 respectively (Flaunt, Belitz, and Hanson, 2009). Groundwater withdrawal from wells has lowered the water table and altered the flow direction, causing land subsidence (Williamson et al., 1989). On the contrary, increase in surface water delivery and excess irrigation loss as infiltration caused the water table to rise (Flaunt, Belitz and Hanson, 2009). Williamson (1989) computed the groundwater flow and storage from pre-developed conditions to 1977 using a numerical model.

The hypothesis is that the groundwater level increased since 1955, as there is more dependency on surface water diversion from the San Joaquin River. The objective is to simulate three dimensional groundwater flows to calculate the hydraulic head distribution in the entire study area. This research also focused on mapping the potential zones of recharge and discharge in the field.

## **4.1 Materials and Methods**

### **4.1.1. Study area**

The 402 km<sup>2</sup> Paramount Farm is located at the Lost Hill of Kern County in southern San Joaquin Valley of Central Valley, California (35°30'N, 119°39'W) (Figure 4-1). The valley occupies two-thirds of the southern Central Valley in California. San Joaquin River flows in the northern part of the San Joaquin Valley and drains to the San Francisco Bay. Majority of the basin's population focuses on agricultural activities. Southern San Joaquin is the world's largest supplier of almonds with more than 4,000 acres of almond orchards. Geographically, the southern part of the San Joaquin Valley is the Tulare Basin, bordered by the Sierra Nevada on the east, the Tehachapi Mountains on the south, and the Coast Ranges on the west. The northern extent corresponds to the Kings River. Significant geographic features include the Tulare Lake Basin and the Kettleman Hills.

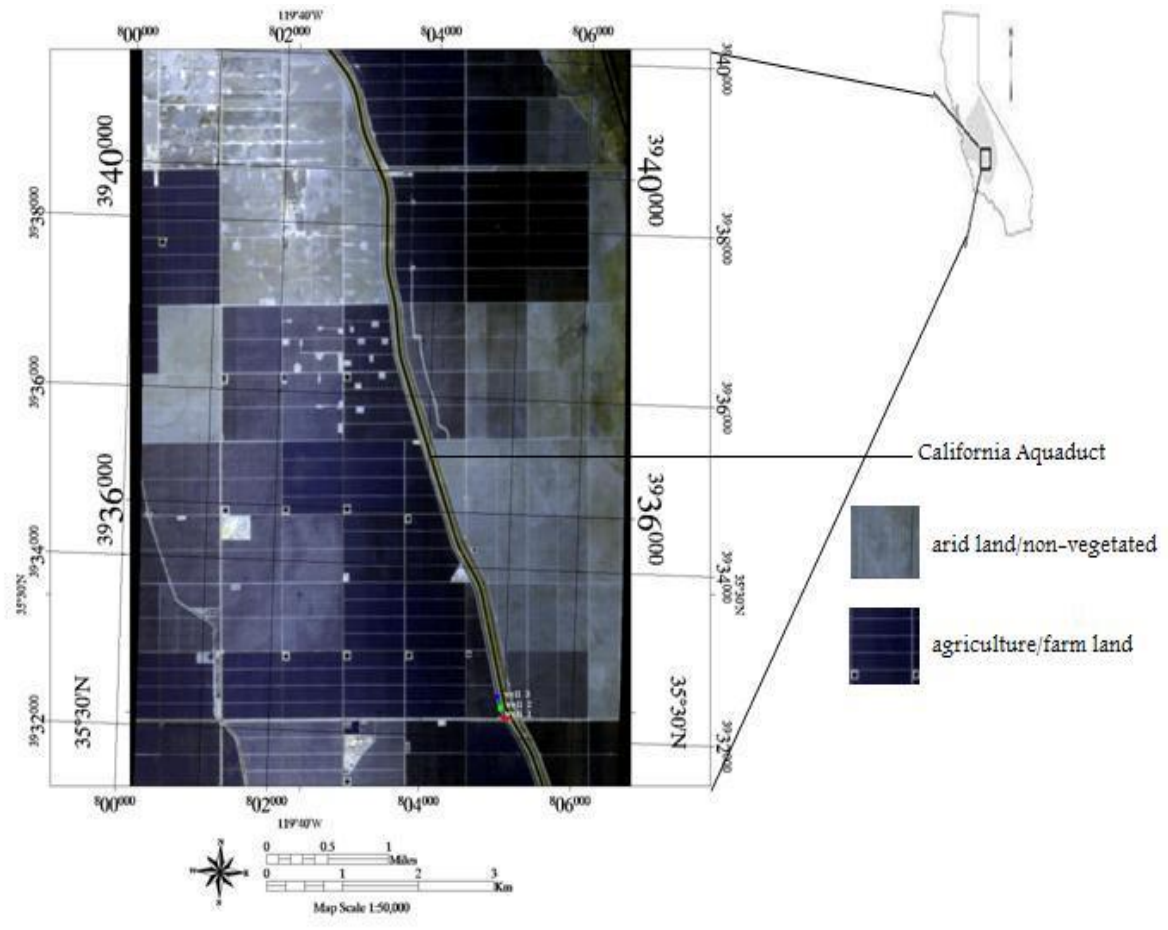


**Figure 4-1.** Remotely sensed false color composite (Band 1, Band 2 and Band 6) of MASTER image showing Paramount farm in Southern San Joaquin Valley, California. Blocks show reflectance of various types of crops in dark tone. Bright tone shows reflectance of non-vegetated/arid areas (Land cover classification of this image shown in Figure 2-3a).



#### **4.1.2. Hydrogeology**

The hydrogeology of the study area is derived from the large, northwest trending asymmetric structural trough which comprises marine and continental sediments up to 10 km thick (Gronberg et al., 1998). These sediments are significantly deposited largely by streams draining from the mountains from time to time. The alluvial fan in this area is derived from the glaciated portion of the Sierra Nevada (Faunt, Hanson, and Belitz, 2009). Fine-grained sediments (clay, sandy clay, sandy silt, and silt) are distributed throughout the San Joaquin Valley (Faunt, Hanson, and Belitz, 2009).

The Corcoran Clay forms a separation in the basin-fill deposits into an upper unconfined to semi-confined zone and a lower confined zone in southern San Joaquin Valley (Williamson and others, 1989, Burow et al., 2004). The Sierra Nevada rises to an elevation of more than 4200 m in the east of the valley; whereas, west of the valley area is bounded by the Coast Ranges which are a series of parallel ridges with moderate elevations (Mendenhall et al., 1916). Development of the groundwater basin initiated the irrigation water to percolate, which became the primary form of groundwater recharge, and irrigation drawdown became the primary form of groundwater discharge in the southern San Joaquin Valley (Davis et al., 1959).

### **Available Data**

The distribution of upper Miocene sand (Webb, 1977), known as Stevens Sand (Bazeley, 1972) in late Miocene occurring in *Bolivina vaughni* zone of southern San Joaquin Valley comprises of discontinuous sand bodies separated by thin shale interbeds. The base map of the study area was developed from a topographic map of scale 1:250000 acquired from the United States Geological Survey (USGS) website. Soil texture and soil moisture capacity of the Paramount Farm is shown in the Table 4-1. Figure 4-2 shows the elevation model constructed from the USGS topographic map. The land-use/land cover map is produced from the remote sensing image acquired from MASTER (MODIS/ASTER) sensor onboard the aircraft NASA-DC-8. It shows that about 80% of the land is under agriculture and less than 10 % is urban (Figure 4-3).

The litho-stratigraphic data was acquired from geophysical electric log in 1978. Five monitoring wells record the dynamics of the water table. California Department of Water Resources monitors these wells. Meteorological data is available from California Irrigation Management Information System located in Belridge. Meteorological and hydrological data are used as input data to characterize the groundwater conditions in this aquifer and to simulate potential recharge and discharge scenario.

**Table 4-1.** Soil moisture capacity of the Paramount Farm (Ratliff et al. 1983)

<b>Soil texture</b>	<b>Available water capacity (mm per meter of thickness)</b>	<b>Maximum soil water capacity (mm)</b>
Sand	14400	182.88
Loamy Sand	22800	289.56
Sandy Loam	30000	381
Loam	38400	487.68
Silt loam	43200	548.64
Sandy clay Loam	42000	533.4
Sandy clay	40800	518.16
Clay loam	45600	579.12
Silty clay loam	51600	655.32
Silty clay	57600	731.52
Clay	4.8	28.8

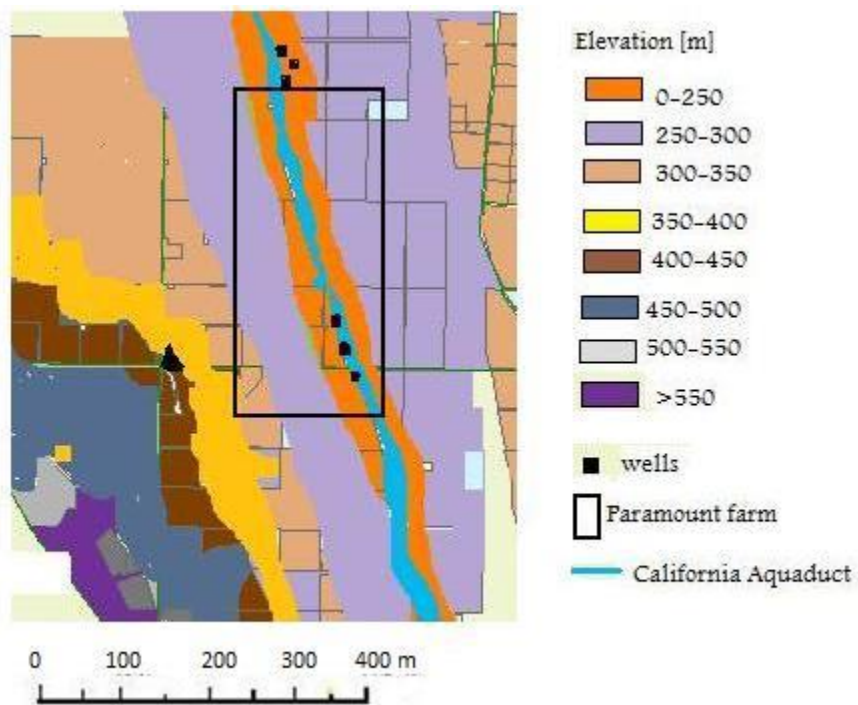


**Figure 4-2.** Map showing elevation derived from U.S.G.S topographic base map

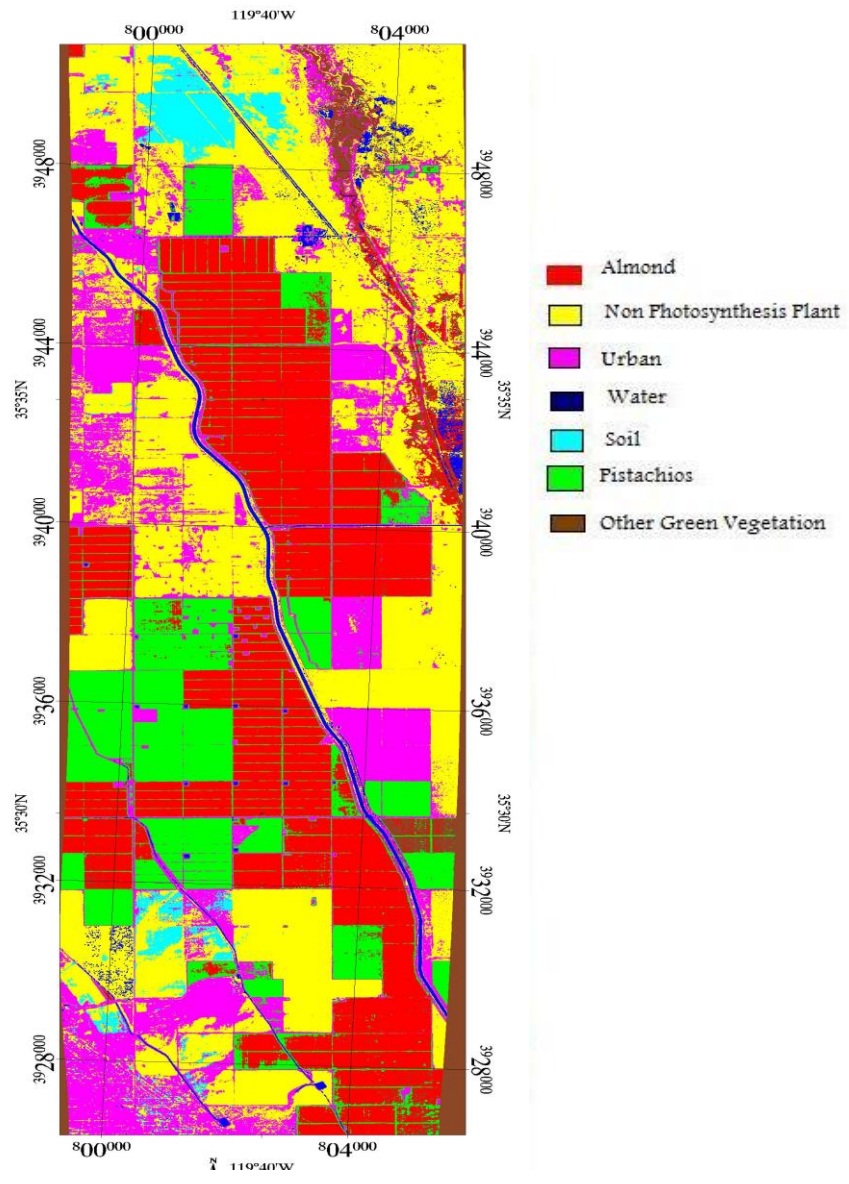


**Figure 4-3.** Supervised classification using maximum likelihood for almond orchards, non-photosynthetic plant (NPV), urban, water, soil, pistachio orchards, and other green vegetations.

#### 4.1.3 Hydrologic framework and conceptualization

The conceptual model of the study area was done by selecting a domain of 17000 m by 24000 m in X and Y directions respectively (Figure 4-4). The Z dimension comprises of five litho-stratigraphic layers derived from borehole log data. Based on well logs data the aquifer parameters were specified accordingly (Table 4-2). The borehole log data obtained by Shell oil Co. at the location in Elk Hills were used to know the aquifer properties. The available data show that the hydraulic conductivity ranges between 0.0008 to 100 m/day. The aquifer is divided into 5 layers based on sub-surface lithology. The first layer is unconfined, 200 m thick and comprises of sand followed by sandy loam, silt loam, sandy clay and clay in layers 2, 3, 4, and 5 respectively. The second, third and fourth layers were assumed to be 100 m, 50 m, 25 m thick respectively. The top boundary was assigned by specifying a hydraulic head value, which is equal to the surface elevation at each node denoted as constant head. The bottom boundary is a confining boundary represented by the Corcoran clay. The California Aqueduct bounds the eastern side of the study area that was considered a no-flow boundary. On the west of the study area is another highway running between Antelope Valley and Elk hills, which is assumed to be no-flow boundary. The north and south of the area bounded by Emigrant Hill and West Elk Hill respectively are considered to be a no-flow boundary. There are five observation wells in the study area monitored by USGS California Water Science Center (CAWSC) and California Department of Water Resources (DWR). The water surface elevation in the observation wells are shown in Table 4-3.

**Table 4-2.** Aquifer parameters

Model	Top	Bottom	Litho-	Hydraulic	Vertical
Layer	Elevation	Elevation	stratigraphic of	Conductivity	Anisotropy
	(m)	(m)	layers	(m/day)	(m/day)
1	600	200	Top soil: Stevens Sand	100	6
2	200	100	Sandy Loam	0.15	3
3	100	50	Silt Loam	0.018	3
4	50	25	Sandy clay	0.001	3
5	25	0	Clay	0.0008	3

**Table 4-3.** Description of observational wells in the locations monitored by DWR

Wells	Well site number	Location of the wells (coordinates)	XY grid cell	Ground Surface Elevation (m)	Water surface Elevation (m) msl	Depth to the water (m)
1	28S22E18C002M	35.49N, 119.64W	14,29	302	268.1	28.7
2	28S22E08D002M	35.51N, 119.63W	15,30	258.29	249.16	15.9
3	26S21E27P061	35.63N, 119.66W	7,28	233.8	221.6	13.1
4	26S21E27R061	35.63N, 119.69W	5,27	242.5	231.2	11.6
5	28S22E05F002M	35.52N, 119.63W	6,28	235.7	222.4	15.3



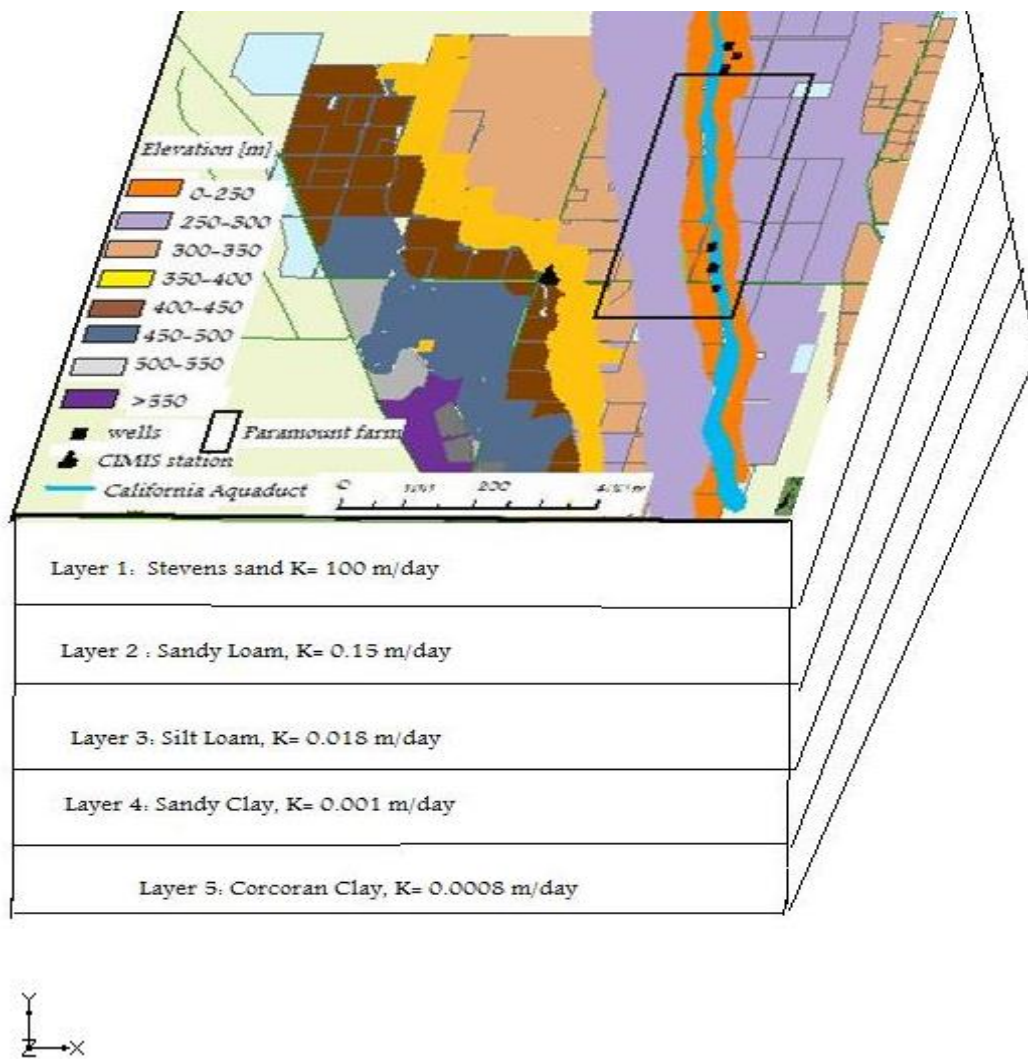


**Figure 4-4.** Conceptual framework of hydrostratigraphic units in the study area

#### 4.1.4 Numerical Model:

The next step in modeling is converting the conceptual design into a numerical model. The finite difference method uses a numerical solution for the following groundwater flow equation for three-dimensional saturated flow in saturated porous media:

$$\frac{\partial}{\partial x} \left( K_{xx} \frac{\partial h}{\partial x} \right) + \frac{\partial}{\partial y} \left( K_{yy} \frac{\partial h}{\partial y} \right) + \frac{\partial}{\partial z} \left( K_{zz} \frac{\partial h}{\partial z} \right) - Q = Ss \frac{\partial h}{\partial t} \quad (4-1)$$

Where  $K_{xx}$ ,  $K_{yy}$ ,  $K_{zz}$  are hydraulic conductivity along the x, y, z axes which are assumed to be parallel to the major axes of hydraulic conductivity;

$h$  = hydraulic head;

$Q$  = discharge flux per unit volume

$Ss$  = specific storage coefficient in which the volume of water released from storage per unit change in head per unit volume of porous material.

The equation that describes three dimensional steady-state groundwater movements through porous earth material under equilibrium condition is given by the partial differential equation (Don et al., 2006):

$$\frac{\partial}{\partial x} \left( K_{xx} \frac{\partial h}{\partial x} \right) + \frac{\partial}{\partial y} \left( K_{yy} \frac{\partial h}{\partial y} \right) + \frac{\partial}{\partial z} \left( K_{zz} \frac{\partial h}{\partial z} \right) = 0 \quad (4-2)$$

Where  $K_{xx}$ ,  $K_{yy}$ , and  $K_{zz}$  are the hydraulic conductivities ( $LT^{-1}$ ) in the x, y and z directions respectively,  $h$  is the piezometric head (L). In this study, three dimensional finite difference numerical model called MODFLOW 2000 (McDonald and Harbaugh, 1988) was used to solves Eq. (4-1) and (4-2) for computing hydraulic heads in the study

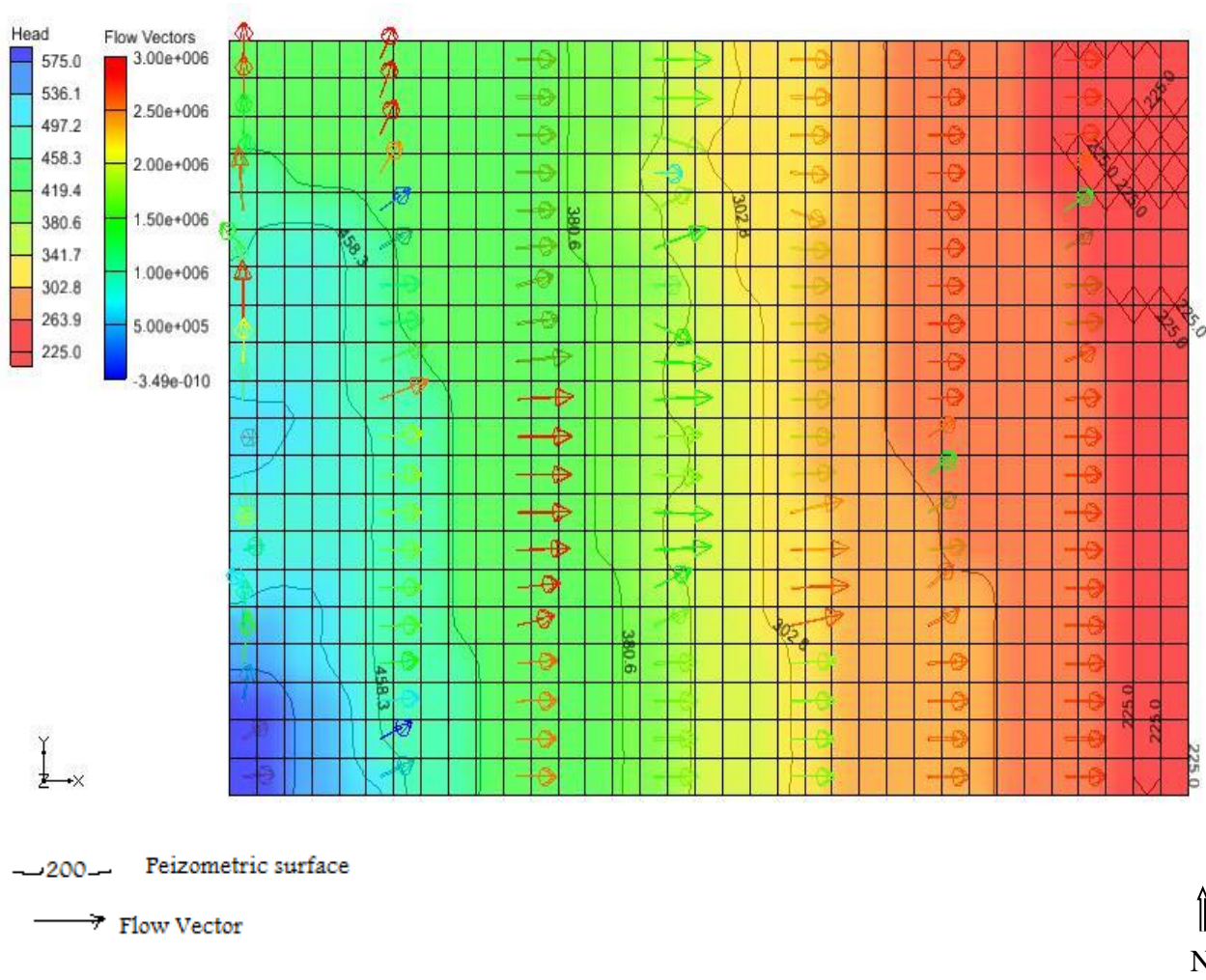
area. The conceptual model was numerically converted into grids. The MODFLOW code is a three dimensional, cell-centered, finite difference, saturated flow model developed by the United States Geological Survey (McDonald and Harbaugh, 1996). The finite difference grid consists of 20 rows and 35 columns uniformly spaced with 700 active cells in X and Y directions respectively. The cell size is 1 by 1 m representing an area of 1 m<sup>2</sup>. The model was divided vertically into 5 layers of variable thickness that extend from the top soil to the basement.

#### **4.2. Result and Discussion**

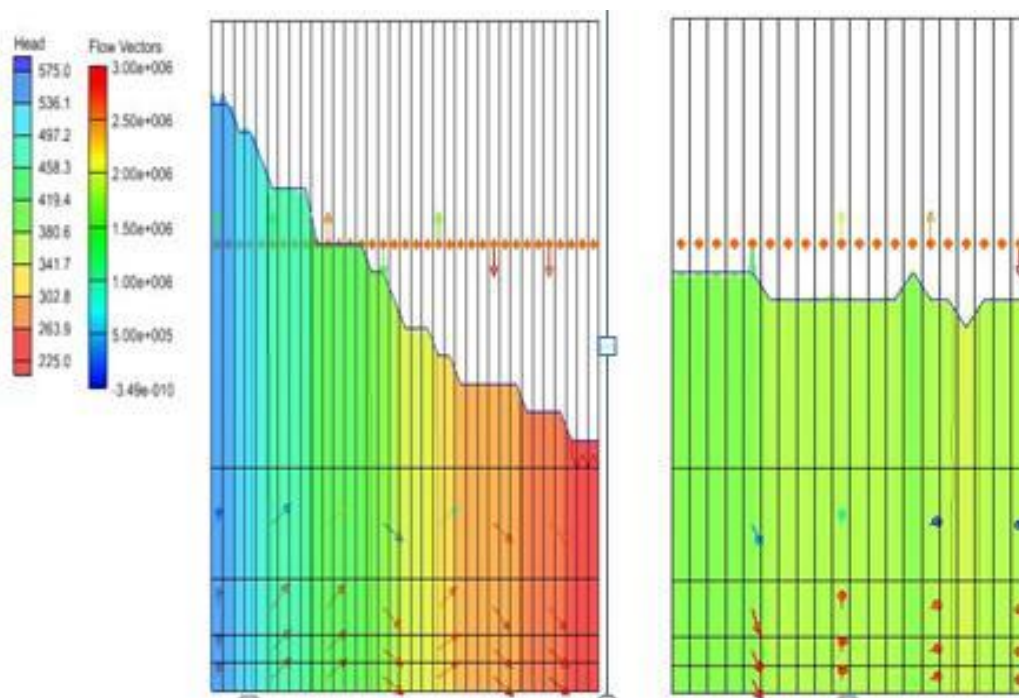
Initially, homogeneous and isotropic conditions were assumed throughout the basin. The numerical model was developed from the piezometric data. With the hydraulic head distributed in the first layer, the mathematical finite difference model was generated in each node to determine the equipotential lines in the surface and study the flow distribution of groundwater in the area. The flow vectors are tangential to the equipotential lines, and thus indicate the direction of groundwater flow at every point in the flow domain. The flow arrows indicate that the groundwater flow direction is from west to east where the Paramount Farm is located. It is moving towards the California Aqueduct. Figure 4-5a shows groundwater contours from the steady-state simulation model. It was observed that the highest hydraulic head in the entire model area is located in the southwest side of the area. Aquifer recharge mainly occurs from canal seepage, irrigation, precipitation, and percolation from surface water bodies whereas discharge

occurs from pumping of wells, evapotranspiration, outflows to the canals and subsurface flows from one zone to another.

The computed recharge-discharge shown in Figure 4-5b indicate a series of alternating recharge and discharge areas. The discharge in Figure 4-8b shown with upward arrows are those nodes where there is massive drawdown of groundwater. The downward arrows show the recharge of water from the agricultural areas. Therefore, the irrigated water, which is mostly percolated from the well-irrigated region of the farm, is flowing towards the California Aqueduct. Hence, in future studies, the subsurface artificial recharge structure such as percolation tank, infiltration gallery, and subsurface barriers will be proposed in recharge areas particularly where the CWSI of almond orchard is less than 0.5.



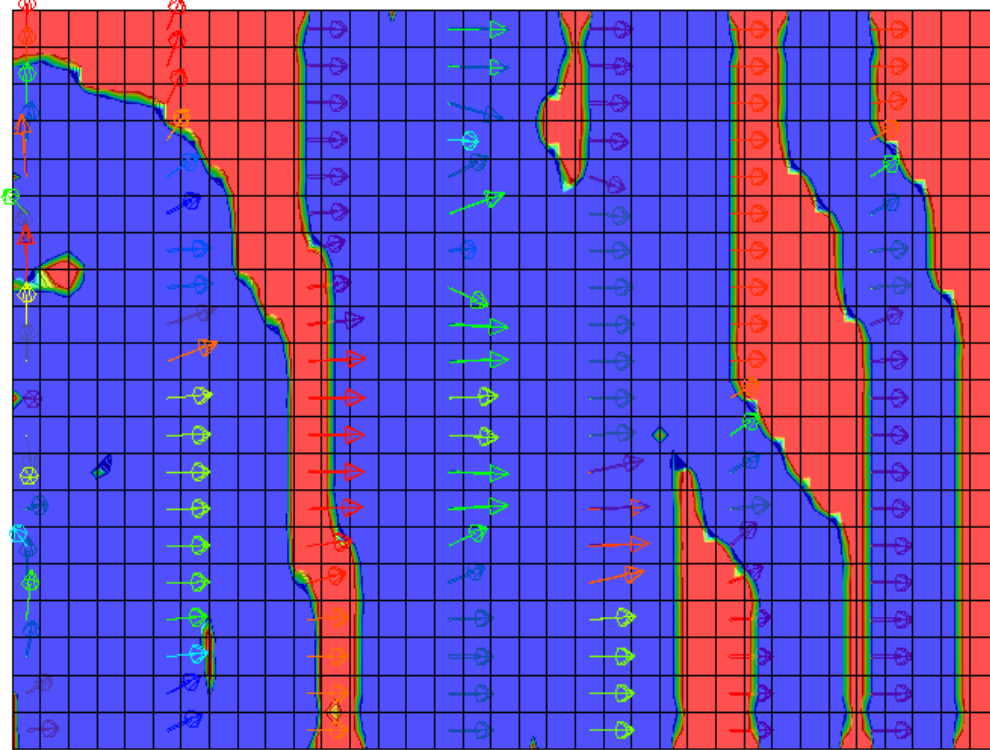
**Figure 4-5a.** Showing horizontal cross section of piezometric surface map (K axis) based on the steady state simulation model.



**Figure 4-5b.** Groundwater flowing in vertical cross-section in I and J axis to analyze the recharge and discharge nodes.

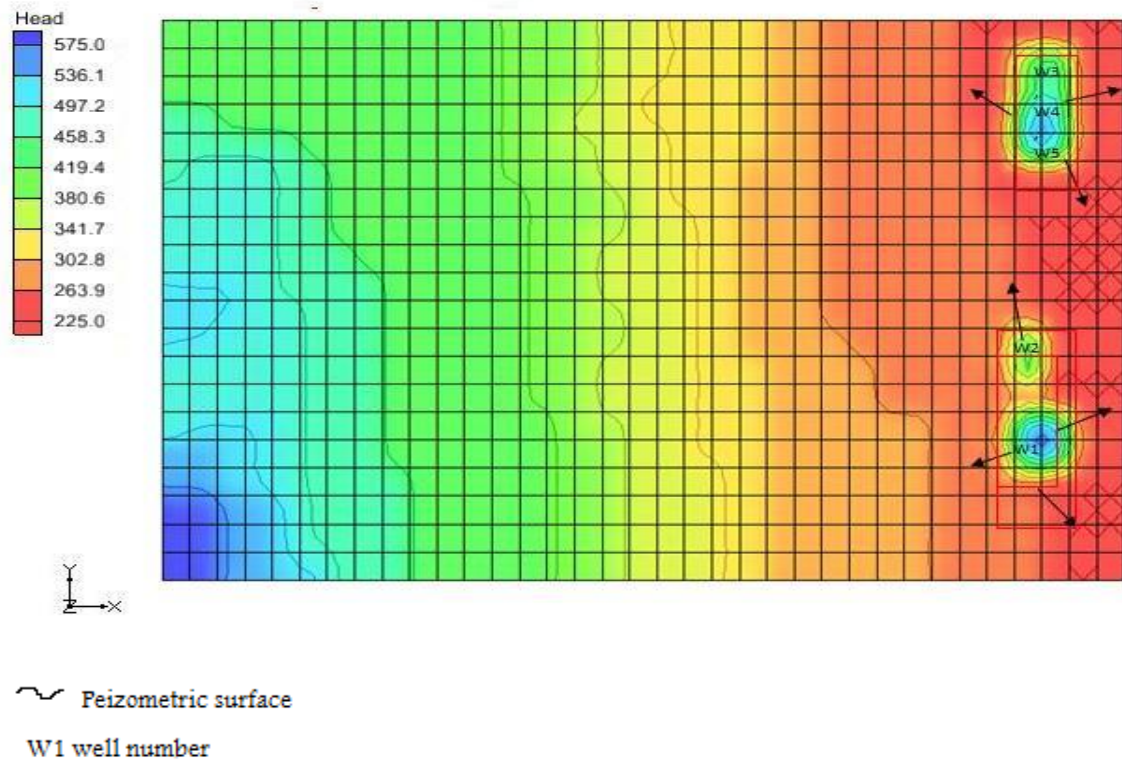
In order to assess the potential zone of recharge (Figure 4-6), the domain is characterized by various infiltration rates of different soil type with variation in groundwater pumpage in the study area. Recharge and discharge can be analyzed quantitatively in order to determine the total groundwater discharge through the system. The models estimated a total discharge that is equal to recharge assuming steady state of  $1.58 \times 10^{-6} \text{ m}^3/\text{s}$ . Steady state conditions were calibrated using water levels in 5 wells in the area in the year 1955. Calibration was achieved by changing the hydraulic conductivities of each layer shown in Figure 4- 4. The transient simulation was carried out from the year 2006 to 2011 for 5 stress periods. Extraction levels were calculated in such a way that the extraction levels do not exceed original steady state hydraulic head.

Figure 4-7 shows the distribution of hydraulic heads and its drawdown at the end of first stress period. It is observed that due to overdraft of groundwater, the water table is declining and it is flowing away from the wells. Under such conditions, where the groundwater was heavily pumped, the groundwater flows beneath the surface water (rivers/streams) instead of discharging into the surface bodies (Bartoldi et al., 1991) resulting in less contamination of groundwater from surface water. The relation between observed and simulated water levels in wells (Figure 4-8) suggested that the hydraulic conductivity was changed constantly to obtain the good regression analysis.



**Figure 4-6.** A horizontal view of bottom layer showing the potential areas of recharge in red.





**Figure 4-7.** Horizontal cross-section view of the map showing groundwater drawdown from the wells w1, w2, w3, w4 and w5 after the first stress period

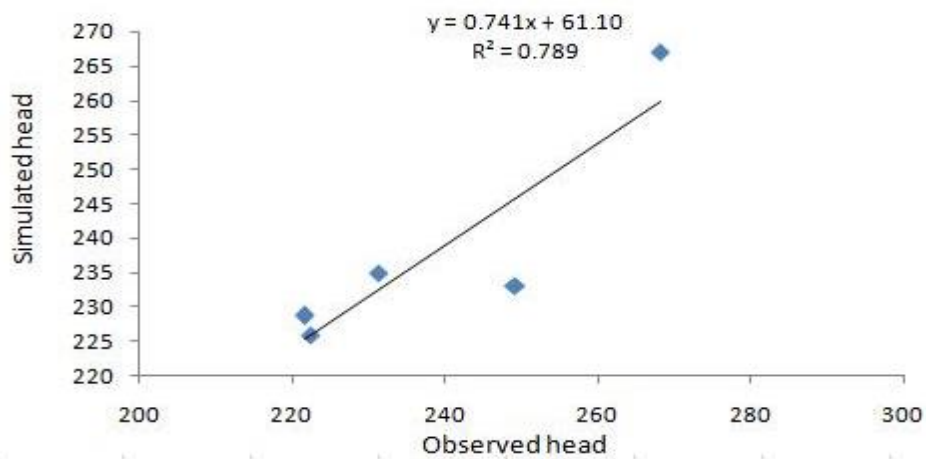


**Figure 4-8.** A plot showing the simulated head and Observed head in 5 wells in the study area

The yearly groundwater demand shown in Figure 4-9 suggests that the demand for groundwater increases in drought period. Therefore, groundwater resources are depleted in order to supply the deficit water for irrigation purposes. Two irrigation periods were observed. The first month begins in March and ends in May, and the other begins in July and ends in September. These are the months where the groundwater is extracted more for irrigation purpose because the crops reach their development stage as shown in Figure 4-9. Orchards are harvested in the month of October. It rains in winter months and the groundwater is replenished. Since irrigation depends on the surface water diversion through California's Central Valley project (CVP) (California Department of Water Resources, 2010). From 1955, the groundwater level had been increasing because of CVP and surface water diversions. As illustrated in Figure 4-10, the average water surface elevation (WSE) in 1955 for the growing season (May to July) is 161.04 m when compared with 2009, 2010, and 2011 are 237.14 m, 236.28 m, and 235.74 m respectively.

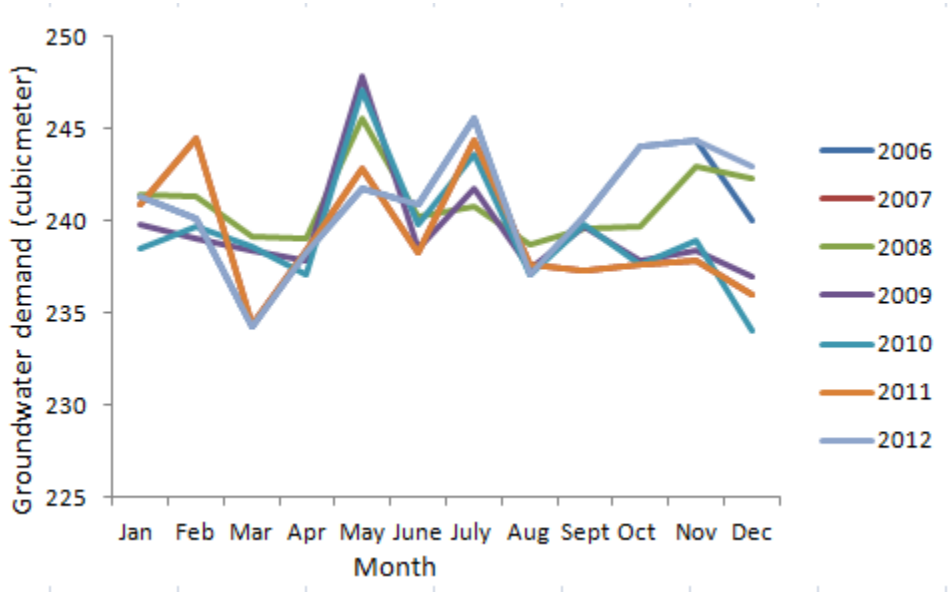


Figure 4-9. Yearly groundwater demand from 2006 through 2012.

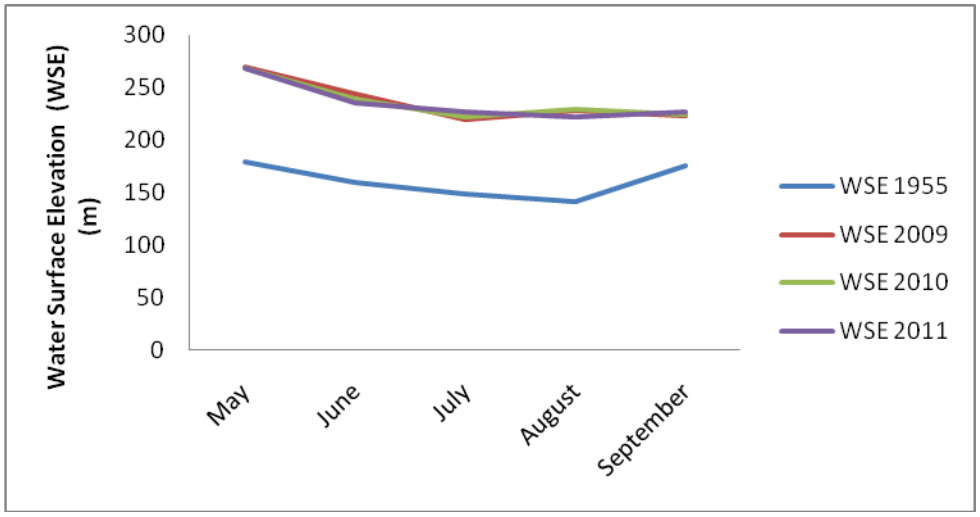


Figure 4-10. A comparison between the groundwater level between 1955 with 2009, 2010 and 2011

### 4.3. Conclusion

San Joaquin Valley is characterized by frequent droughts for the last the few years. There is no accountability on groundwater discharge in San Joaquin Valley and this led to indiscriminate exploitation of aquifer quantity. Hence, aquifer parameters were used to construct hydrologic model to ascertain groundwater flow and its directions. Calibration of the hydraulic head obtained from the model was performed against the observed water level data (hydraulic head) for five wells in the study area. It was observed that the demand of groundwater increased to an average of 255 m<sup>3</sup> for the growing season in summer months. The simulation shows that the irrigated water mostly percolated from the recharge area, and moved towards the California Aqueduct. Hence, in future studies, the subsurface artificial recharge structures (such as such as check dams, subsurface dykes) should perhaps be proposed such that the groundwater is diverted to water stressed crops. This will also prevent the groundwater from flowing away from the farm, which is also necessary for sustainable water conservation. It is observed that the average water surface elevation (WSE) in 1955 for the growing season (May to July) is 161.04 m. This value is low when compared to those of 2009, 2010, and 2011, which are 237.14, 236.28, and 235.74 m respectively.

#### 4.4 References

- Bazeley, W.M. 1972. San Emigdio Nose oil field. *A.A.P.G. Mem.*, No. 16, pp 313-17
- Bertoldi, G.L., R. H. Johnston, and K.D. Evenson, 1991. Ground Water in the Central Valley, California - A Summary Report 1401-A, *U.S. Department of the Interior, Geological Survey*.
- Burow, K.R., Shelton, J.L., Hevesi, J.A., and Weissmann, G.S., 2004.. Hydrogeologic characterization of the Modesto area, San Joaquin Valley, California: *U.S. Geological Survey Scientific Investigations Report*, 2004–5232, pp. 62  
Available at [http://pubs.usgs.gov/sir/2004/5232/sir\\_2004-5232.pdf](http://pubs.usgs.gov/sir/2004/5232/sir_2004-5232.pdf)
- California Dept. of Food and Agriculture. 2009.  
[http://www.cdffa.ca.gov/egov/Press\\_Releases/Press\\_Release.asp?PRnum=09-009](http://www.cdffa.ca.gov/egov/Press_Releases/Press_Release.asp?PRnum=09-009)
- California Department of Water Resources Revised June 18, 2009
- Davis, G.H., Green, J.H., Olmsted, F.H., and Brown, D.W., 1959. Ground-water conditions and storage capacity in the San Joaquin Valley, California: U.S. Geological Survey. *Water-Supply Paper*, Vol. 1469, pp. 287.
- Devin Galloway and Francis S. Riley, *Mining Groundwater*, U.S. Geological Survey, Menlo Park, California,  
<http://pubs.usgs.gov/circ/circ1182/pdf/06SanJoaquinValley.pdf>
- Faunt, C.C., Belitz, Kenneth, and Hanson, R.T. 2009, Chapter B. Groundwater availability in California's Central Valley, in C.C. Faunt, ed., *Groundwater availability of the Central Valley Aquifer, California: U.S. Geological Survey Professional Paper 1766*. Available at <http://pubs.usgs.gov/pp/1766/>.

- Gronberg, J.M., Dubrovsky, N.M., Kratzer, C.R., Domagalski, J.L., Brown, L.R., and Burow, K.R., 1998. Environmental setting of the San Joaquin-Tulare Basins, California: *U.S. Geological Survey Water-Resources Investigations Report 97-4205*, pp. 45
- Maupin, M.A., and Barber, N.L., 2005. Estimated withdrawals from principal aquifers in the United States, 2000: *U.S. Geological Survey Circular 1279*, pp. 46.  
Available at <http://pubs.usgs.gov/circ/2005/1279/>.
- Mendenhall, W.C., Dole, R.B., and Stabler, Herman., 1916. Ground water in San Joaquin Valley, California: *U.S. Geological Survey Water-Supply Paper Vol. 398*, pp. 310.
- McDonald M.G., and A.W. Harbaugh.1988. A modular three-dimensional finite-difference ground-water flow model. *Techniques of Water-Resources Investigations, Book 6. U.S. Geological Survey*
- McDonald M.G., and A.W. Harbaugh, 1996a. User's documentation for MODFLOW-96, an update to the U.S. Geological Survey modular finite-difference ground-water flow model. *Open-File Report 96-485. U.S. Geological Survey.*
- McDonald M.G., and A.W. Harbaugh, 1996. Programmer's documentation for MODFLOW-96, an update to the U.S. Geological Survey modular finite-difference ground-water flow model. *Open-File Report 96-486. U.S. Geological Survey.*

- Ratliff L.F., J.T. Ritchie, D.K.Cassel. 1983. Field-measured limits of soil water availability as related to laboratory-measured properties. *Soil Science Society of America*, Vol. 47(770), pp. 5
- Susan A. Thiros, Laura M. Bexfield, David W. Anning, and Jena M. Huntington, 2009. Conceptual Understanding and Groundwater Quality of the Basin-Fill Aquifer in the Central Valley, California, *National Water-Quality Assessment Program, Professional Paper 1781, U.S. Geological Survey*
- Williamson, A.K., Prudic, D.E., and Swain, L.A., 1989. Ground-water flow in the Central Valley, California: *U.S. Geological Survey Professional Paper 1401-D*, pp. 127.
- Webb, G.W. , 1977. Stevens and earlier Miocene turbidite sands, San Joaquin Valley, California in guidebook: Late Miocene geology and new oil fields of Southern San Joaquin Valley, Pacific sections, *A.A.P.G., SEC., S.E.P.M.*

**CHAPTER 5**

**ASSESSMENT OF WATER BALANCE OF THE SEMI-ARID REGION IN  
SOUTHERN SAN JOAQUIN VALLEY CALIFORNIA USING  
THORNTHWAITE AND MATHER'S MODEL.**

[This chapter was published in Journal of Environmental Hydrology (2012)]

**Abstract**

The demand for water is increasing with growing population and irrigation. Judicious application of limited fresh water resources is a prime focus. Sufficient measures require immediate consideration to avert detrimental crisis to humankind, as agriculture and water resources are one of the most important factors for human survival. The Paramount Farm in southern San Joaquin Valley is known for its largest supplier of almond, albeit water deficit problem. The water resources in this study area is estimated using water-balance assessment approach based on Thornthwaite and Mather (TM) model. The result shows that the total annual precipitation of the farm is 98.5 mm. The month of February received the highest precipitation of 39.6 mm. The potential evapotranspiration (PET) in this region appeared high in July with zero precipitation of 124.3 mm. The actual evapotranspiration (AET) ranges from 36 to 195 mm/month. High soil moisture storage is observed from November to February in the range of 25 to 36 mm, whereas it is low in the months of May to August, as the evapotranspiration process is maximum in May-July. This study also illustrates that there is highest recharge of soil moisture in November to January. To avoid crop water stress, irrigation should apply when the absolute value of Accumulated Potential Water Loss (APWL) is high in the months of



May to July. Further, the water balance calculation in this study implied that the maximum annual runoff is observed from January to March and October to December. There is an annual water deficit of  $135.68 \pm 11.3$  mm and an annual surplus of  $291.47 \pm 24.29$  mm in the farm. It was observed that growers should apply a depth of approximately  $79.37 \pm 11.3$  mm to replenish the soil moisture storage used by the plants over the entire field. Additionally, the field should be irrigated with at least 20 mm of water at each irrigation period to ensure uniform irrigation in the field. This area has a period of moisture surplus from November to February and the remaining months are a period of deficit. This approach is very helpful in finding out the period of moisture deficit and moisture surplus for Paramount Farm.

**Keywords:** Water balance, moisture surplus, TM model, moisture deficit, Paramount Farm.

## 5. Introduction

In semi-arid regions, water resources are limited, and available groundwater for irrigation and other water uses are severely constrained. Southern San Joaquin Valley is located in a semi-arid climatic region, characterized by limited water resources due to expanding urban, industrial and agricultural water demands. In semi-arid regions, the actual evapotranspiration (AET) plays a key role of the hydrological cycle. AET may account for more than 90 % of the precipitation (P) in semi-arid areas (Pilgrim et al., 1988; Huxman et al., 2005). Drought in California is a matter of serious concern particularly when there are extensive agricultural productions in Central Valley. The state experienced massive agricultural loss of \$ 308 million in 2008 due to water scarcity (California Dept. of Food and Agriculture, 2009). The Central Valley Project (CVP) allowed only 10% of water allowance to farmers in 2009 compared to 40% in 2008 and 50% in 2007. Farmers relied on the groundwater to accommodate the water shortage provided by CVP.

The water system especially in agricultural areas requires an understanding through the water balance method for irrigation scheduling. Water balance refers to the balance between incoming water (precipitation) and outgoing water (evapotranspiration, groundwater discharge and stream flow). Therefore, a budgeting exercise is used to evaluate the amount of precipitation that becomes stream flow (or runoff), evapotranspiration, and drainage (or groundwater discharge). Among the several methods for calculating water balance, Thornthwaite and Mather (TM) in 1955 and 1957 introduced one of the most prominent methods that are used widely. The water balance

approach is very helpful in finding out the annual periods of moisture deficit and moisture surplus for an entire area. The long-term average monthly rainfall, long-term average PET, and soil-vegetation characteristics are required to compute the water balance. LaBaugh et al. (1997) used isotopes and hydro-chemical tracers to study the water balance of a lake in North America. Mandal et al. (1999) used the TM model for estimating soil-climatic water balance throughout India for analyzing climatic indices, length of growing period of crops, and their applications in agricultural research. Boulet et al. (2000) estimated simple water and energy balance with a bulk mixed vegetation and bare soil using soil “bucket” and Soil-Vegetation Atmosphere Transfer (SVAT) model. However, the depth of the “bucket” or hydrologically active depth was established to be critical when the water balance was translated to soil moisture (Boulet et al., 2000).

The objective of this study is to investigate the water balance of a region using the TM model and to record the periods of moisture deficit and moisture surplus in the study area.

## **5.1 Materials and Method**

### **5.1.1 Study Area**

The 402 km<sup>2</sup> Paramount Farm is located at the Lost Hill of Kern County in southern San Joaquin valley of Central Valley, California (35°30'N, 119°39'W) (Figure 5-1). The total annual precipitation of the farm is 98.5 mm. The valley occupies two-thirds of the southern Central Valley in California. San Joaquin River flows in the northern part of the San Joaquin Valley and drains to the San Francisco Bay. About 4 percent of the basin

area is urban. Majority of the basin's population focuses on agricultural activities. Geographically, the southern part of the San Joaquin Valley is the Tulare Basin, bordered by the Sierra Nevada on the east, the Tehachapi Mountains on the south, and Coast Ranges on the west. The northern extent corresponds to the Kings River. Significant geographic features include the Tulare Lake Basin and the Kettleman Hills.

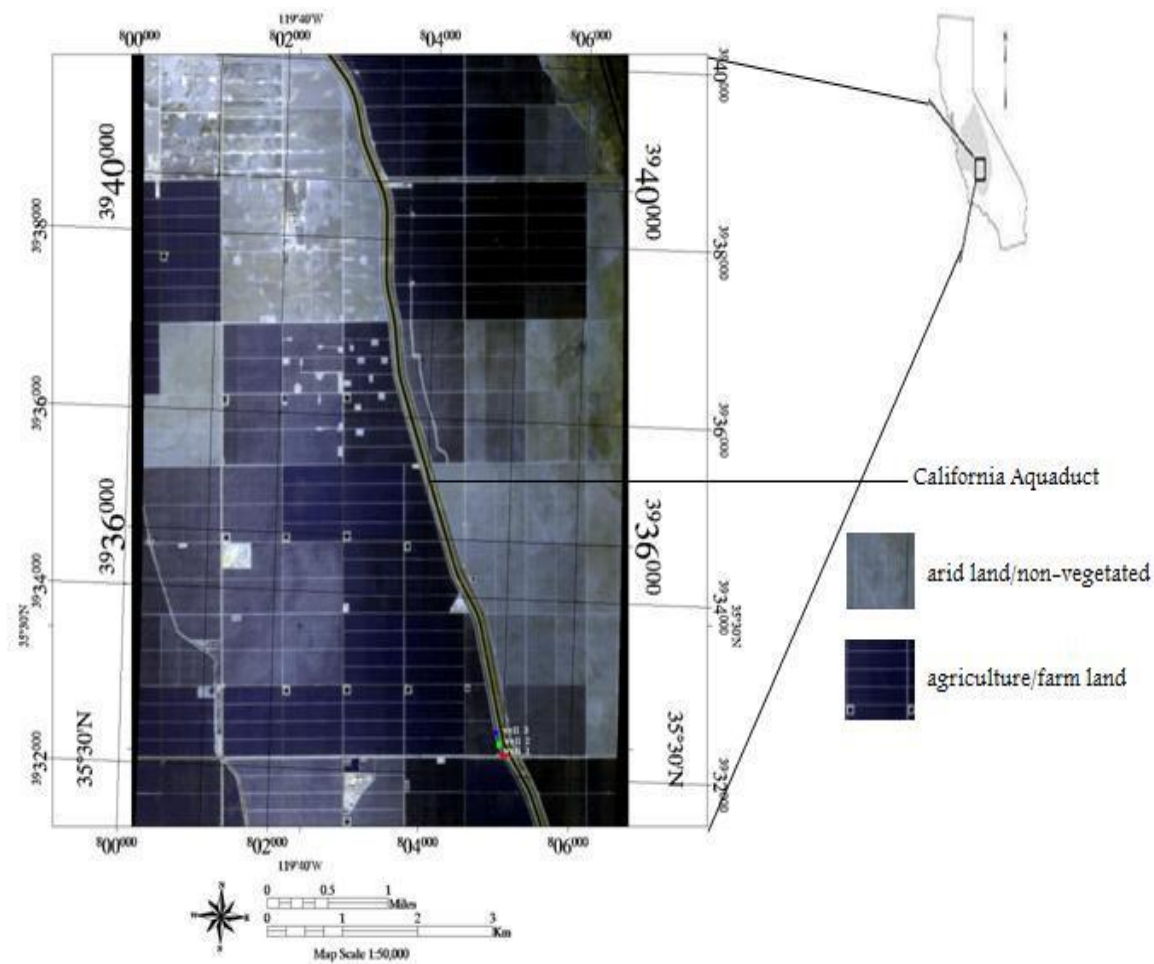


**Figure 5-1.** Remotely sensed false color composite (Band 1, Band 2 and Band 6) of MASTER image showing Paramount farm in Southern San Joaquin Valley, California. Blocks show reflectance of various types of crops in dark tone. Bright tone shows reflectance of non-vegetated/arid areas (Land cover classification of this image shown in Figure 5-2).

### 5.1.2 Hydrogeology

The hydrogeology of the study area is derived from the large, northwest trending asymmetric structural trough which comprises marine and continental sediments up to 10 km thick (Gronberg and others, 1998). The trough is filled with marine sediments that are overlain by continental sediments in some places. These sediments are significantly deposited largely by streams draining from the mountains from time to time. The alluvial fans in this area are derived from the glaciated portion of the Sierra Nevada (Faunt, Hanson, and Belitz, 2009). Fine-grained sediments (clay, sandy clay, sandy silt, and silt) are distributed throughout the San Joaquin Valley. The Corcoran Clay forms a separation in the basin-fill deposits into an upper unconfined to semi-confined zone and a lower confined zone in southern San Joaquin Valley (Williamson et al., 1989, Burow et al., 2004). The Sierra Nevada Mountains rise to an elevation of more than 4200 m in the east of the valley; whereas, west of the valley area is bounded by the Coast Ranges which are a series of parallel ridges with moderate elevations (Mendenhall et al., 1916). Before the development of surface water diversion, ground water generally moved toward the center of the valley and northward to the San Francisco Bay. A prolong period of surface waters diversions altered the natural flow of groundwater. Development of the groundwater basin initiated the irrigation water to percolate, which became the primary form of groundwater recharge and irrigation drawdown became the primary form of groundwater discharge in the southern San Joaquin Valley (Davis et al., 1959). The soil texture in southern San Joaquin valley comprises alluvial fans that are derived from the glaciated parts of the Sierra Nevada. They are coarser grained than the alluvial fans to the

north (Faunt, Hanson, and Belitz, 2009). Generally, thin, discontinuous lenses of fine-grained sediments (clay, sandy clay, sandy silt, and silt) are distributed throughout the San Joaquin Valley (Table 5-1).

**Table 5-1.** Estimated available water capacities for various soil-texture group (Ratliff et al., 1983)

<b>Soil texture</b>	<b>Available water capacity (mm per meter of thickness)</b>	<b>Maximum soil water capacity (mm)</b>
Sand	14400	182.88
Loamy Sand	22800	289.56
Sandy Laom	30000	381
Loam	38400	487.68
Silt loam	43200	548.64
Sandy clay Loam	42000	533.4
Sandy clay	40800	518.16
Clay loam	45600	579.12
Silty clay loam	51600	655.32
Silty clay	57600	731.52
Clay	4.8	28.8



The available water capacity of a soil was typically given as inches of water holding capacity per foot of soil thickness. Ratliff et al., (1983) computed the field measurement of soil water availability for each soil type shown in the Table 5-1. The rooting depth of the orchards was 1.8 m. The maximum soil water capacity was calculated as available water capacity multiplied by the rooting depth. If the infiltrated water exceeds the maximum soil water capacity then the water contributes as recharge to groundwater.

### **5.1.3 Available data**

Within the study area, California Irrigation Management System (CIMIS) station is located in Belridge. The climatic stations contain daily measurements of wind speed, global radiation, and daily minimum and maximum values of both air temperature and relative humidity. These data are used to calculate the daily PET by the Penman-Monteith method. There are 70 different types of topsoil identified in the catchment. However many of the soil types are similar in description, therefore the 70 soils types were reclassified into eleven major soil types (Table 5-1). A land use map is shown in Figure 5-2 (see Chapter 2). The vegetation is classified into almond orchards, pistachio crops, and other photosynthesis vegetation. The classification also includes urban land, non-photosynthesis vegetation, soil, and water.

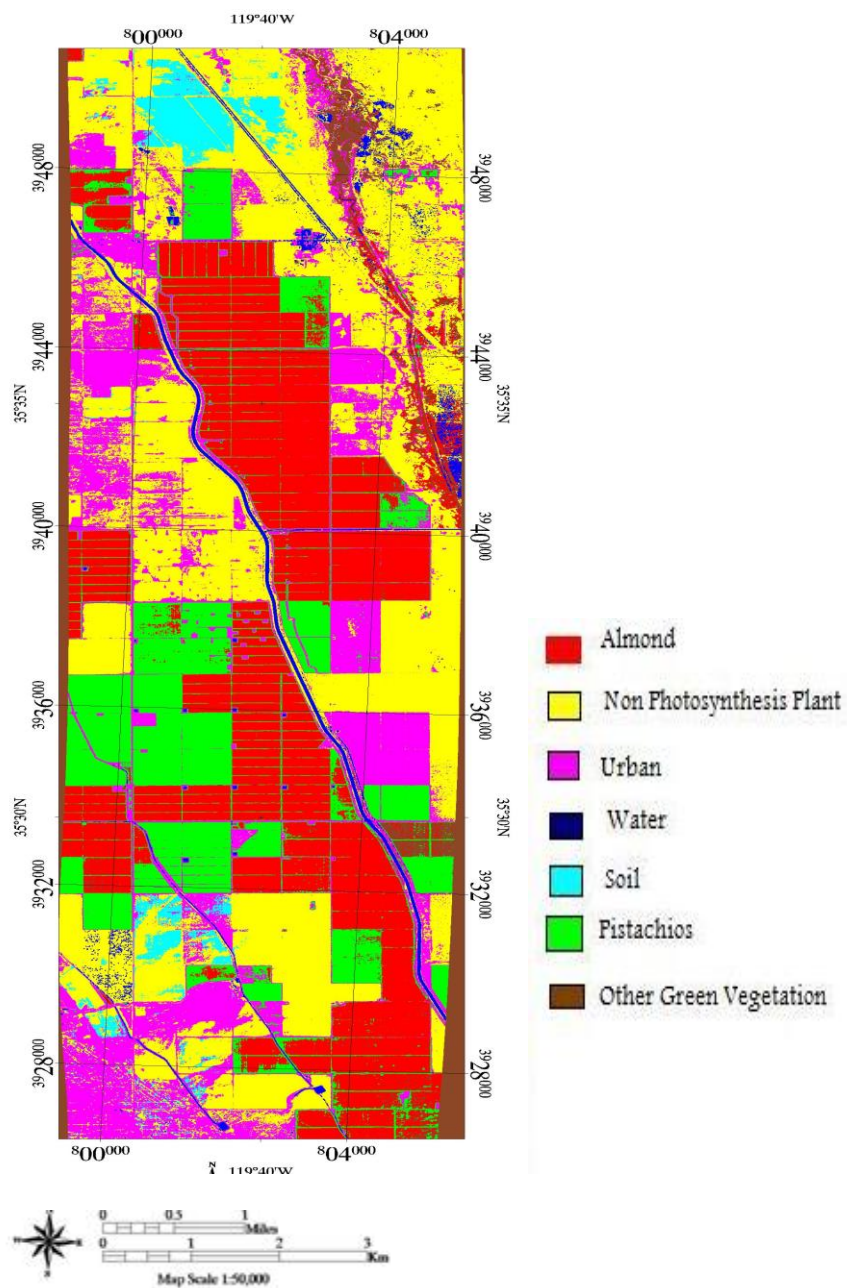


**Figure 5-2.** Supervised classification using maximum likelihood for almond orchards, non-photosynthetic plant (NPV), urban, water, soil, pistachio orchards, and other green vegetations.

#### 5.1.4 The Thornthwaite and Mather's (TM ) Model

The TM model is one of the simplest models to determine water balance of a region from individual fields to small watersheds. Monthly water balance is used to examine the various components of the hydrologic cycle (for example, precipitation, evapotranspiration and runoff). The monthly potential evapotranspiration is computed using the following equation (Singh et al., 2004)

$$PET = 1.6 \times C \times \left(10 \times \frac{T}{I}\right)^a \quad (5-1)$$

Where PET is the potential evapotranspiration (mm month<sup>-1</sup>); T is the mean monthly temperature (°C); I is the annual heat index for the 12 months in a year ( $I = \sum i$ );

i is the monthly heat index ( $i = [T/5]^{1.514}$ );  $a = 6.75 \times 10^{-7} \times I^3 - 7.71 \times 10^{-5} \times I^2 + 1.792 \times 10^{-2} \times I + 0.49239$ ; and C is a correction factor for each month ( $C = [m/30] \times [d/12]$ ),

Where m is the number of days in the month and d is the monthly mean daily duration (number of hours between sunrise and sunset, expressed as the average for the month).

$P - PET$ , is a quantitative estimation of the water excess (+) or deficit (-). Accumulated potential water loss (APWL) is the potential deficiency of soil moisture associated with low moisture contents of soil below its water holding capacity. Accumulated potential water loss is 1) increased during dry seasons to meet the demands of PET when there is insufficient supply of water, 2) reduced during wet seasons from soil moisture recharge, and 3) equals zero when soil moisture equal to the available water holding capacity of the soil. The accumulated values APWL for each months, were calculated by running the sum of the daily  $P - PET$  values during the periods when ( $P - PET$ ) is a negative value as given in Table 5-2. APWL will be zero for the months having positive ( $P - PET$ ).

Therefore, the actual storage of soil moisture (STOR) for each month was calculated as follows:

$$STOR = AWC \times e^{(APWL/AWC)} \quad (5-2)$$

Where, AWC is the moisture storage capacity, also known as available water capacity of the soil, which is based upon the land use, soil texture and rooting depth as suggested by Thornthwaite and Mather (1955, 1957). The results are summarized in Table 5-2. Change of actual storage was calculated as

$$\Delta SM_{\text{month}} = STOR_{\text{month}} - STOR_{\text{previous month}} \quad (5-3)$$

A negative value of  $\Delta SM$  means discharge of water from the storage because of evapotranspiration, whereas a positive value of  $\Delta SM$  implies infiltration of water into the soil that contributes to the soil moisture storage.

The actual evapotranspiration (*AET*) was computed for all the months, as given in equations (5-4) and (5-5):

$$AET = \Delta SM + P \quad \Delta SM < 0 \quad (5-4)$$

$$AET = PET \quad \Delta SM > 0 \quad (5-5)$$

Where PET is the potential evapotranspiration.

The water deficit (DEF) was calculated for those months having negative value of P-PET as follows:

$$DEF = PET - AET \quad (5-6)$$

Moisture surplus (SUR) is defined as the excess water that cannot be stored when soil moisture storage attains its saturation; SUR is calculated using equation (5-7):

$$SUR = P - PET \quad (5-7)$$

No surplus exists if soil storage is not at its capacity. If moisture storage capacity of the soil is just satisfied, then, SUR is obtained using equation (5-8)

$$\text{SUR} = \text{P} - (\text{AET} + \Delta\text{SM}) \quad (5-8)$$

Where  $\Delta\text{SM}$  is the change in actual soil moisture storage. Previous studies show that actual runoff should be equal to the available annual surplus (Singh et al., 2004). Considering the study area was classified as homogeneous land use /land cover occupying only almond orchards; the total amount of annual ET and runoff is calculated from the monthly water balance. Thus, the monthly runoff and the monthly AET from the farm are area-weighted values (Table 5-3).

**Table 5-2.** Calculation of Accumulated Potential Water Loss (APWL) in mm

	<b>P</b>	<b>PET</b>	<b>P-PET</b>	<b>APWL</b>
<b>Jan</b>	13.72	39.88	-26.16	-36.06
<b>Feb</b>	39.62	56.90	-17.27	-51.62
<b>Mar</b>	3.56	115.32	-111.76	-111.50
<b>Apr</b>	5.84	154.43	-148.59	-155.70
<b>May</b>	0.25	197.87	-197.61	-197.86
<b>Jun</b>	0.00	197.10	-197.10	-204.21
<b>Jul</b>	0.00	214.12	-214.12	-213.10
<b>Aug</b>	0.00	181.61	-181.61	-181.61
<b>Sep</b>	0.00	146.56	-146.55	-151.89
<b>Oct</b>	3.30	98.30	-94.99	-94.99
<b>Nov</b>	5.84	55.88	-50.03	-53.08
<b>Dec</b>	26.42	34.54	-8.13	-29.97
<b>Total</b>	98.50	1492.50	1393.95	1481.59

## 5.2 Result and Discussion

### 5.2.1 Water Balance Computations

The accumulated potential water loss (APWL) for the Paramount Farm was calculated from monthly rainfall and temperature data using TM model. In Table 5-2, monthly APWL for almond farm was calculated. The available soil moisture capacity for different types of soil texture shown in Table 5-1 was considered for computation of actual storage of soil moisture. The top soil of the study area is dominated by sandy loam with AWC of root zone of 63.5 mm. The monthly water balance in the farm was calculated as shown in Table 5-3. Paramount Farm has the annual deficit of 135.68 mm and annual surplus of 1.77 mm. The total annual runoff from the farm is calculated as 1086.56 mm.

Table 5-4 gives us information regarding the water balance of the farm. The monthly variation of P, PET, AET and runoff in the area indicates the periods of soil moisture deficit, recharge and utilization. The moisture deficit from May to August suggests maximum crop water stress where CWSI is approximately 1. This indicates that the crop is dried up and the yield is affected. Therefore, irrigation is necessary in that area. Soil moisture recharge occurs from late October. The period from November to early February was the period of water surplus as the area was subjected to rainfall during winter months. The amount of AET and runoff from the farm was calculated as the area-weighted values.

**Table 5-3.** Average monthly water balance computation for almond orchard in mm

(AWC= 63.5 mm for sandy loam)

	<b>P</b>	<b>PET</b>	<b>P-PET</b>	<b>Store</b>	<b><math>\Delta</math>SM</b>	<b>AET</b>	<b>Deficit</b>	<b>Surplus</b>	<b>Runoff</b>
<b>Jan</b>	13.71	39.87	-26.16	35.98	-314.01	36.25	3.62	291.47	53.85
<b>Feb</b>	39.62	56.89	-17.27	28.16	-7.82	51.72	5.17	0	120.07
<b>Mar</b>	3.55	115.31	-111.76	10.96	-17.19	104.83	10.48	0	212.73
<b>Apr</b>	5.84	154.43	-148.59	5.46	-5.50	140.39	14.039	0	0
<b>May</b>	0.25	197.86	-197.61	2.81	-2.65	179.87	17.98	0	0
<b>Jun</b>	0	197.10	-197.10	2.54	-0.26	179.18	17.91	0	0
<b>Jul</b>	0	214.12	-214.12	2.21	-0.382	194.65	19.46	0	0
<b>Aug</b>	0	181.61	-181.61	3.63	1.42	165.1	16.51	0	0
<b>Sep</b>	0	146.55	-146.55	5.80	2.170	133.23	13.32	0	0
<b>Oct</b>	3.30	98.29	-94.99	14.22	8.41	89.36	8.93	0	176.73
<b>Nov</b>	5.84	55.88	-50.03	27.52	13.29	50.8	5.08	0	84.99
<b>Dec</b>	26.41	34.54	-8.12	39.60	12.08	31.40	3.14	0	52.75
<b>Total</b>	98.55	1492.50	-1393.95	178.97	-310.39	1356.82	135.68	291.48	701.15



**Table 5-4.** Summary of P, PET, AET, and Runoff in mm

	<b>P</b>	<b>PET</b>	<b>AET</b>	<b>Runoff</b>
<b>Jan</b>	13.72	39.88	36.25	256.75
<b>Feb</b>	39.62	56.9	51.72	184.48
<b>Mar</b>	3.56	115.32	104.83	60.63
<b>Apr</b>	5.84	154.43	140.39	0
<b>May</b>	0.25	197.87	179.88	0
<b>Jun</b>	0	197.1	179.19	0
<b>Jul</b>	0	214.12	194.66	0
<b>Aug</b>	0	181.61	165.1	0
<b>Sep</b>	0	146.56	133.23	0
<b>Oct</b>	3.3	98.3	89.36	105.96
<b>Nov</b>	5.84	55.88	50.8	218.93
<b>Dec</b>	26.42	34.54	31.4	259.81

The output was compiled by collating the data into long-term averages. This is useful to track soil moisture status throughout the year in order to determine periods of soil water deficit, soil water recharge, soil water utilization, and soil water surplus. Figure 5-3 demonstrated the different status of soil moisture throughout the year with AWC of 63.5 mm at 1.8 m rooting depth. It was observed that the area-weighted average annual deficit in the farm was 11.30 mm and the annual surplus was 24.29 mm. To avoid crop water stress, irrigation should apply when the absolute value of APWL is above 200. APWL was maximum in the month of May, June, and July.

Table 5-3 shows that in the month of July 2009, there was 19.46 mm of deficit when irrigation efficiency was 80 percent. Therefore, the amount of water required for effective irrigation was obtained by dividing the amount of water required to replenish the soil moisture storage (or AWC) by the efficiency of irrigation system (CIMIS drought tips 90-20). In this study, the total amount of water required is calculated as  $(63.5 / 0.80) = 79.37 \pm 11.3$  mm for effective irrigation. Hence, the grower should apply a minimum depth of  $79.3 \pm 11.3$  mm of water to replenish the soil moisture loss over the entire field for the month of July.

The water is applied unevenly, therefore, at each irrigation; the total water applied should be more than the soil water deficit. This is to assure that the part of the field receiving least amount of water or water stressed ( $CWSI > 5$ ) is adequately irrigated. The total water to apply at each irrigation (CIMIS drought tip 90-20) is calculated as deficit + irrigation efficiency ( $19.46 + 0.8 = 20.26$  mm). Therefore, the field should be irrigated with at least 20 mm of water at each irrigation.

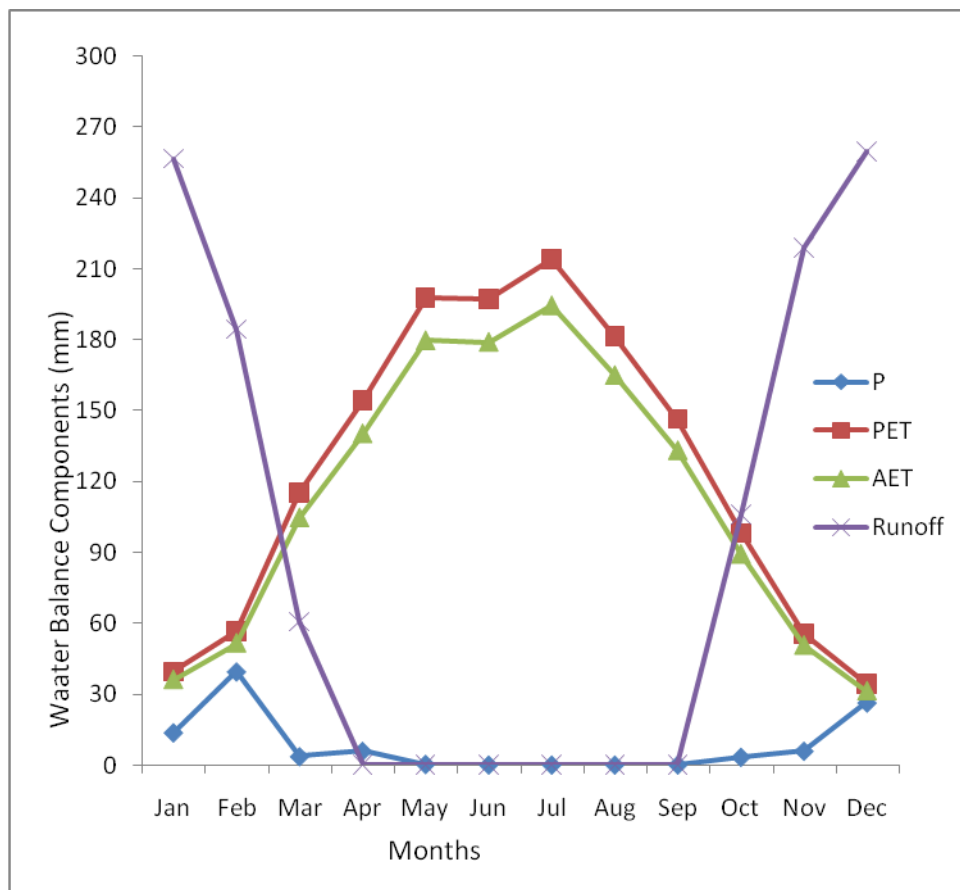


**Figure 5-3.** Water balance status of the study area

### 5.3 Conclusion

This study uses TM water balance model to evaluate various components of water balance in the Paramount Farm region. Such estimation of water balance components is useful in agricultural areas that account for all water addition and subtraction from the soil root zone for planning irrigation scheduling. Water balance study is also helpful in finding out the periods of moisture deficit and moisture surplus for the region. The model computes evapotranspiration, runoff, soil moisture, and recharge separately on monthly basis. The TM model uses rainfall data, temperature data, soils, land-use and rooting depth of almond orchard vegetation for calculating the soil moisture deficit, soil moisture surplus, evapotranspiration, and surface runoff. The average annual precipitation of the farm is 8.21 mm. February receives the highest precipitation of 39.6 mm. Average PET of this region was 124.3 mm. The range of AET is 45 to 246 mm/month. These AET estimates can be used to determine day-to-day soil water depletion from available water capacity and thus can be used to schedule irrigation. High soil moisture storage was observed from November to February in the range of 25 to 36 mm, but least in May to August as the ET was high. This shows that there was highest recharge of soil moisture in November to January. To avoid crop water stress, irrigation should be applied when the absolute value of APWL is maximum in the months of May to July. The water balance calculation shows that the maximum annual runoff was observed from January to March and October to December. The total runoff was calculated as 1086.56 mm. Runoff exceeds rainfall, suggesting the melting snow from snow-covered mountain in Sierra Nevada that contributes to most of the surface and groundwater runoff in this region. The

total annual deficit in the watershed is  $135.66 \pm 11.3$  mm and the annual surplus is  $291.47 \pm 24.29$  mm. This region undergoes a period of moisture deficit in the months of May to July. September to October are months of soil water recharge; from November to early February is the period of water surplus as the area is subjected to winter rainfall. Winter months are subjected to surplus, whereas deficit in the remaining time of the year shows strong exchange phenomenon among atmosphere, surface water, groundwater, energy balance and water balance in the farm. Result shows that for efficient irrigation, water balance studies are important to estimate the quantity of water required for irrigation without much loss. It was observed that growers should apply a depth of approximately  $79.37 \pm 11.3$  mm to replenish the soil moisture storage over the entire field for the month of July. At least 20 mm of total water should be applied in each irrigation period to ensure that most of the field is evenly irrigated to avoid crop water stress. This study helps the farmers to decide their crop calendar, irrigation requirements, and water conservation, based upon the periods of deficit or surplus.

## 5.4 References

- Boulet, G., A. Chehbouni, I. Braud, M. Vauclin, R. Haverkamp, and C. Zammit, 2000. A simple water and energy balance model designed for spatialisation and remote sensing data utilization. *Agric. For. Met.* (SALSA Special Issue). Vol. 105, pp. 117–132.
- Burow , Karen R., L. Jennifer, Joseph A. Shelton, Hevesi, and Gary S. Weissmann, 2004. Hydrogeologic Characterization of the Modesto Area, San Joaquin Valley, California. *U.S. Geological Survey, Scientific Investigations Report 5232*.
- California Dept. of Food and Agriculture, 2009. Retrieved on February 26, 2011 from [http://www.cdfa.ca.gov/egov/Press\\_Releases/Press\\_Release.asp?PRnum=09-009](http://www.cdfa.ca.gov/egov/Press_Releases/Press_Release.asp?PRnum=09-009)[http://www.cdfa.ca.gov/egov/Press\\_Releases/Press\\_Release.asp?PRnum=09-009](http://www.cdfa.ca.gov/egov/Press_Releases/Press_Release.asp?PRnum=09-009)
- California Department of Water Resources Revised June 18, 2009
- Davis, G.H., J.H. Green, F.H. Olmsted, and D.W. Brown, 1959. Ground-water conditions and storage capacity in the San Joaquin Valley, California: *U.S. Geological Survey Water-Supply*, Paper 1469, pp. 287.
- Faunt, C.C., Kenneth Belitz, and R.T. Hanson, 2009. Chapter B. Groundwater availability in California's Central Valley, in C.C. Faunt, ed., Groundwater availability of the Central Valley Aquifer, California: *U.S. Geological Survey. Professional Paper 1766*.
- Gronberg, J.M., N.M. Dubrovsky, C.R. Kratzer, J.L. Domagalski, L.R. Brown, and K.R. Burow, 1998. Environmental setting of the San Joaquin-Tulare Basins,

- California: *U.S. Geological Survey Water-Resources Investigations Report 97-4205*, pp. 45.
- Huxman, T. E., B. P. Wilcox, D. D. Breshears, R. L. Scott, K. A. Snyder, E. E. Small, K. Hultine, W. T. Pockman, and R. B. Jackson, 2005. Ecohydrological implication of woody plant Encroachment. *Ecological Society of America*. Vol. 86(2), pp. 308-319.
- Hultine, W. T. Pockman, and R. B. Jackson, 2005. Ecohydrological implication of woody plant Encroachment. *Ecological Society of America*, Vol. 86(2), pp. 308-319
- LaBaugh, J. W., T.C. Winter, D.O. Rosenberry, P.F. Schuster, M.M. Reddy, and G.R. Aiken, 1997. Hydrological and chemical estimates of the water balance of a closed lake in north central Minnesota. *Water Resour. Res.*, Vol. 33, pp. 2799-2812.
- Mandal, C., D.K. Mandal, C.V. Srinivas, J. Sehgal, and M. Velayutham, 1999. Soil climatic database for crop planning in India. National Bureau of Soil Survey. Paper 53.
- Mendenhall, W.C., R.B. Dole, and Herman Stabler, 1916. Ground water in San Joaquin Valley, California: U.S. Geological Survey Water-Supply. Paper 398, pp. 310.
- Pilgrim, D. H., T. G. Chapman, and D. G. Doran, 1988. Problems of rainfall-runoff modelling in arid and semiarid regions. *Hydrological Sciences Journal - des Sciences Hydrologiques*, Vol. 33, pp. 379-400.

- Ratliff L.F., J.T. Ritchie, D.K.Cassel, 1983. Field-measured limits of soil water availability as related to laboratory-measured properties. *Soil Science Society of America*, Vol. 47(770), pp. 5
- Singh, R.K, V.Hari Prasad, 2004. Remote sensing and GIS approach for assessment of the water balance of a watershed. *Hydrological sciences*, Vol. 49(1), pp. 131-141
- Snyder, R.L., and H.L. Sheradin, 1993. Water Balance Irrigation Scheduling Using CIMIS ETo. University of California Drought Tip 90-60.
- Thornthwaite, C. W., and J.R. Mather, 1955. The water balance: Centeron, N.J., Laboratory of Climatology. *Publications in Climatology*, Vol. 8, no. 1, pp. 1–104.
- Thornthwaite, C. W., and J.R. Mather, 1957. Instructions and tables for computing potential evapotranspiration and the waterbalance: Centeron, N.J., Laboratory of Climatology. *Publication in Climatology*, Vol. 10, no. 3, pp. 185-311.
- Williamson, A.K., D.E Prudic, and L.A.Swain, 1989. Ground-water flow in the Central Valley, California: U.S. Geological Survey. Professional Paper 1401–D, pp. 127.



## Summary

Water resources are limited in semi-arid regions and thereby the available water for irrigation and other purposes are constrained. However, there is always need for optimum use and planning of limited water resources. The Central Valley in California is one of the most productive agricultural regions in the world. This project focused on the Paramount Farm (35°30'N, 119°39'W) in Central Valley, California with an annual rainfall of 98.5 mm. An optimum amount of water is required for irrigation as well as conservation. The objective was to integrate remote sensing and hydrologies to (1) evaluate energy fluxes for estimation of crop evapotranspiration (ET). (2) Compute water stress of crop using Crop Water Stress Index (CWSI). (3) Analyze the movement of the groundwater table. (4) Compute the water balance of the farm.

The crop water requirement is studied by estimating the ET. ET is one of the most important parameters of water balance, which is used for irrigation scheduling, and analyzing crop water stress. The remote sensing approach allows for a more complete understanding of ET over large area. Bastiaanssen et al. (1998, 2005) developed a Surface Energy Balance Algorithm for Land (SEBAL) model. For this study, airborne images were obtained from NASA DC-8 aircraft by MASTER (MODIS/ASTER) simulator. This sensor has 50 spectral bands in four spectral regions (visible through thermal infrared) with greater than 10m spatial resolution. Results show that the remote sensing estimate of ET is an alternative to conventional methods using Penman-Monteith. Average actual evapotranspiration (ET<sub>a</sub>) estimated from SEBAL, and Penman-Monteith (PM) was 0.67 mm/h and 0.75 mm/h respectively, with a mean percent difference of

0.109%. The average ET<sub>a</sub> estimated from SEBAL is 0.65 mm/h. The amount of water required to reimburse evapotranspiration loss from the farm is defined as crop water requirement. Therefore, Crop Water Stress Index (CWSI) was used to quantify the water requirement. The estimation of water stress in crop is not only used to monitor vegetative activity and predict productivity, but it also assesses the efficient use of water in arid agricultural areas. This method is suggested by Idso et al. (1981), to quantify plant stress associated with water deficit under field conditions. Remote Sensing allows efficient irrigation by applying water when symptom of water stress appears. The empirical relationship for canopy- air temperatures difference ( $T_c - T_a$ ) versus Vapor Pressure Deficit (VPD) will represent water status of the vegetation. The average value of CWSI for well-irrigated (non-stressed) almonds was 0.24 while the yield would decline when the average CWSI values for water stress crop are greater than 0.5. Therefore, to avoid the water stress and poor productivity, the irrigated agriculture relies heavily on surface-water diversions, and groundwater. Identification of potential recharge area in the field was required to study soil-water moisture status. The source of recharge is through percolation of irrigation water and thereby, the groundwater flow direction was studied to analyze the fluctuation of the groundwater table. A mathematical groundwater flow model was developed in the study. For this purpose, Groundwater Modeling Software (GMS) was used which supports MODFLOW- 2000 code. The model was calibrated using groundwater elevation data against the historical water level data in 1955 under steady-state conditions. Transient simulation of groundwater flow was carried out from the year 2006 to 2011 for 5 stress periods. It was observed that the groundwater is

flowing from west to east in the study area. The average water surface elevation (WSE) in 1955 for the growing season (May to July) is 161.04 m in comparison with 2009, 2010, and 2011 elevations of 237.14 m, 236.28 m, and 235.74 m respectively. Therefore, the irrigated water is mostly percolating and moving towards the California Aqueduct. In future studies, the subsurface artificial recharge structure (such as check dams, percolation tank, and infiltration gallery) will be proposed such that the percolating water can be conserved to be used by water stressed crops. In addition, a thorough understanding of the ET processes as well as precipitation is required to obtain water balance computations of the farm annually. It was observed that the annual deficit in the watershed is  $135.66 \pm 11.3$  mm and the annual surplus is  $291.47 \pm 24.29$  mm. This region undergoes a period of moisture deficit in the months of May to July. From September to October are months of soil water recharge; from November to early February is the period of water surplus from winter rainfall. To avoid crop water stress, irrigation should be done when the APWL observed is maximum in the months of May, June, and July. Considering that Central Valley Project (CVP) allowed only 10% of water allowance to farmers in 2009 compared to 40% in 2008 and 50% in 2007. Growers should apply a depth of approximately  $79.37 \pm 11.3$  mm to replenish the soil moisture storage over the entire field for the orchard growing season. At least 20 mm of total water should be applied in each irrigation period to ensure that most of the field is evenly irrigated to avoid crop water stress.

Results obtained from this study will help the water managers to predict the irrigation scheduling, understand how water moves through the aquifer system, and to

predict water supply scenarios based on the water balance. Such studies can be very beneficial for the local population who can decide their crop calendar and irrigation requirements based upon the periods of deficit or surplus. Water conservation measures are also planned based upon the duration of deficit and surplus for drought affected agricultural regions in the farm. This research can also be applicable to other arid to semi-arid agricultural areas of the world (for example India, northern China, Israel, West Africa, Mexico, Australia) for water conservation and management in the farms. Therefore, high-resolution satellite image, field data (thermal measurement of water, canopy, soil), and weather data are required to compute energy balance for estimating ET, water balance, and water stress indices (CWSI or WDI depending upon the canopy cover). However, the applicability of this study can also be difficult in extreme spatial heterogeneity of soil, vegetation, and climatic characteristics in semi-arid agricultural areas of the world. Scarcity of weather and field data at inaccessible regions can hinder the model output. Therefore, for such areas, distributed hydrological model can be proposed.

Climate change is largely determined by an increase in the area of arid land driven by global warming, and rising green house gases. In southwest US, diminishing snow pack and reduction of soil moisture affects groundwater recharge rates, less surface water runoff and low groundwater table. Long-term study of climate change from this study requires regional historical data on precipitation, temperature, evapotranspiration, soil moisture, and evaporative demand, which is determined by net radiation at surface, humidity, vapor pressure, wind speed, and air temperature for computation of projected

water balance of the farm in drought years. However, there are uncertainties in projected changes in hydrological system due to variability of weather parameters, anthropogenic changes in land cover/use, uncertainty of future greenhouse gases, and declining availability of moisture in the summer from snowmelt as the snowpack is melting earlier, in the spring. The study has demonstrated the potential reason for using remote sensing data for deriving important variables for studying hydrologic modeling in semi-arid agricultural regions.

